PAUL SCHERRER INSTITUT

PSI

UNIVERSITÄT BERN

LABOR FÜR RADIO- UND UMWELTCHEMIE
DER UNIVERSITÄT BERN UND
DES PAUL SCHERRER INSTITUTS

Annual Report 2009

January 2010

COVER:

What the Periodic Table of the Elements is to the normal chemist is the Chart of Nuclides to the nuclear chemist, independently of his or her specialty. Since its first appearance over 50 years ago, the Karlsruhe Chart of Nuclides nowadays contains data on almost 3000 nuclides and it is still expanding as new elements and new nuclides are being discovered. The sketch of the Chart of Nuclides, designed by Prof. H.H. Coenen (FZ Jülich) for the NRC6 conference, accurately reflects the vitality and drive of our field. With this dynamic motion in mind, leadership of the Laboratory of Radiochemistry and Environmental Chemistry is passed on from Heinz Gäggeler (left) to Andreas Türler.

PAUL SCHERRER INSTITUT

LABOR FÜR RADIO- UND UMWELTCHEMIE
DER UNIVERSITÄT BERN UND
DES PAUL SCHERRER INSTITUTS

UNIVERSITÄT BERN

Annual Report 2009

January 2010

Editors: A. Türler
M. Schwikowski
A. Blattmann

Reports are available from:
Angela Blattmann (angela.blattmann@psi.ch), Paul Scherrer Institut, 5232 Villigen PSI, Switzerland (See also our web-page: http://lch.web.psi.ch/)

Paul Scherrer Institut
Labor für Radio- und Umweltchemie
5232 Villigen PSI
Switzerland

Durchwahl +41 (0)56 310 24 04
Sekretariat +41 (0)56 310 24 01
Fax +41 (0)56 310 44 35

Universität Bern
Departement für Chemie und Biochemie
Labor für Radio- und Umweltchemie
Freiestrasse 3, 3012 Bern, Switzerland

Durchwahl +41 (0)31 631 42 64
Sekretariat +41 (0)31 631 42 42
Fax +41 (0)31 631 42 20

TABLE OF CONTENTS

Analytical Chemistry

Radwaste Analytics

Environmental Radionuclides Universität Bern

EDITORIAL

The past year has seen many changes. On August 28 we celebrated the 25th anniversary of the "Laboratory of Radiochemistry and Environmental Chemistry" (as it is now officially called at Paul Scherrer Institut), but also the retirement of Heinz Gäggeler, its head. In addition, the department TEM (particles and matter), that he was also heading, was dissolved. Thus, the laboratory needed a new head as well as a new home at PSI.

This situation might have been problematic, but it wasn't, since the transition had been carefully planned in advance. It is thus with great pleasure and also a certain pride, that I am writing now my first editorial to the already traditional annual report of the Laboratory of Radiochemistry and Environmental Chemistry. After gathering 8 years of experience as head of the Institute of Radiochemistry at Technical University of Munich, I accepted the offer to succeed Heinz. The time in Munich has been an interesting one, but it has been a bumpy ride, with many ups but also downs. In coming here, I leave my former co-workers in a difficult situation. This is especially troubling, since they all have been supporting me and my ideas with a dedication that went far beyond the ordinary. It is, however, equally fantastic that I was received with the same spirit here at PSI and at Bern University.

Our laboratory is now part of the newly formed department BIO (biology and chemistry). Thanks to the excellent work of Heinz, I am now in the comfortable situation of taking over a smoothly running unit that is conducting internationally recognized research. This leaves me with the freedom to do what I like to do most, namely science! The laboratory will not see drastic changes in its research focus, but rather additions, which will integrate it even better into our new department. One such example will be a new group, which is a joint venture between the center for radiopharmaceutical science and our unit. The group will apply its radiochemical knowledge to the synthesis and development of new nuclides suitable for diagnosis and therapy in nuclear medicine. This lies in line with developments at the Insel Hospital of Bern University, where a cyclotron will be installed in a new building containing lab space dedicated to the production of novel radiopharmaceuticals. The new group will be headed by Konstantin Zhernosekov, one of my former group leaders in Munich and renowned specialist in the field.

Two promotions are the result of the excellent work that is being accomplished at our laboratory. My deputy Margit Schwikowski has been awarded the title of titular professor by Bern University for her outstanding contributions to paleo-climate science. Sönke Szidat obtained his "venia legendii" and, even more important, a permanent position as docent at Bern University. Both, Margit and Sönke are now allowed to accept and supervise PhD students.

Our annual report summarizes the so far unpublished scientific results of ongoing research in our unit. Again, some of our results ended up in high ranking journals, such as work performed by the Radwaste Analytics group of Dorothea Schumann, which led them to become co-authors of two Physical Review Letter publications.

A social event allowed us to get acquainted outside of work. Heinz had organized an impressive two day excursion to the Puschlav, a region of Switzerland he is especially fond of. On the first day we visited the rapidly retreating Morteratsch glacier. After a night at the Saoseo hut, a quite strenuous but rewarding hike took us to Livigno in Italy.

It is now my duty to take over Heinz`s responsibilities and to thank him for the long years of service that have resulted in the formation of this outstanding unit. The torch has now been passed on and I will do my best to carry on in his spirit, while Heinz enjoys his well deserved retirement. Retirement? Heinz is busier than ever, but exclusively with things he likes to do, things like science!

Andreas Türler

NEW ATTEMPT TO CHEMICALLY INVESTIGATE ^{283}112 AND ^{287}114

R. Eichler (Univ. Bern & PSI) for the PSI – Univ. Bern – FLNR – ITE collaboration

Three experiments were carried out at varied conditions to chemically identify ^{283}112 and ^{287}114.

The adsorption of elements 112 and 114 on gold surfaces was observed in our previous experiments [1-3]. Using the nuclear reaction of ^{48}Ca with ^{242}Pu we produced ^{287}114 ($T_{1/2}$~0.5 s), which decays by alpha decay to ^{283}112 ($T_{1/2}$~4 s) decaying further by alpha particle emission to the spontaneously fissioning (SF) ^{279}Ds ($T_{1/2}$~0.2 s). To improve the transport efficiency for short-lived isotopes the irradiation channel at FLNR was rebuilt and a new experimental platform was installed. Thus a transport time from the target to the COLD detector of 0.8 s was achieved. Two $^{242}PuO_2$ targets of 0.9 mg/cm^2 (A) and 1.4 mg/cm^2 (B) (^{242}Pu) have been prepared by the painting technique on Rh metal foil of 1.7 µm thickness. This target was irradiated in three separate experiments in the stationary target assembly as shown in [4]. The recoiling nuclear reaction products are thermalized in the recoil volume in pure argon carrier gas flowing at 2 l/min. Subsequently, they had to pass through the aerosol filter and getter oven held at 850°C (see Fig. 1). The products were further separated according to their adsorption properties on gold by a gold containing trap (see Fig. 2). Only quite inert reaction products reach the COLD thermochromatography detector described in [1-3].

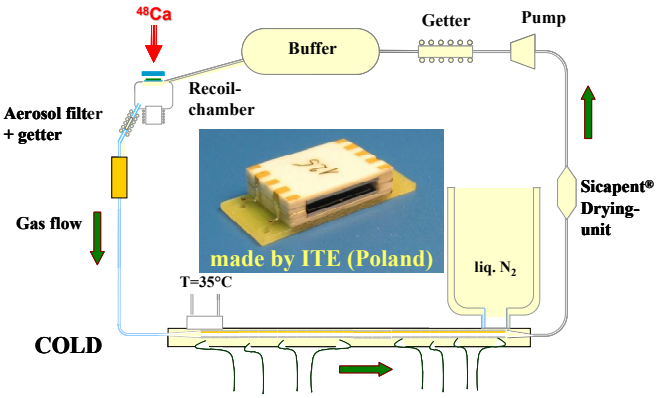

Fig. 1: The experimental setup. Note the difference to the experiments described in [1-3]: shortened transport time, the gold trap (yellow box) and the target backing material.

Fig. 2: The Gold trap.

Experiment 1: Target (A) was mounted with the target material facing the beam. Nuclear fusion reaction products recoil through the target material and the Rh backing foil. The ^{48}Ca beam was delivered from the U400 cyclotron with an energy of 270 MeV yielding a center of target energy (E_{cot}) of 237 MeV. In 11 days a total of $2.6 \cdot 10^{18}$ ^{48}Ca particles have been accumulated on the target. The gold trap was held at ambient temperatures between 5-12 °C.
Experiment 2: Target (A) was mounted with the target backing facing the beam. Nuclear fusion reaction products recoil through the target material only. The ^{48}Ca beam energy was 303 MeV (E_{cot} = 235 MeV). In 14 days a total of $3.4 \cdot 10^{18}$ ^{48}Ca particles have been accumulated. The gold trap was held at ambient temperatures between 10-15°C.
Experiment 3: Target (B) was installed as in Experiment 2. In 18 days a total of $5.3 \cdot 10^{18}$ ^{48}Ca particles (E_{cot} =242 MeV) have been applied. The gold trap was heated up to 100°C.
Only one decay chain, that can be unambiguously attributed to the decay of ^{283}112 has been observed (see Fig. 3) in Experiment 3 at an expected number of $6 \cdot 10^{-3}$ events of random origin. The observed deposition temperature of -7°C fully confirms previous observations of element 112 adsorbing on gold.

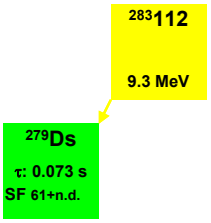

Fig. 3: The observed decay chain of ^{283}112.

The one event sensitivity limits for ^{287}114 were estimated in: Experiment 1: 2 pb; Experiment 2: 1 pb; Experiment 3: 0.7 pb. ^{283}112 could only be observed in Experiment 3, where the gold trap was heated to 100°C. Otherwise, ^{283}112 was completely retarded by the gold trap, according to its adsorption properties on gold. The cross section estimated from the observation of 1 event of ^{283}112 in Experiment 3 was 0.3 pb. The significantly lower yields for ^{283}112 and ^{287}114 measured in Experiment 3 can be explained so far only by one significant difference compared to previous experiments [1-3] – the use of pure Ar as carrier gas instead of an Ar/He mixture, assuming that the adsorption of elements 112 and 114 in the gold trap is unlikely. The heat load of 150 W (higher energy loss of the ^{48}Ca beam in pure Ar) and also the low thermal conductance of pure Ar lead to gas temperatures in the recoil volume estimated to be in the range between 600°C and 800°C. At these conditions up to a factor of 3 larger recoil ranges are expected for the nuclear fusion reaction products. The stopping volume was most probably a factor 1.5 too small. However, this hypothesis has to be confirmed by an in-situ temperature measurement in the recoil chamber.

REFERENCES

[1] R. Eichler et al., Nature **447**, 72-75 (2007).
[2] R. Eichler et al., Ang. Chem. Int. Ed. **47,** 3262 (2008).
[3] R. Eichler et al., Radiochim. Acta in press.
[4] R. Eichler et al., this report, p. 8.

BEAM INDUCED AEROSOL PRODUCTION IN HEAVY ION EXPERIMENTS PART I: VERY SHORT LIVED α-α CORRELATIONS

R. Dressler, D. Piguet, A. Vögele (PSI), R. Eichler, A. Serov, D. Wittwer (Univ. Bern & PSI)

The transport of less volatile multi-nucleon transfer products to the COLD detector indicates a decreasing efficiency of the aerosol particle filter in our experimental set-up at high carrier gas flow rates.

The unambiguous detection of the decay chains of exotic elements is one of the most important prerequisites for the investigation of the chemical properties these elements. In the case of transactinide isotopes α-particles with energies between 8.5 MeV and 11.0 MeV are emitted and correlations between consecutive decays or detected spontaneous fission fragments must be identified on a high significance level.

In the course of our experiments [1-3] a very high chemical separation of multi-nucleon transfer products from the wanted isotopes of element 112 and 114 is achieved due to large differences in their volatilities. Only the light volatile elements e.g. At and Rn reach the thermochromatographic detector COLD due to a pure gas phase transport. Therefore, it was surprising that the overall count-rate in the region above 9.0 MeV is quite high under certain experimental conditions. Fig. 1 shows the sums of α–spectra over the first 26 detector pairs of the COLD using different transport gas flow rates. These spectra were obtained in experiments bombarding ^{244}Pu with ^{48}Ca [2, 3]. The reaction products were swept out of the recoil chamber using a He/Ar gas mixture 50/50 vol.% with a flow rate of either 1.50 l/min (green line) or 1.85 l/min (blue line) at very dry conditions (water dew point of the transport gas less than -96°C). The region between 8.85 MeV and 9.50 MeV is dominated by β-α pile-up events from the consecutive decay of ^{212}Bi and ^{212}Po. The events above 9.5 MeV must originate from α-α pile-up events of very short-lived isotopes with half-lives less than 1 ms not resolved by the spectroscopic electronics applied. This observation prevented experiments at gas flow rates above 1.50 l/min [2].

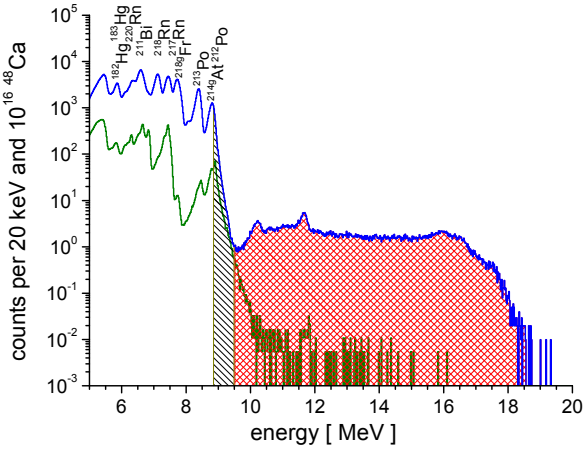

Fig. 1: Sum of spectra of the COLD in the ^{48}Ca on ^{244}Pu reaction taken at flow rates of 1500 ml/min (green) and 1850 ml/min (blue). The β-α pile-up region (yellow) and the α-α pile-up region (red) are indicated.

The final assignment of the observed events is based on an analysis of short time α-α correlations. Fig. 2 depicts a two-dimensional plot of all α-events coincidently detected in detectors facing each other. The effective time window to register such events is about 25 µs. Within this time the acknowledged event is processed by the data acquisition system and the CAMAC-ADCs are inhibited to accept further events. The minimum time required for readout of the measurement electronics is at least 185 µs or longer in dependence of the number of involved ADC's.

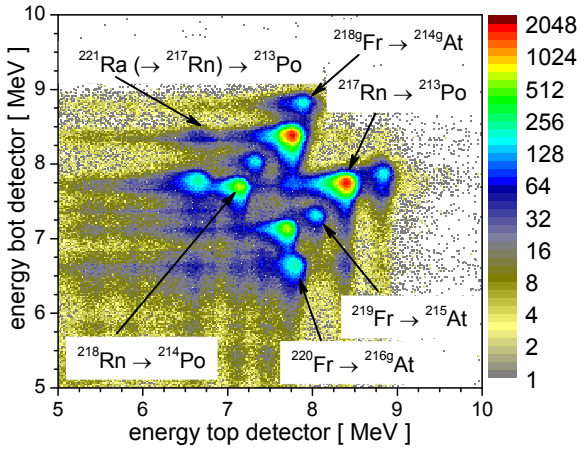

Fig. 2: Correlation plot for an events occurring within less than 25 µs in the same detector pair of COLD.

The consecutive decays of ^{217}Rn, ^{218}Rn, ^{218}Fr, ^{219}Fr, and ^{220}Fr and their daughter isotopes are clearly visible. These isotopes (with exception of ^{220}Fr) exhibit too short half-lives for a direct transport to the detector in the measured amounts even at 1.85 l/min. Therefore, they must be transported in the state of their precursors, e.g. ^{221}Ra, ^{222}Ra, ^{222}Ac, and ^{223}Ac. However, neither Ra nor Ac can be transported efficiently to the COLD without aerosols. Hence, a certain amount of aerosols are able to pass the aerosol filter of the setup consisting of a quartz tube filled with a tantalum roll and by a quartz-wool plug kept at 850°C. We expect that the formation of aerosols is a common feature of experiments where pure very dry inert-gases are used to transport volatile nuclear reaction products. Their efficient separation and monitoring using the method discussed above is a prerequisite for the determination of chemical properties of transactinide elements as demonstrated [1-3]

REFERENCES

[1] R. Eichler, et al., Nature **447**, 72 (2007).
[2] R. Eichler, et al., Ang. Chem. Int. Ed **47**, 3262 (2008).
[3] R. Eichler, et al., Radiochim. Acta, in press.

BEAM INDUCED AEROSOL PRODUCTION IN HEAVY ION EXPERIMENTS PART II: TIME DEPENDENCE OF OVERALL COUNT RATE

R. Dressler, D. Piguet, A. Vögele (PSI), R. Eichler, A. Serov, D. Wittwer (Univ. Bern & PSI)

Part I of this report [1] discusses the observation of the transport and detection of non volatile At, Fr, Ra, and Ac isotopes from the recoil chamber to the COLD system under certain experimental conditions. An experiment performed at FLNR (Dubna) in 2009 was aimed at the investigation of chemical properties of element 114 produced using the ^{48}Ca on ^{242}Pu reaction. For details regarding this experiment see [2,3].

Here, we discuss experimental conditions at which an efficient production and transport of aerosols within the experimental setup was observed reproducibly. A typical time schedule for a warm-up cycle of COLD represents the following:

1. 10.5. 2009/02:05→ beam off
2. 03:27 → warm up COLD
3. 03:48 → dew point behind COLD increases
4. 03:58 → dew point maximum of -54°C
5. 04:19 → dew point at -100°C
6. 07:35 → cool down COLD
7. 09:00 → temperature gradient established
8. 10:44 → beam on target; start run 170
9. 14:00 → no beam on target
10. 17:03 → stop run 170; start run 171
11. 11.05.2009/01.04 → stop run 171

Fig. 1 shows the beam current and the overall count rate of two consecutive runs #170 and #171 (both performed at the 10.05.2009). The overall count rate in run 170 is obviously much higher and the response to beam current variation is not as immediate as in run 171.

This behavior can be explained assuming the following:

1. During the warm-up phase of the COLD system the water content accumulated frozen on the detectors held at temperatures below the dew point is remobilized and partially deposits on the dry surfaces of the whole loop.
2. In the following time the water remaining in the transport gas is removed by the drying units until a dew point of less then -100°C is reached. Water adsorbed on very dry surfaces will only slowly be remobilized and therefore stays mainly on these surfaces, especially in the recoil chamber.
3. After the cool down of the COLD system the detector itself acts as water trap and decreases further the dew point. This is not recognized by the dew point meters that have detection limits of -100°C.
4. The incoming beam heats up the beam dump, the recoil chamber and the transport gas. The gas will reach temperatures in the range between 600°C and 800°C [2]. At these temperatures the adsorbed water will be released and forms aerosols in addition to the material sputtered of the Cu beam dump.
5. These aerosols are only partially retained by the IVO oven and carry non-volatile reaction by-products to the COLD which strongly increase the overall count rate as well as the α-α pile-up rate.
6. After about 50 min this effect disappears and the generation of aerosols stops. The overall count rate drops down according to the half-live of the accumulate reaction products.
7. After about five hours stable conditions with a minimum of aerosols and transported reaction by-products are reached.

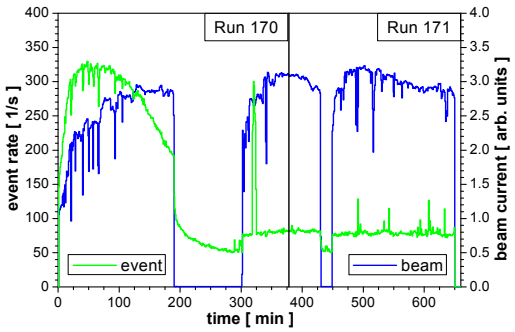

Fig. 1: Beam current and overall count rate in COLD during the runs 170 and 171 (experimental details see [2], Experiment 3).

We expect that the formation of aerosols is a common feature of experiments where pure, very dry inert gases in combination with cryo-detectors are used to transport and detect volatile nuclear reaction products. The monitoring of such effects and the documentation of their amount in experiments performed at a few pb level sensitivities are crucial to bolster the interpretation of the obtained data. Only data form experiments, where such transport effects can be excludes are legible to chemical interpretations. Therefore, the experimental runs where such transport phenomena were observed have been excluded from chemical data analysis.

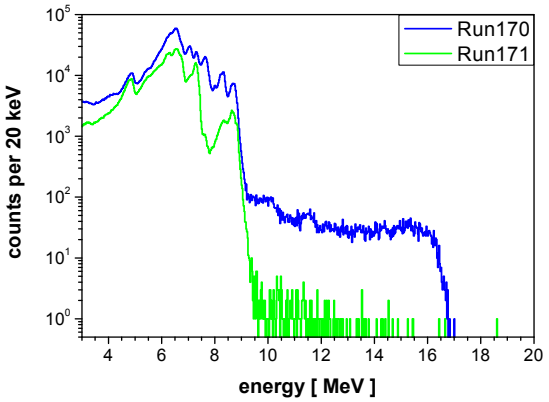

Fig. 2: Sums of α-spectra of the first 24 detector pairs in consecutive run 170 and 171 (experimental details see [2]).

REFERENCES

[1] R. Dressler et al., this annual report, p. 4.
[2] R. Eichler et al., this annual report, p. 3.
[3] R. Eichler et al., Radiochim. Acta, in press.

ADSORPTION INTERACTION OF ^{125}Sb ISOTOPES WITH QUARTZ

A. Serov, R. Eichler, A. Vögele, H.W. Gäggeler (Univ. Bern & PSI)

Antimony-125 was prepared by thermal and epithermal neutron activation of natural tin. Their adsorption properties on quartz were investigated by thermochromatography.

INTRODUCTION

Presently several newly synthesized elements are successfully added to the periodic table of elements. This was possible due to significant efforts in improving production techniques (accelerators, ion sources, new target-projectile combinations, and new target setups) as well as developing new detection systems. Up to now the elements with atomic numbers up to 118 were produced and physically characterized [1]. Only a limited number of methods are available for studying the chemical behaviour of SHE and their lighter analogues on an one-atom-at-a-time basis: Liquid phase –, gas-phase – and electrochemical methods [2]. Here, we report on gas-phase thermochromatographic investigations of the adsorption interaction of carrier-free ^{125}Sb as a homologue of element 115 with quartz surfaces. For the first time deposition temperatures of Sb-hydroxide on a quartz surface were obtained, whereas the deposition of Sb in the elemental state was confirming available literature data.

EXPERIMENTAL

An isotope of antimony, ^{125}Sb ($T_{1/2}$=2.7582 y), which serves as a lighter homologue of element 115, can be prepared by neutron irradiation of natural metallic tin. For that purpose 0.5g of ^{nat}Sn were irradiated at the neutron activation facility (SINQ-NAA) at Paul Scherrer Institute for 2 h at a neutron flux of 10^{13} s^{-1} cm^{-2}. The analysis of the gamma spectra from neutron irradiated ^{nat}Sn shows that the isotopes produced are mainly ^{113}Sn, ^{113m}In, ^{111}In, ^{117m}Sn, ^{122}Sb, and ^{125}Sb (**Fig. 1**). The presence of ^{111}In and ^{122}Sb can be ex-plained by macroscopic amounts of In and Sb in the initial metallic tin sample. Such irradiated samples can be directly used for experiments with carrier-added amounts of antimony.

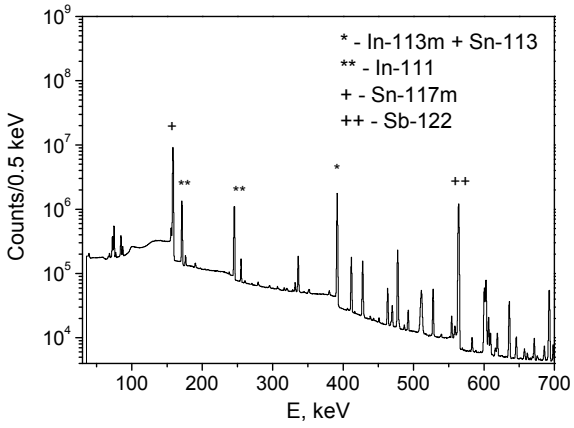

Fig. 1: Gamma spectrum of irradiated ^{nat}Sn.

RESULTS AND CONCLUSIONS

The interaction of antimony species with quartz surfaces was investigated using highly purified carrier gases to exclude trace amounts of water and oxygen. The entire thermochromatography column was encapsulated in a steel tube. The carrier gas had to pass a Ta getter (1000°C) before hitting the antimony source heated up to 1300°C. The reproducibility of the obtained data was ensured by several repetitions of the same experiment at the same conditions. A Monte-Carlo simulation approach [3] was applied to deduce the standard adsorption enthalpy of the antimony species at zero surface coverage on quartz surfaces (ΔH_{ads}^{SiO2}(SbX)) from the thermochromatograms shown in (**Fig**. **2**).

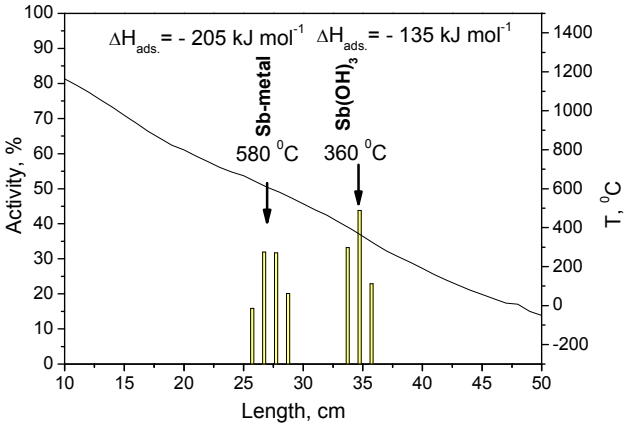

Fig. 2: Thermochromatogram of ^{125}Sb and ^{125}Sb(OH)$_3$ in a quartz column (carrier gas H_2, 15 ml·min^{-1}).

It was observed that carrier-free, metallic Sb is volatile with deposition temperatures on the quartz surface of $T_{dep.}$=580±10 ºC (ΔH_{ads} = -205 kJ·mol^{-1}) whereas Sb(OH)$_3$ is deposited at $T_{dep.}$=360±10 ºC (ΔH_{ads} = -135 kJ·mol^{-1}). The data obtained in this investigation for elemental antimony are in good agreement with previously obtained adsorption data [4]. For the first time adsorption interaction of Sb(OH)$_3$ with a quartz surface was investigated. Form the correlation established between ΔH_{ads} and ΔH_{subl} shown in [5] the sublimation enthalpy of Sb(OH)$_3$ could be estimated as 183 kJ·mol^{-1} for the first time.

ACKNOWLEDGEMENT

Authors kindly appreciate the financial support by SNF.

REFERENCES

[1] Yu. Ts. Oganessian et al., J. Phys. **G 34,** R165-R242 (2007).
[2] M. Schädel, Angew.Chem. Int. Ed. **45,** 368 (2006).
[3] I. Zvara, Radiochim. Acta. **38,** 95 (1983).
[4] B. Eichler, JINR-Dubna report **P12-6662,** 3 (1972).
[5] A. Serov et al., this report, p. 7.

ADSORPTION INTERACTION OF CARRIER-FREE $^{125m}TeO_2$ WITH QUARTZ

A. Serov, R. Eichler, H.W. Gäggeler (Univ. Bern & PSI)

Tellurium-125 was prepared by neutron activation of natural tin. Adsorption properties of $^{125m}TeO_2$ on quartz were investigated by thermochromatography.

INTRODUCTION

Transactinide elements, artificially produced in heavy-ion-induced nuclear fusion reactions, are well known since several decades. During this period a significant efforts allowed researchers to synthesize and to identify new elements with Z up to 118 [1]. Nowadays, in chemical investigations of tansactinides mainly techniques based on the following three separation methods are applied: 1) gas/vacuum adsorption thermochromatography or isothermal chromatography, 2) liquid phase ion-exchange and extraction chromatographic methods and 3) electrochemical deposition methods [2]. We report here on gas-phase adsorption thermochromatographic investigations of no carrier added ^{125m}Te species as a homologue of element 116 in quartz columns.

EXPERIMENTAL

Lighter homologue of element 116, ^{125m}Te ($T_{1/2}$=57.49 d) can be prepared by neutron irradiation of natural metallic tin. For that purposes 0.5g of ^{nat}Sn were irradiated at the neutron activation facility (SINQ-NAA) at Paul Scherrer Institute for 2 h at a neutron flux of 10^{13} s^{-1} cm^{-2}. Produced during this irradiation ^{125}Sb decays into isotope of interest – ^{125m}Te. Such irradiated sample can be directly used for experiments with carrier-free tellurium species. The thermochromatographic setup used in [3] was applied. The interaction of tellurium species with quartz surface was investigated using 25 ml/min pure oxygen as a carrier gas. The entire thermochromatography column was encapsulated in a steel tube. The dry irradiated tin sample serving as ^{125m}Te source was heated up to 1300°C. Reproducibility of obtained data was achieved by several repetition of experiment at the same conditions.

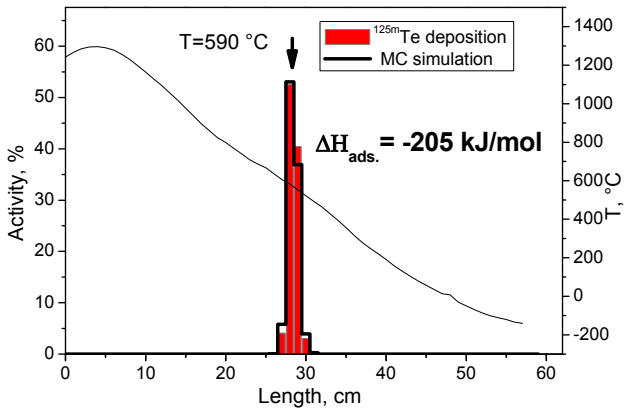

Fig. 1: Thermochromatogram of $^{125m}TeO_2$ on quartz surface.

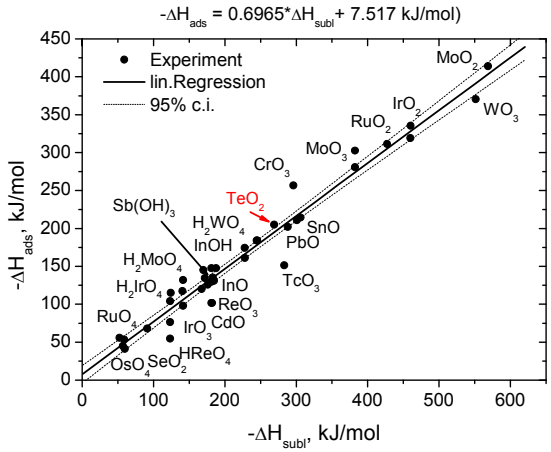

Fig. 2: Correlation of the molecular property adsorption enthalpy ΔH^o_{ads} of oxygen containing species on quartz with their macroscopic property sublimation enthalpy ΔH^o_{subl} [6].

RESULTS AND CONCLUSIONS

From the measured thermochromatographic deposition pattern the standard adsorption enthalpy of TeO_2 on quartz at zero surface coverage ($\Delta H_{ads}^{SiO2}(TeO_2)$) Was deduced using the Monte-Carlo simulation approach [4] (see Fig. 1).

It was observed that carrier-free TeO_2 is deposited at $T_{dep.}$ = 590 ± 20 ^{0}C (ΔH_{ads} = - 205 kJ mol^{-1}). To validate the suggested speciation of the observed TeO_2 depositions the correlation between macroscopic (ΔH_{subl}) and microscopic (ΔH_{ads}) properties were used (Fig. 2). The sublimation data for TeO_2 [5] (ΔH_{subl}=269 kJ/mol) fit this correlation well.

ACKNOWLEDGEMENT

Authors kindly appreciate the financial support by SNF.

REFERENCES

[1] Yu. Ts. Oganessian et al., J. Phys. **G 34,** R165-R242 (2007).
[2] M. Schädel, Angew.Chem. Int. Ed. **45,** 368 (2006).
[3] A. Serov et al., this report, p. 6.
[4] I. Zvara, Radiochim. Acta 38. 95 (1983).
[5] T.S. Lakshmi Narasimhan et al. Thermochim. Acta **427,** 137 (2005).
[6] B. Eichler et al., in *Chemistry of Superheavy Elements.* (ed. M. Schädel) Kluwer Academic Publishers, Dodrecht, 2003**,** p. 205.

A NOVEL TARGET SETUP BASED ON Rh AS TARGET BACKING MATERIAL

R. Eichler (Univ. Bern & PSI) for the PSI-Univ. Bern-FLNR-ITE collaboration

Experiences with thick stationary $^{244}PuO_2$ targets based on Ti and Rh backings are reported. The results clearly demonstrate that action is needed regarding high power production target development for SHE research.

The increasing heavy ion beam intensities nowadays available at particle accelerators represent a challenge for the development of suitable target technologies. We report here on the use of high melting noble metals as backing materials for heavy ion targets. The performance of these targets is compared with the performance achieved by the "classical" targets based on thin Ti target backings. During the experiments aimed at the chemical investigation of elements 112 and 114 long-term heavy duty irradiations of plutonium targets mounted in stationary target assemblies (see Figure 1) have been performed.

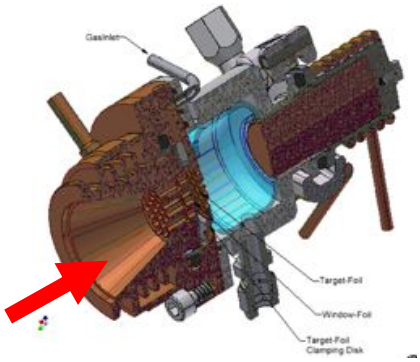

Fig. 1: Cartoon of the water-cooled collimator–target–recoil chamber–beam stop assembly as used for the described experiments (red arrow – incoming beam).

The target assembly consisted of a water-cooled copper collimator with a honeycomb grid having 80% geometrical transmission. The stationary vacuum window was a titanium foil with a thickness of 4 µm mounted on a Ti grid with the same geometry as the collimator grid. Finally, the target foil was mounted onto a third copper grid of same geometry. The target material $^{242}PuO_2$ was painted as a 0.9-1.4 mg/cm^2 circle with 1.8 cm diameter onto the respective backing foil. Backing foils made of Ti (thickness 1.5 µm) and of Rh (1.7 µm) with 2x2 cm^2 size were used. The target foils were mounted with the target material facing the incoming beam onto the copper cooling grid. Assuming a thermal load due to the ^{48}Ca beam (0.8 pµA, 270 MeV) of about 200 W onto the collimator grid and about 40 W on the Ti entrance window foil (energy deposition of ^{48}Ca in Ti is about 24 MeV) a finite-element calculation yielded the highest temperature in the centers of the honeycomb grid openings of about 1328°C (see Fig.2). At the experimental conditions the Ti vacuum window withstood a beam dose of >3*10^{18} particles without leaking. So far no calculations exist of the target temperatures at these conditions. The ^{48}Ca beam deposits an energy of 9 MeV in the Ti-backing, i.e. a thermal load of 16 W. In the case of the Rh-backing the energy release is 22 MeV or 37 W. A maximum target temperature below the melting point of Ti can be assumed.

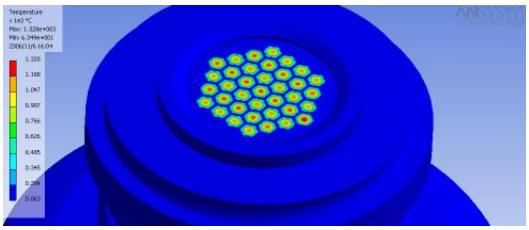

Fig. 2: Results of a finite element calculation of the thermal load in the Ti vacuum window.

However, the destruction of the targets was considerable. Typically the Ti based targets were destroyed at overall ^{48}Ca doses of 1·10^{18} particles (see Fig. 3 (1)). A chemical reaction of Ti with the PuO_2 has to be considered leading to the destruction of the Ti backing.

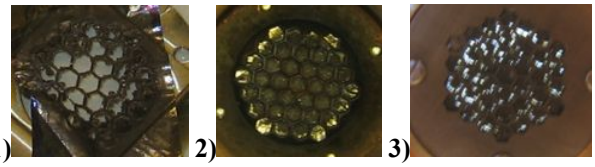

Fig. 3: The targets after irradiation.
1) 1·10^{18} ^{48}Ca particles were passed through the Ti-backing based target; 2) 1·10^{18} ^{48}Ca particles passed through the Rh-based structure. 3) Rh-based structure after 6·10^{18} ^{48}Ca particles passed through (back light photo).

The Rh-based structure irradiated with 1·10^{18} particles looked almost like before the irradiation. After passing 6·10^{18} particles also the Rh backing revealed severe damage. The degradation of the target material on the Rh target was monitored directly through the production yield of ^{185}Hg produced in the reaction of ^{nat}Nd(^{48}Ca,5n)^{185}Hg from a thin (50µg/cm^2) natural neodymium layer situated in the middle of the target material (see Fig. 4). Other effects, e.g., stopping range changes for ^{185}Hg due to the target degradation, are not included in this analysis. A Rh based structure can safely be operated using the shown stationary target assembly until an overall beam dose of 3·10^{18} ^{48}Ca particles at ^{48}Ca beam intensities of 0.8 pµA have been accumulated.

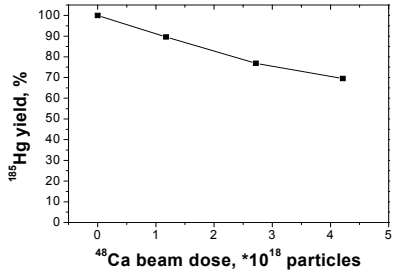

Fig. 4: The ^{185}Hg yield dependent on applied beam dose.

LANTHANIDE TARGET PREPARATION ON NOBLE METAL BACKINGS

D. Wittwer, P. Steinegger, R. Eichler, A. Türler (Univ. Bern & PSI), R. Dressler (PSI)

A method to efficiently produce a rare earth - noble metal compound as high power heavy ion target is under development. A model study for the preparation of a new type of actinide targets for the production of super heavy elements is presented.

Chemical investigations of the so called superheavy elements (Z>110) require producing neutron-rich, long-lived nuclei applying heavy ion induced nuclear fusion reactions based on the use of actinide targets. These investigations face the problem of decreasing production cross-sections with increasing Z. Both circumstances require the further development of particle accelerators. Nowadays, increasing beam intensities by a factor of two up to an order of magnitude compared to available beams are discussed. These increased beam intensities will certainly help working with low production cross-sections, but open up the new challenge of high power target preparation. The targets used nowadays are not capable of withstanding these beam intensities promised for the near future. The techniques used for target preparation are electrochemical deposition, evaporation, spin-coating or just simply painting of actinide compounds onto conducting backing foil (Al, C, Be, Ti). The targets prepared by these methods and also the backing foils reveal mostly mechanical or thermal instability against increasing intensity. Heats and charges induced by the beam cannot be distributed, leading to a destruction of the targets. Therefore, in terms of thermodynamic stability as well as the thermal and electrical conductivity, high melting noble metal (Ru, Rh, Pd, Pt) – actinide alloys were suggested to be a promising choice towards higher power target technology [1,2]. This alloy formation was investigated using coupled reduction of actinide oxides with highly purified hydrogen gas in contact with noble metals [3,4]. Another way to produce the alloy is via amalgamation [5].

First experiments were conducted by using rare earth metals as model elements for actinides. To find out which noble metal fits best as a host for the rare earth target material the enthalpies of solid solution at infinite dilution were calculated using the semi-empirical macroscopic model by Miedema [6]. All high melting noble metals appear to be suitable. The initial materials used were europium oxide and platinum. To monitor the reaction yields during the experiments an ^{152}Eu tracer in form of $^{152}Eu(NO_3)_3$ was added. The Eu_2O_3 was converted to the nitrate by dissolution in concentrated HNO_3 and the formed europium nitrate was obtained after evaporation to dryness. In a classical alkaliothermic approach a melt of either metallic lithium or sodium was used to reduce the europium to its metallic state in-situ prior to its reaction with the noble metal. Therefore, the $Eu(NO_3)_3$ together with the alkali metal and the noble metal foil were heated up at vacuum conditions (10^{-4} mbar) in a tantalum crucible to the melting point of the alkali metal and kept for few minutes up to an hour at this temperature. In this phase the reduction of the Eu took place. Subsequently, the crucible was heated up to 1450°C and kept for several hours to accelerate the diffusion of the Eu into the noble metal foil. From the very first experiments a further task turned out to be the selection of the appropriate alkali depending on its reactivity with the noble metal backing foil. Empirically, it was established that the enthalpy of solid solution of the alkali metal in the noble metal (see Figure 1) should not be lower than -50 kJ/mol. Otherwise, the foil was partly destroyed by the alkali metal. If this enthalpy is larger than zero, no alloy formation was observed at all. Therefore, it can be assumed that the reaction of the alkali element with the surface of the noble metal promotes the transfer of the lanthanide into the surface of the noble metal.

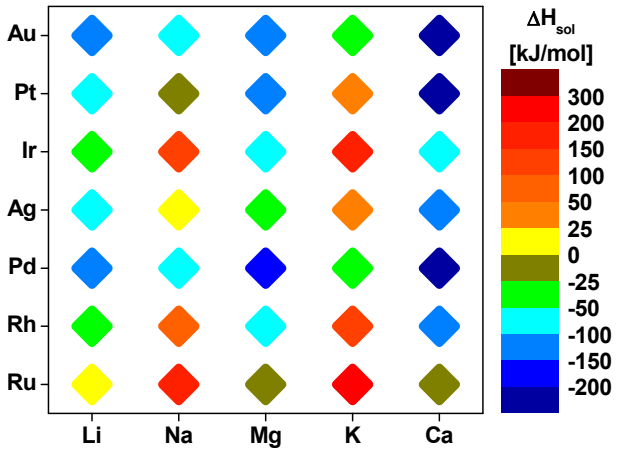

Fig. 1: The enthalpies of solid solution of: Li, Na, K, Mg, and Ca in the noble metals: Ru, Rh, Pd, Ag, Ir, Pt, and Au at infinite dilution.

The final product foil was cleaned with water, diluted HCl and concentrated HCl as well as concentrated HNO_3 to remove traces of not reacted lanthanide and alkali oxide and to test the chemical or thermodynamic stability of the product. The leaching was monitored by γ-spectrometric measurements of the foil after each leaching step and stored for further analysis.

So far several promising Pt - Eu foils were produced using Li as reagent and a Pd - Eu foil using Na as reagent. The final lanthanide content in the noble metal could not be leached out, even not by concentrated HCl or HNO_3 pointing to a high stability of the formed product. The distribution of the lanthanide in the noble metal foil samples will be further analyzed using REM-EDX. Later on the process will be optimized for high yields.

REFERENCES

[1] R. Eichler, NRC6 conference, Aachen 2004.
[2] R. Eichler, this report, p. 8.
[3] B. Erdmann, C. Keller, Inorg. Nucl. Chem. Letters, **7**, 675 (1971).
[4] B. Erdmann, C. Keller, J. Solid State Chem., **7**, 40 (1973).
[5] C. Guminski, J. of Material. Sci., **24**, 2661 (1989).
[6] A. R. Miedema, J. Less-Common Met., **45**, 237 (1976).

ISOTHERMAL VACUUM CHROMATOGRAPHY OF ^{211}Pb ON QUARTZ

R. Eichler, A. Serov, D. Wittwer (Univ. Bern & PSI), R. Dressler, D. Piguet (PSI)

The adsorption behavior of lead on fused silica quartz surfaces is revisited.

The investigation of adsorption enthalpies at zero surface coverage of lead on quartz ($-\Delta H_{ads}^{SiO2}$(Pb)) yielded wide spread results: from theoretically calculated 27.34 kJ/mol [1] up to experimentally determined values between 135 kJ/mol [2] and 222 kJ/mol [3]. The problem with the experimental investigation of lead at carrier-free amounts is the likely content of "macroscopic" amounts of lead (>1 ppt) from simple sample handling. A new Isothermal VAcuum Chromatography apparatus (IVAC) was developed at PSI [4] (see Fig. 1). This system consists of a source oven, which can be heated up to 1400°C; an isothermal chromatographic oven operational between 50°C and 950°C; and a detection unit with a PIPS α–detector.

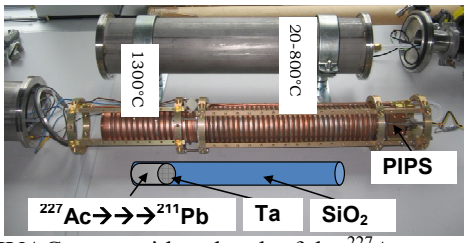

Fig. 1: IVAC setup with a sketch of the ^{227}Ac source.

An ^{227}Ac source was prepared from a nitric acid solution dried in a tubular Ta crucible and heated up in vacuum to 1400°C. This source was placed into a quartz column one side of which was closed. This column (see Fig 1, sketch) was placed into the oven array of IVAC. The ^{227}Ac source was positioned in the middle of the source oven. The entire system was evacuated to a pressure of $2\cdot10^{-6}$ mbar. ^{219}Rn emanates permanently from the source and travels chromatographically through the column. By chance it is decaying in-flight. Therefore, on the PIPS alpha detector installed opposite to the column exit a low background rate of ^{211}Bi at equilibrium conditions is measured which is a factor of 400 below the activity maximum measured. The source oven was heated up within 30 min to 1300°C to reproducibly volatilize the entire equilibrium ^{211}Pb/^{211}Bi activity from the ^{227}Ac/Ta source. Thus these atoms start their chromatography with several hits to a very hot Ta surface leading to their elemental atomic state. The high temperatures secured the injection of the entire amount of ^{211}Pb/^{211}Bi into the isothermal part of the setup. The equilibrium temperature distribution in the column and the equilibration of the ^{211}Pb (T_{05}=36 min) amount in the source was obtained within ~12 h between consecutive experiments. The real temperatures along the "isothermal" part of the column are shown in Fig 2. The consecutive experiments were performed at temperatures as shown in Fig. 3 (upper panel) to eventually reveal hysteresis-like adsorption effects. After the experiment the ovens are shut down and after a 30 min oven cooling time, where the initial ^{211}Bi($T_{0.5}$=2 min) decays, the ^{211}Pb deposited on the surface of the detector is measured indirectly via ^{211}Bi(α) without breaking the vacuum. The system was never opened in between the experiments to avoid any contamination with macroscopic amounts of lead.

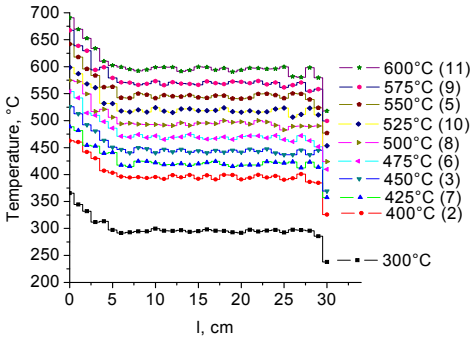

Fig. 2: Temperature distribution along the 30 cm quartz column having installed the nominal isothermal temperature in the "isothermal" oven (N_{Exp}) as shown in the legend.

The external chromatogram, i.e. the measured ^{211}Pb yield dependening on the nominal isothermal temperature of the quartz surface is shown in Fig. 3. From the chromatogram the adsorption enthalpy of Pb on quartz was deduced using the Monte Carlo simulation of vacuum chromatography adopted from [5] as $-\Delta H_{ads}^{SiO2}$(Pb)= 173±5 kJ/mol. In the Monte-Carlo simulations the real temperatures inside the columns (Fig 2) have been used. The experimental design of this study guarantees the investigation of the adsorption properties of lead at real carrier free single atom conditions. The theoretical calculations seem to underestimate the reversible chemical adsorption of lead on quartz that energetically predominates the physisorption process assumed in [1]. Investigations using Teflon as chromatographic surface will follow. These model investigations are also crucial for the design of future experiments investigating the behavior of super heavy elements at such conditions.

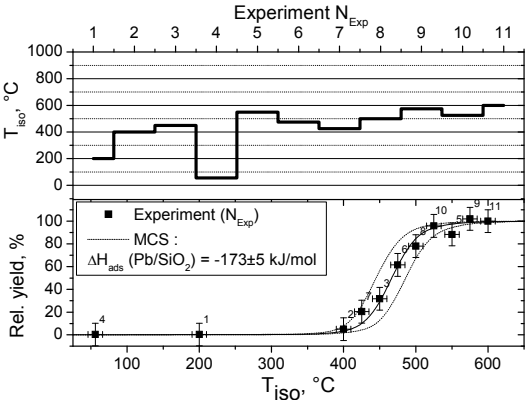

Fig. 3: External chromatogram of lead adsorption on quartz (lower panel). Consecutive temperature steps chosen during the experiments (N_{Exp})(upper panel).

REFERENCES

[1] V. Pershina et al., J. Chem. Phys, **128**, 024707 (2008).
[2] B. Eichler et al., ZFK Report **346,** (1977).
[3] W. Fan et al., Radiochim. Acta, **31,** 95 (1982).
[4] A. Serov et al., Ann. Rep. Lab. of Radio- and Environ. Chemistry, Uni Bern & PSI (2008), p. 4.
[5] R. Eichler et al., J. Phys. Chem B **106,** 1413(2002).

Th-228 CALIBRATION SOURCE FOR THE GERDA-EXPERIMENT PART I: REQUIREMENTS & SOURCE PREPARATION

L. Baudis, A.D. Ferella, F. Froborg, R. Santorelli, M. Tarka (Univ. Zurich), R. Dressler, R. Eichler, D. Schumann (PSI), G. Bruno, S. Fattori (Univ. L'Aquila), E. Bellotti (Univ. Milano Bicocca and INFN), C.M. Cattadori (INFN Milano Bicocca and Univ. Milano), U. Graf (Isotope Prod. GmbH Berlin)

The preparation of a ^{228}Th low neutron emitting calibration source meeting the background requirements of the GERDA experiment is presented.

Search experiments for neutrinoless double β-decay are sensitive probes to determine the fundamental properties of neutrinos. The questions whether or not neutrinos carry a mass or are distinguishable from there antiparticles are of particular interest. Among others, the decay of ^{76}Ge is of exceptional interest, due to the expected low upper limit of the deduced electron neutrino. One additional advantage is the possibility to build up high purity Ge (HPGe) detector crystals with enriched ^{76}Ge content. In this case the source material is incorporated into the detector itself leading to an enhanced sensitivity of the setup.

The GERDA-experiment (GERmanium Detector Array) [1-3] is using 8 ^{76}Ge enriched detector crystals (total mass 18 kg) during the experimental phase I. The envisaged sensitivity of the neutrino mass of less than 0.27 eV requires a minimized and well understood radiation background. Therefore, the experiment is installed at the LNGS (Laboratori Nazionali del Gran Sasso) underground laboratory in Italy. The muon flux drops down to about 1 event $m^{-2}\,h^{-1}$ at the place GERDA is set up due to the shielding of approximately 3500 m.w.e. against cosmic radiation at the LNGS. Additionally, special requirements for the used materials must be fulfilled to reach the desired γ-background rate of less than 10^{-2} cts kg^{-1} keV^{-1} $year^{-1}$. Neutrons from natural spontaneous fission sources and from neutron evaporation reactions induced by high energetic α-particles – so called (α, xn) reactions – must be taken into account in addition to the γ-background. In Fig. 1 the threshold energies (E_{thr}) for the (α, n) reaction of all isotopes of the 2003 mass evaluation [4] are depicted. Only 17 stable isotopes with $Z < 50$ exhibit $E_{thr} > 8.8$ MeV. In the case of $E_{thr} > 10.6$ MeV the isotopes ^{2}H, ^{3,4}He, ^{12}C, ^{16}O and ^{40}Ca remain.

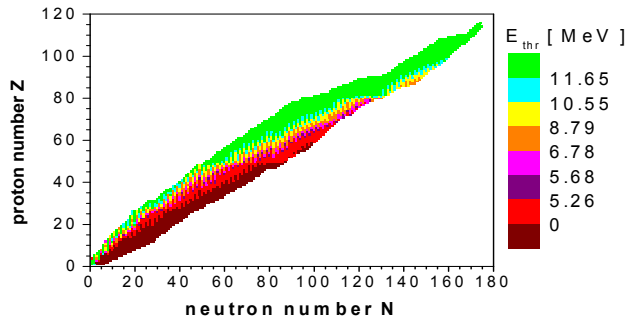

Fig. 1: Energy thresholds of (α, n) reactions for all isotopes of the 2003 mass evaluation [4]. The transition of the colour codes indicates the α-decay energies of ^{232}U, ^{224}Ra, ^{216}Po, ^{212}Po, ^{212}Bi (βα), and ^{212m2}Po in ascending order.

^{228}Th has been established as a good isotope for calibration sources in GERDA due to the γ-emissions from 0.073 MeV up to 2.615 MeV. Especially the single escape line of its progeny ^{208}Tl at 2.104 MeV in the region of interest around $Q_{ββ} = 2.04$ MeV, the energy release of the neutrinoless double β-decay, is highly important. In total three ^{228}Th sources (each with an activity of about 20 kBq) will be integrated in the phase I of the GERDA experimental setup and contribute permanently to the γ- and neutron background during the whole data taking period.

The chemical speciation as well as the container materials of the calibration sources must be chosen carefully particularly with regards to the use of ^{228}Th. α-particles with energies ranging from 5.34 MeV to 8.78 MeV are emitted during the whole decay chain of ^{228}Th. Apart from ^{212}Po, ^{212}Bi is able to produce high energetic α-particles of 10.55 MeV with an abundance of 0.026%. Therefore, the prevention of (α, xn) channels, populated in the encapsulating materials, is crucial. ThO_2 enclosed into an Au foil was suggested for a prototype source. This prototype was produced starting from a nominal ^{228}Th solution of 20 kBq delivered by Eckert & Ziegler Nuclitec GmbH. This solution contained in addition to Th about 10 μg Zr as carrier material in 1 M HCl solution. This initial solution is evaporated to dryness in a Teflon beaker. The residue is converted into the nitrate form by fuming several times with concentrated HNO_3. After this treatment, the residue is dissolved in a minimal volume of diluted HNO_3 and transferred into a crucible made out of 25 μm thick gold foil and evaporated to dryness. The procedure is repeated in order to avoid activity losses in the delivery vial as well as the Teflon beaker. Afterwards, the crucible is heated to 750°C in air to transfer the nitrates into oxides. Subsequently the gold crucible is folded to produce a closed encapsulation by gold. The overall process yield was close to 100%. Subsequently, this source was sealed into a P02 capsule. The sealing work, the tightness tests and the ISO C 11111 certification was performed by Eckert & Ziegler Nuclitec GmbH Prague. The final ^{228}Th source is shown in Fig. 2.

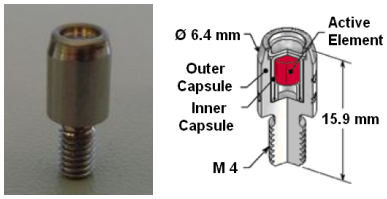

Fig. 2: The final ^{228}Th source enclosed in a P02 capsule.

REFERENCES

[1] A. Bettini, Nucl. Phys. B **168**, 67 (2007).
[2] V. A. Rodin et al., Nucl. Phys. A **366**, 107 (2006).
[3] V. A. Rodin et al., Nucl. Phys. A **793**, 213 (2007).
[4] G. Audi, et al., Nucl. Phys. A **729**, 337 (2003).

Th-228 CALIBRATION SOURCE FOR THE GERDA-EXPERIMENT PART II: RESULTS OF NEUTRON MEASURMENTS

L. Baudis, A.D. Ferella, F. Froborg, R. Santorelli, M. Tarka, (Univ. Zurich), R. Dressler, R. Eichler, D. Schumann (PSI), G. Bruno, S. Fattori (Univ. L'Aquila), E. Bellotti (Univ. Milano Bicocca and INFN), C.M. Cattadori (INFN Milano Bicocca and Univ. Milano), U. Graf (Isotope Prod. GmbH Berlin)

First measurements of a customized ^{228}Th source for the GERDA-experiment and MC-calculations to compare the neutron-flux with commercially available sources are discussed.

Part I of this report [1] discusses the experimental requirements and the preparation procedure of a prototype of a 20 kBq low neutron emitting ^{228}Th source.

A γ-spectrum taken with an HPGe detector at University Zürich confirms the high overall process yield of the source preparation. In order to estimate the total activity of the source after the treatment, a full Monte Carlo simulation of the HPGe detector has been carried out in the framework of GEANT4. In Fig. 1 the simulated spectrum (red) between 100 keV and 2.7 MeV is compared with the real data (black). The activity has been estimated in a χ^2-minimization of the fit of the data to the MC spectrum. The obtained value for the activity is (20.2 +/- 0.4) kBq, thus showing no significant losses compared to the initial nominal activity.

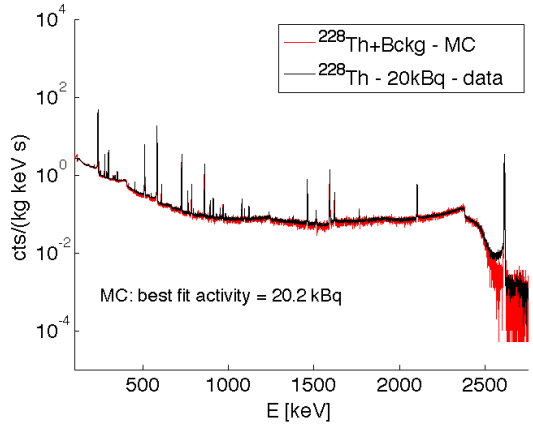

Fig. 1: Measured γ-spectrum of the prepared ^{228}Th source and MC-simulated spectrum.

Further, the significance of the neutron background from (α, xn) reactions induced by the emitted α-particles of ^{228}Th interacting with the intrinsic components of the calibration source was determined. For this scenario a parking position of the source inside a separate lock about 3.5 m above the detector array was assumed during data taking period. The source will be periodically moved down to the detector array for calibration purposes. Commercially available sources for cryogenic applications consist of porous $NaAlSiO_2$ ceramics saturated with a chloride solution of the used isotopes and sealed inside a stainless steel capsule. The performance of the prepared source prototype from [1] was compared with such a commercial source. The neutron flux can be calculated using the software package SOURCES4mv [2] knowing isotopic abundances for each chemical element in the source material. Such calculations lead to a neutron rate of 5.0×10^{-4} s^{-1} kBq^{-1} for the source prototype in contrast to 3.8×10^{-2} s^{-1} kBq^{-1} for a commercial source. These rates lead to a neutron background rate in the region from 1.5 MeV to 2.5 MeV of about 8.6×10^{-8} or 1×10^{-5} kg^{-1} keV^{-1} year^{-1} kBq^{-1}, respectively for both types of sources, detected in GERDA according to a GEANT4 based Monte Carlo (MC) simulation of the whole experimental setup. These calculations were confirmed experimentally for the prototype source using a ^{3}He neutron detector at LNGS. A moderator of 12.5 cm polyethylene was installed between the source and the ^{3}He counter to moderate the high energy neutrons produced in (α, n) reactions down to thermal energies. Fig. 1 shows the energy spectrum of a measurement lasting about 28 days live time. The total full energy efficiency for neutrons of the ^{3}He neutron detector used is 0.2%. The neutron rate was determined to be (0.017 ± 0.003) s^{-1} which is in reasonable agreement with the predicted value of 0.01 s^{-1} obtained from the MC-simulations. Contaminations of Zr and Fe in the ^{228}Th solution, which had not been taken into consideration in the calculations of the neutron flux, could explain the difference between the measured and the calculated rates. Additional measurements using the commercial ^{228}Th source are also planned to confirm the neutron-flux reduction achieved by using the prototype source.

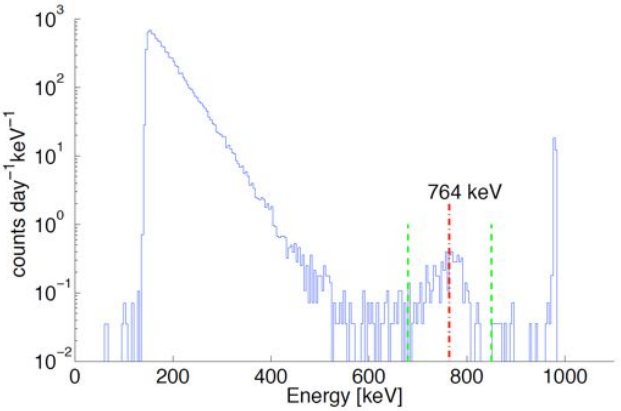

Fig. 2: The neutron spectrum of the 20 kBq ThO_2 prototype source with a ^{3}He counter at LNGS. Indicated is the region of the full energy peak for neutron detection around 764 keV.

REFERENCES

[1] L. Baudis et al., this report, p. 11.

[2] M. Tarka "Simulation of the (α, n)-induced Background in the CDMS-II Dark Matter Search Experiment" Univ. Zürich 2007.

PHOTOENHANCED NITROUS ACID FORMATION UPON NO_2 UPTAKE ON A GENTISIC ACID FILM

Y. Sosedova (Univ. Bern & PSI), A. Rouvière, M. Ammann, H.W. Gäggeler (PSI)

Increased nitrous acid (HONO) concentrations were detected in the gas phase at the exit of a flow tube coated with gentisic acid and being in contact with gaseous nitrogen dioxide (NO_2) upon irradiation with UV light. Under visible light irradiation enhancement of HONO production occurred only when a photosensitizer was added to the coating.

INTRODUCTION

The heterogeneous chemistry of NO_2 is a potential source of reactive intermediates such as HONO. Hydroxy and methoxy substituted phenols may play a significant role in the aqueous-phase chemistry occurring on the ground or within aerosol particles in air masses affected by biomass burning. It is well established that electron transfer between phenols and NO_2 in alkaline aqueous solutions is fast (k_2 ~10^7 - 10^9 mole $L^{-1}s^{-1}$) and could be a source of nitrite in the aqueous phase and HONO in the gas phase. However its kinetics is very slow under atmospheric conditions. The role of phenolic species as electron donors has also been suspected to be responsible for the photoenhanced transformation of NO_2 to HONO over humic acids [1]. In this study we used gentisic acid (GA) as another proxy for atmospheric phenolic compounds.

EXPERIMENTAL

The experiments were performed in a horizontal coated wall flow tube (40 cm × 5.9 cm i.d.) at ambient pressure. 7 fluorescence lamps (Vis lamps: Osram Luminux Deluxe 954, 58 W, 400-750 nm; or UV lamps: Phillips Cleo Effect 70 W, 300-420 nm) in an air cooled lamp housing surrounded the flow tube in a circular arrangement.

The inner surface of the sandblasted glass tube with surface to volume ratio of 5 cm^{-1} was coated with a thin layer of coating solution and then gently dried under a flow of nitrogen. The coatings were prepared from a mixture of gentisic and citric acid in water, resulting in a quantity of ~0.5 mg·cm^{-2}, and were operated under 40-60% RH and a temperature of 21-23°C.

The total concentration of NO_x leaving the flow tube was monitored with a chemiluminescence detector (Monitor Labs 9841) and was adjusted in the 0-335 ppb range. At the residence times used in this experiment, loss of NO_2 in the tube due to photolysis was negligible. At the flow tube exit a LOPAP (Long Path Absorption Spectrometer) was used to determine the concentration of HONO in the gas phase. The instrument scrubs HONO by a fast chemical reaction in a stripping coil and converts it into a dye, which is measured in a long path absorption cell with a detection limit of 5 ppt and a total accuracy of ±10%.

RESULTS AND DISCUSSION

The interactions of aqueous films containing GA with gaseous NO_2 were investigated in the dark and under UV or visible light. Similar to the NO_2 uptake on a 1,2,10-trihydroxyanthracene film [2], the reactive uptake coefficient (γ) leading to HONO formation in the dark was a few 10^{-6} and decreased with increasing gas phase NO_2 concentration, $[NO_2]_g$ (Fig. 1a). HONO formation for both dark and illuminated conditions increased linearly with increasing $[NO_2]_g$ from 0 to 30 ppb and approached saturation for $[NO_2]_g$ above 100 ppb (data not shown). This behavior could be explained by adsorption saturation preceding the photochemical reaction or by a limiting production of a photochemical intermediate.

The photochemically enhanced HONO production is demonstrated in Fig. 1 (a, b). As GA does not absorb light at wavelengths above 400 nm, no enhancement in HONO formation was monitored under irradiation of a GA coating with visible light. If 1% of a photosensitizer (methylene blue) was added to the coating, some increase in HONO production was observed, but less pronounced as upon UV irradiation.

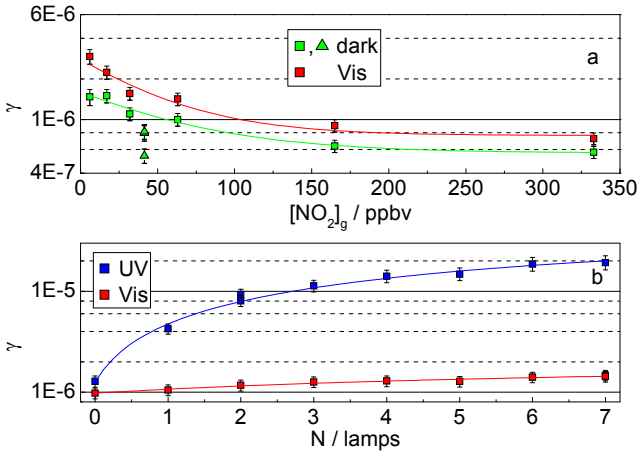

Fig. 1: **(a)** Dependence of the uptake coefficient of NO_2 on $[NO_2]_g$ for a GA surface in the dark and for a GA surface containing 1% methylene blue under irradiation with 7 visible lamps. **(b)** Dependence of the uptake coefficient under UV and visible light on irradiation. $[NO_2]_g$ in (b) is 64 ppbv. For the UV experiments the irradiation was performed during 0.95 s; for visible light during 0.8 s.

ACKNOWLEDGEMENT

This work was supported the Swiss National Science Foundation.

REFERENCES

[1] Stemmler, K. et al., Atmospheric Chemistry and Physics (2007), *7*, 4237.

[2] Arens, F. et al., Phys. Chem. Chem. Phys. (2002), 4, 3684.

KINETICS OF PROTEIN NITRATION BY O_3 AND NO_2

M. Shiraiwa, U. Pöschl (MPI-CH), Y. Sosedova, A. Rouvière, M. Ammann (PSI)

The kinetics of nitration of protein particles by O_3 and NO_2 was measured using the short-lived radioactive tracer ^{13}N. The observed uptake coefficients of NO_2 ($\sim 10^{-5}$) depend strongly on O_3 concentrations.

INTRODUCTION

The effects of air pollution on allergic diseases are not yet well-understood. Proteins contained in biogenic aerosol particles (pollen, spores, bacteria, etc.), which account for up to 5% of urban air particulate matter, are efficiently nitrated in polluted environments before inhalation and deposition in the human respiratory tract [1], which is likely to trigger immune reactions for allergies. Proteins undergo a nitration reaction that leads to the formation of 3-nitrotyrosine residues. The kinetics and reaction mechanism of protein nitration is still largely unknown.

EXPERIMENTAL

The routine for the online production of ^{13}N-labeled nitrogen dioxide and the main experimental setup were reported previously [2]. Bovine serum albumin (BSA) was used as a model protein compound. Deliquesced NaCl particles were also used as a reference. Particles generated by an ultrasonic nebulizer were mixed with O_3 (0 – 150 ppb) and NO_2 (5 – 100 ppb) under humid conditions (30 – 75 % RH) in a flow tube reactor. The reaction time was varied in the range of 4-10 min by changing the position of the inlet of the reactor. The surface concentration of particles was monitored by a scanning mobility particle sizer (SMPS). After passing through the flow tube reactor, the gas and aerosol flow entered a narrow parallel-plate diffusion denuder coated to selectively absorb gas phase NO_2, followed by a particle filter collecting the particles. The γ detectors were attached to each denuders and the filter to count the amount of gamma quanta, which are emitted in the decay of ^{13}N. From the count-rate, the concentration of the corresponding species was derived, which was used for the calculation of uptake coefficients of NO_2 (γ_{NO2}). Fig.1 shows a typical experimental profile of NO_2 uptake by BSA particles along with the surface concentration of particles.

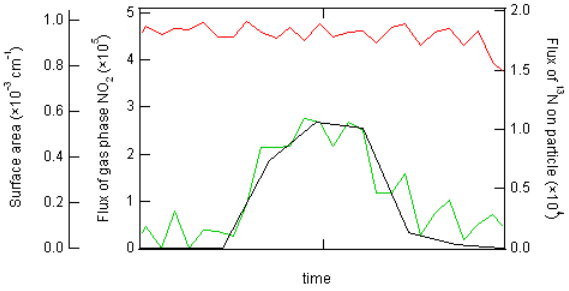

Fig. 1: Typical experimental profile of flux of $^{13}NO_2$ in gas phase (red) and on protein particle (green) along with surface area concentration (black).

RESULTS AND DISCUSSION

In absence of O_3 in the flow tube reactor, NO_2 uptake by both BSA and deliquesced NaCl were below the detection limit ($\gamma_{NO2} < \sim 10^{-6}$). Fig. 2 shows measured γ_{NO2} by BSA and deliquesced NaCl particles. The γ_{NO2} by BSA is of the order of 10^{-5}, strongly depending on gas phase ozone concentration, which indicates that O_3 plays an important role in NO_2 uptake. The γ_{NO2} by deliquesced NaCl is one order of magnitude smaller, which is likely to be attributed to the formation of gas phase NO_3 and N_2O_5, as neither O_3 nor NO_2 are expected to rapidly react with deliquesced NaCl. This amount of uptake is considered to be the maximum potential contribution of gas phase NO_3 radicals and N_2O_5 to uptake of ^{13}N-labeled species by protein particles. The possible mechanisms of high NO_2 uptake by protein particles are: 1) surface reaction between adsorbed O_3 and NO_2 forming NO_3 radicals on the surface which react with protein [3], 2) O_3 first reacts with protein forming intermediates, followed by reaction with NO_2. Further experiments and modelling are in progress.

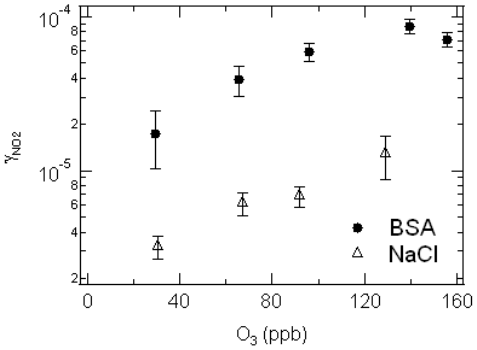

Fig. 2: Observed γ_{NO2} by BSA and deliquesced NaCl vs. gas phase O_3 concentration at 26 ppb NO_2 and 60% RH.

ACKNOWLEDGEMENT

Support of the PSI accelerator facilities for providing stable proton beams and of IP-2 for handling our target are greatly appreciated. MS is supported by the Max Planck Graduate Center.

REFERENCES

[1] T. Franze et al., Environ. Sci. Tech., **39**, 1673 (2005).
[2] Y. Sosedova et al., J. Phys. Chem A., **113**, 10979 (2009).
[3] M. Shiraiwa et al., Atmos. Chem. Phys. Discuss, **9**, 18021 (2009).

.

INFLUENCE OF FATTY ACIDS ON THE UPTAKE OF OZONE TO DELIQUESCED KI/NaCl AEROSOL PARTICLES

A. Rouvière, M. Birrer, M. Ammann (PSI)

The reactive uptake of ozone on deliquesced KI/NaCl aerosol particles coated with amphiphilic surfactants was investigated. The effects of fatty acids from C_9 to C_{20} were studied.

INTRODUCTION

The aim of this study was to determine the effect of surfactants (fatty acids) on the phase transfer of ozone to the underlying condensed phase. Stemmler et al. [1] have shown earlier that surfactants inhibit the phase transfer of HNO_3. Indeed, an organic coating can reduce the mass transfer between the gas and the aerosol phases. Surfactants may also affect the interfacial halide enhancement [2, 3].

EXPERIMENTAL

The experimental set-up is similar to that described in [4] (Fig. 1). The aerosol flow passes over a heated reservoir containing a given fatty acid (FA). The amount of fatty acid condensed on the particles was controlled by changing the evaporator temperature. We don't know whether the organics form a homogeneous coating on the dry particles or condense as a separate droplet attached to the particle. However, once deliquesced, we assume that FA spontaneously forms a monolayer with the excess accumulating as a "lens" at the aqueous surface.

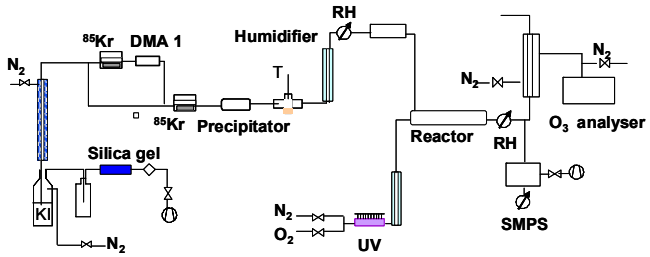

Fig. 1: Experimental set-up.

RESULTS

Under appropriate steady state approximations, the uptake coefficient of gas molecules from the gas-phase into a liquid can be expressed in terms of a sequence of resistances similar to the following equation. The uptake coefficient is directly related to the resistance at the surface due to transport across the surfactant layer including also transfer into the liquid, usually expressed by the bulk accommodation coefficient, and the resistance due to the bulk liquid phase reaction expressed by $1/\Gamma_b$:

$$\frac{1}{\gamma} = \frac{1}{R} + \frac{1}{\Gamma_b}$$

Uptake coefficients obtained for particles containing a mixture of sodium chloride and potassium iodide in presence of fatty acids are shown as a function of iodide concentration in Fig. 2 for the example of stearic acid. These results show that for low mass ratios of surfactant we have a bulk reaction limited uptake, where the term $1/R$ is negligible and the uptake coefficient increases linearly with the square root of the iodide concentration. Then, for sufficiently high mass ratios of surfactants, the uptake coefficient is not depending on the iodide concentration. In this case, uptake of ozone is limited by transport across the surfactant layer, which allows retrieving an estimate for $R_{C18}=3.3\times10^{-4}$.

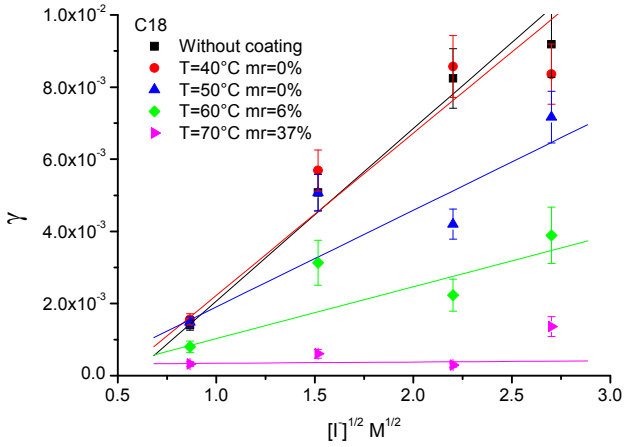

Fig. 2: The uptake coefficient as a function of the square root of the iodide concentration $\sqrt{[I^-]}$ for different mass ratios of surfactant for C_{18}.

CONCLUSION

This study highlights the effectiveness of an organic layer to act as a barrier to the uptake of a trace gas species from the gas phase to the bulk aqueous phase. Similar results were obtained for other FA. Considering the long chained surfactants ($>C_{15}$), the monolayer formed is in the liquid condensed state [5]. These films are well structured and hardly compressible, which explains their capability to inhibit the ozone uptake.

ACKNOWLEDGEMENT

This work was supported by the Swiss National Science Foundation (grant no. 200020-109341).

REFERENCES

[1] K. Stemmler et al., Atmos. Chem. Phys. 8, 5127 (2008).
[2] M. Krisch et al., J. Phys. Chem. C 111, 13497 (2007).
[3] M. Latif and P. Brimblecombe, Environ. Sci. Technol., 38, 6501 (2004).
[4] A. Rouviere et al., Ann. Rep. Lab. of Radio- & Environ. Chemistry, Uni Bern & PSI (2008), p 10.
[5] W. Seidl, Atmos. Environ, 34, 4917 (2000).

EFFECT OF PHOTOSENSITIZED CHEMISTRY ON ORGANIC AEROSOL

A. Rouvière, Y. Sosedova, T. Bartels-Rausch, M. Birrer (PSI), B. D'Anna, C. George (IRCELYON), M. Ammann (PSI)

Photochemistry in aerosol particles is an emerging new field of atmospheric science. We report evidence that the absorption of organic acids in presence of a photosensitizer showed a light induced shift from UV to the visible, which is likely induced by oligomerisation of the acids.

INTRODUCTION

Organic compounds constitute a significant fraction of atmospheric aerosol particles. They either originate directly from primary sources such as combustion or are formed through oxidation of volatile organic compounds in the gas phase and subsequent condensation. The particle phase organics continue to undergo oxidative and photochemical processing as well as repeated exchange with the gas phase. Photochemical processes in the condensed phase are not well understood. Partially oxidized aromatic compounds such as aromatic ketones may act as photosensitizer to promote charge and energy transfer (triplet-triplet) to other organic compounds under conditions, where direct photolysis processes of the latter are not possible. The resulting radicals undergo numerous secondary chemical reactions; some of them may lead to polymerization.

Ultraviolet or visible light absorbing organic constituents of atmospheric aerosols may act as photosensitizers for a number of processes [1]. Photosensitizers may be primary organics from combustion sources or be formed in situ during oxidation in the atmosphere [2]. The significance of photosensitized processes has been demonstrated by showing enhanced uptake of atmospheric oxidants to organic films or aerosol particles [3]. Photosensitizers are known to absorb light and cause photochemical reactions. UV-VIS spectroscopy experiments of organic acid solutions in presence of a photosensitizer were performed.

EXPERIMENTAL

Organic acids and benzophenone type photosensitizers were dissolved and irradiated using 7 sunlight lamps (Phillips Effect, 70W, diffuse) for different times of exposure. Solutions of acetic acid and BBA (Benzoyl Benzoic Acid) and succinic acid and benzophenone were studied.

RESULTS

Light induced reactions can change the chemical composition of a bulk solution containing an organic acid and a photosensitizer. In fact, we observed that the absorption shifted from the UV to the visible in presence of the photosensitizer, which indicates an oligomerisation of the acids. Moreover, increasing absorption at UV-VIS wavelengths are correlated with the irradiation time (Fig.1 and Fig. 2). Additional evidence has been obtained through coated wall flow tube experiments in a photoreactor coupled to a Chemical Ionization Mass Spectrometer (CIMS) and an aerosol photoreactor coupled to an aerosol mass spectrometer (AMS). In first experiments, we have observed significant depletion of succinic acid from the aerosol phase in presence of ammonium sulfate and Benzoyl Benzoic Acid (BBA) as sensitizer.

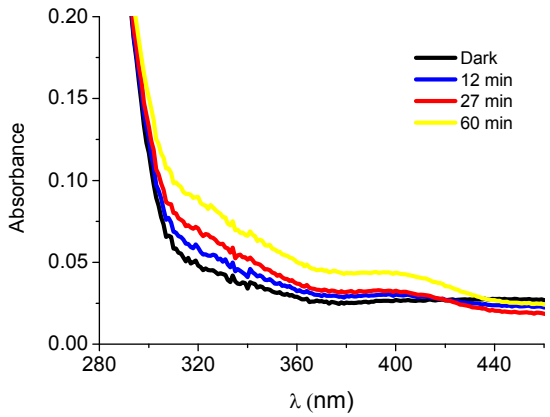

Fig. 1: UV-Visible spectra of a solution containing succinic acid (0.1 mM) and benzophenone (0.1 mM) at different times of exposure to light.

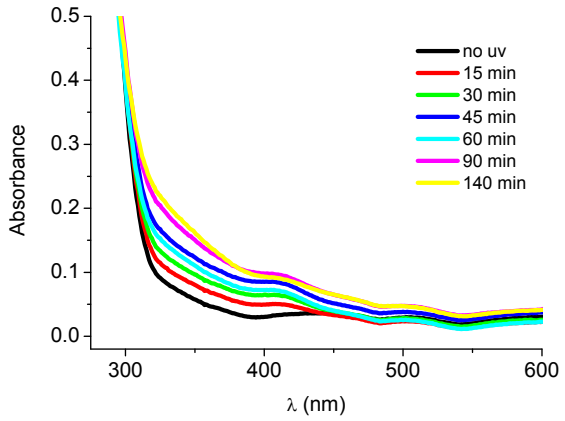

Fig. 2: UV-Visible spectra of a solution containing acetic acid (0.4 mM) and BBA (0.4 mM) at different times of exposure to light.

ACKNOWLEDGEMENT

This project was supported by the EU FP 6 project EUCAARI (European Integrated project on Aerosol Cloud Climate and Air Quality interactions) No 036833-2. Support by P. De Carlo with the AMS is appreciated.

REFERENCES

[1] S. Canonica et al., J. Phys. Chem. A, 104, 1226, 2000.
[2] A. Gelencser et al., J. Atmos. Chem., 45, 25, 2003.
[3] B. D'Anna et al., J. Geophys. Res., 114, D12301, 2009.

MICROSCOPIC, SPECTROSCOPIC AND HYGROSCOPIC CHARACTERIZATION OF SINGLE SOOT PARTICLES

V. Zelenay (PSI), T. Huthwelker (PSI/SLS), A. Křepelovà (PSI), M.G.C. Vernooij (EMPA), M. Birrer (PSI), R. Chirico, T. Tritscher (PSI/LAC), B. Watts, J. Raabe (PSI/SLS), M. Ammann (PSI)

In this work, we characterized single soot particles from two different diesel vehicles (EURO 2 and EURO 3) using TEM and X-ray microspectroscopy.

INTRODUCTION

Soot is estimated to have the second strongest contribution to global warming besides CO_2. This influence depends on the optical properties of soot. These properties change with aging in the atmosphere and water uptake. Freshly emitted soot is assumed to be hydrophobic and its optical properties are shown to be independent of relative humidity (RH), whereas soot mixed with hygroscopic substances, e.g. organics as it can happen during the aging, exhibits significant enhancement in light absorption and scattering depending on mass of hygroscopic substance and RH [1].

EXPERIMENTAL

Soot particles were sampled from the smogchamber, where atmospheric aging of diesel exhaust is simulated using ozone and light. A van without oxidation catalyst and a passenger car with oxidation catalyst, further referred to as EURO 2 and EURO 3, respectively, were used. Oxidation of volatile precursors leads to partitioning of secondary organic material to the primary soot particles. Particles were sampled before and after processing in the chamber. The x-ray absorption spectroscopy (XAS) and TEM measurements were used to characterize the soot particles, while the hygroscopicity measurements were performed in the homebuilt microreactor [2] at the PolLux beamline.

RESULTS

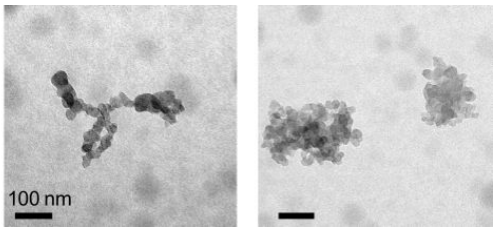

Fig. 1: TEM images of soot particles from a EURO 3 car, left: unprocessed soot showing a chain-like structure, right: processed soot showing a more collapsed agglomerate structure.

The soot particles were characterized with TEM (Figure 1) and XAS (Figure 2). The XAS spectra were used to analyze the aromatics (285 eV), carboxyls (288 eV) and aliphatics (292 eV). We could show that particles with a high carboxylic and aliphatic content, which were found in the emissions from the EURO 2 van (processed and unprocessed particles), showed a high water uptake. High aromatic and low aliphatic/carboxylic content, which was found in the unprocessed EURO 3 soot, did not lead to significant water uptake (Figure 3 and 4).

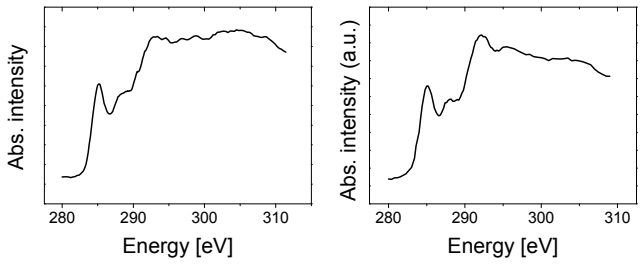

Fig. 2: NEXAFS spectra of unprocessed soot from a EURO 2 car (left) and of processed soot from a EURO 3 car.

We showed that the assumed conversion from hydrophobic to hydrophilic soot as estimated in the literature is not always as obvious (e.g. EURO 2), and water uptake can already occur in freshly emitted soot (Fig. 3). But this property depends on individual cars as e.g. in contrast to the EURO 2 soot, the unprocessed EURO 3 soot is very hydrophobic and does not show any uptake (Fig. 4).

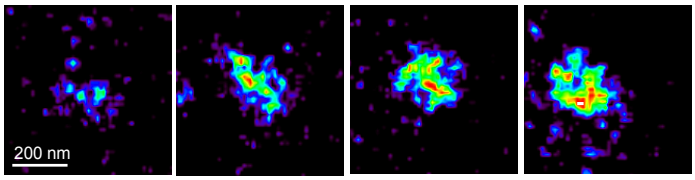

Fig. 3: Unprocessed single soot particle from a EURO 2 car measured under different conditions, from left to right: 0%, 50%, 80% and 90% RH showing a continuous increase in absorption intensity.

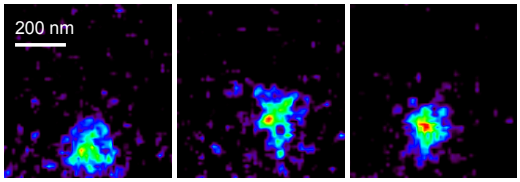

Fig. 4: Unprocessed single soot particle from the EURO 3 car measured at (from left to right) 0%, 90% and again 0% RH showing no change in absorption intensity i.e. no water uptake.

ACKNOWLEDGEMENT

This work is supported by the NEADS project within the Center of Excellence in Energy and Mobility (CCEM-CH).

REFERENCES

[1] Khalizov et al., J. Phys. Chem. A, **113**, 1066 (2009).
[2] V. Zelenay et al., Ann. Rep. Lab. of Radio- & Environ. Chemistry, Uni Bern & PSI (2007).

TRACKING MORPHOLOGICAL CHANGES IN FULVIC ACIDS UPON WATER UPTAKE USING X-RAY MICROSPECTROSCOPY

V. Zelenay, A. Křepelovà (PSI), T. Huthwelker (SLS/PSI), M. Birrer (PSI), B. Watts, J. Raabe (SLS/PSI), U. Krieger, G. Ciobanu (ETHZ), Y. Rudich (Weizmann), M. Ammann (PSI)

Microspectroscopy – spectroscopy at the nanometer scale – at the PolLux beamline was used to observe morphological changes as a function of humidity in fulvic acids, a proxy for atmospheric humic like substances (HULIS).

INTRODUCTION

Atmospheric humic like substances constitute a major fraction of organic material in atmospheric aerosol particles generated by oxidation of primary organic compounds. Such atmospheric aerosol particles have a substantial effect on our climate, both through direct and indirect effects [1]. Many questions are still open as e.g. the influence of the relative humidity on the morphology of atmospheric particles. We try to approach this question using x-ray absorption micro-spectroscopy in a new developed microreactor at the x-ray microscope at the PolLux beamline (SLS) [2]. We use the Swannee River fulvic acids as a proxy for these humic like substances since the fulvic acids resemble them to some degree.

EXPERIMENTAL

Two different preparation methods were used to apply the fulvic acid on the sample holder: 1. a piezo-driven microdispenser, which deposited about 30 µm large droplets on the sample holder, 2. a nebulizer, which was used to produce aerosol of about 200-500 nm in size and that were deposited on the sample holder as dry particles.

RESULTS

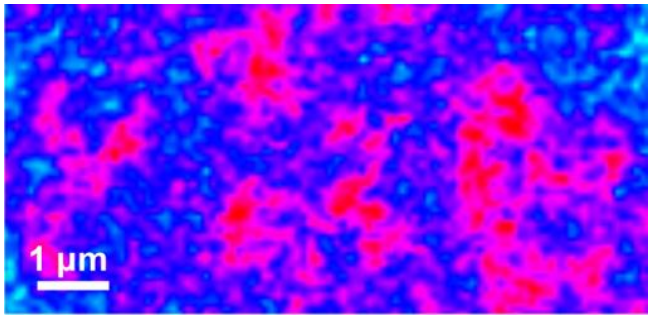

Fig. 1: Image measured at 288 eV and 90% RH showing an emulsion like system with colloidal particles (red) of more phenolic nature contained in a solution (blue) of more carboxylic character.

The near edge X-ray absorption spectra at the C K-edge show characteristic peaks at 284.8, 286.5 288.4 eV to represent aromatic, phenolic and carboxylic functional groups, respectively. Images taken at these energies, and ratios thereof, allow obtaining chemical contrast within the sample.

The SRFA prepared with the microdispenser shows an interesting behaviour upon water uptake: In the dried droplet residue on the wafer window the phenolic species are found to be more concentrated at the border of the dry particles, while carboxylic species are found preferably in the middle of this droplet. Enhancing the relative humidity (RH) to 90% causes a rearrangement in the droplet and a two phase system ('emulsion') is formed (Figure 1). Small colloidal particles of more hydrophobic molecules are found undissolved in a solution of the more hydrophilic components of fulvic acids. In these droplet residues the hydrophobic particles range from 1 µm diameter particles to rather big structures of up to 10 µm. We found the more water soluble components of the fulvics acids to be of carboxylic, while the more insoluble are of more phenolic nature.

The quantitative analysis of the spectra and images show that the carboxylic species take up 4 times more water than the phenolic species.

In contrast, the smaller, micron sized particles generated with the nebulizer method remained widely homogeneous within the resolution constraints of the microscope. However, after water uptake at 80% some of the particles show inhomogeneous morphology. But this morphology did not persist and starting from about 90% RH the fulvic acid appeared again as a homogeneous solution (Figure 2).

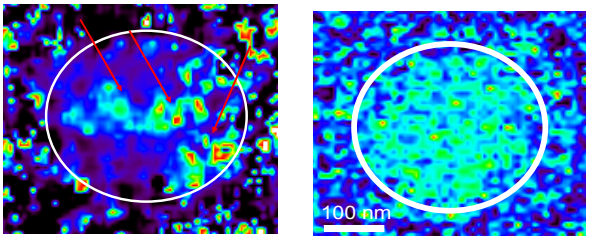

Fig. 2: One single particle measured at 81% (left) showing an inhomogeneous mixture and at 91% RH (right) showing the same particle as left but here the fulvic acid forms a homogenous solution.

ACKNOWLEDGEMENT

This work is supported by the NEADS project within the Center of Excellence in Energy and Mobility (CCEM-CH) and by the EU FP-7 project EUCAARI.

REFERENCES

[1] V. Ramanathan, et al., Science, **294**, 2119 (2001).
[2] V. Zelenay et al., submitted to J. Phys. Chem. A (2010).

PHASE CHANGES IN HALIDE SALT AEROSOL PARTICLES

A. Křepelová, V. Zelenay, T. Huthwelker, M. Ammann (PSI)

X-ray microspectroscopy was applied to observe the phase changes in halogen salt aerosol particles under controlled gas phase composition and temperature. The measurements were carried out at a soft X-ray beamline with a microfocus (PolLux) at the Swiss Light Source (SLS).

INTRODUCTION

Aerosol particles play an important role in atmospheric chemistry and climate. Sea salt aerosol emitted from the oceans is a major contributor to the global aerosol burden. Sea salt particles can serve as a substrate for heterogeneous chemistry or as cloud condensation nuclei. In this work, we studied the phase changes in NaCl and NaBr particles using a Scanning Transmission X-ray Microscope (STXM). Near Edge X-ray Absorption Fine Structure (NEXAFS) spectra of individual aerosol particles were measured at different conditions.

EXPERIMENTAL

To study aerosol particles under defined conditions, a microreactor allowing controlling gas composition and temperature of the sample was constructed and tested [1]. The aerosol particles were generated with an ultrasonic nebulizer using N_2 as a carrier gas with 2 g·L^{-1} solutions of NaCl or NaBr. The particles were electrostatically deposited on a silicon nitride membrane window. The membrane was previously glued with wax onto the small device of the microreactor [2]. The measurements were performed at the PolLux beamline at SLS. The microreactor with the collected aerosol particles was placed in a He-filled microscope sample chamber maintained at 1 atm.

RESULTS

Significant absorption at the oxygen edge occurred only after deliquescence of the particles. Fig. 2 and 3 show the oxygen K-edge NEXAFS spectra of NaCl and NaBr particles as a function of temperature and relative humidity (RH) after deliquescence. The spectra exhibit a shape comparable to that of more dilute halide solutions [3], with the ratio of the intensity at 538 eV to that at 542 eV increasing with increasing concentration towards the supersaturated solutions, when the RH was lowered below the deliquescence humidity (78% for NaCl, 60% for NaBr).

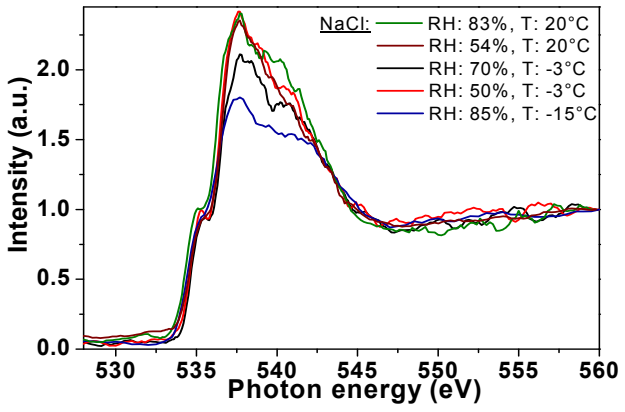

Fig. 1: Oxygen NEXAFS spectra of NaCl aerosols at different temperatures and RHs.

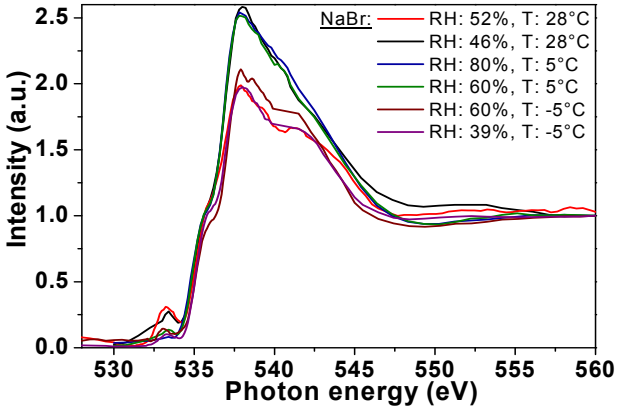

Fig. 2: Oxygen NEXAFS spectra of NaBr aerosols at different temperatures and RHs.

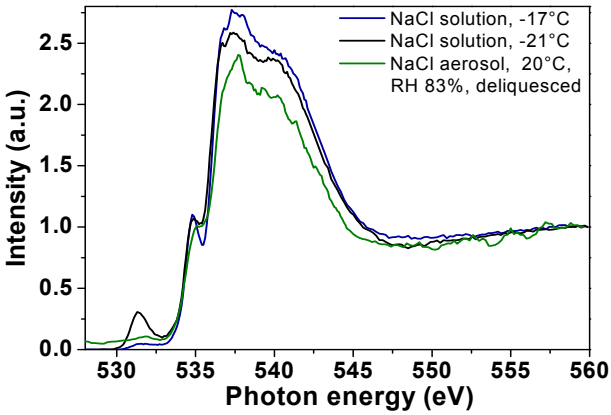

Fig. 3: Comparison of oxygen NEXAFS spectra of NaCl solutions [1] with NaCl aerosol spectra from this work measured under wet conditions.

Fig. 3 compares the spectra of NaCl particles after deliquescence (liquid state) with the surface sensitive Auger electron yield spectra of NaCl solutions obtained at the ALS [4]. The good agreement shows the comparability of surface and bulk probes for this type of solution.

ACKNOWLEDGEMENT

This work is part of our contribution to the EU FP6 project SCOUT-O3.

REFERENCES

[1] V. Zelenay et al., Ann. Rep. Lab. of Radio- & Environ. Chemistry, Uni Bern & PSI (2007), p. 17.
[2] V. Zelenay et al, submitted to J. Phys. Chem.
[3] C.D. Cappa et al., J. Phys. Chem. B, **109**, 7046 (2005).
[4] A. Křepelová et al., this report, p. 20.

X-RAY PHOTOELECTRON SPECTROSCOPY OF HALOGEN SALT IMPURITIES IN ICE

A. Křepelová (PSI), H. Bluhm (LBNL), T. Huthwelker, M. Ammann (PSI)

X-ray photoelectron spectroscopy (XPS) and electron yield near edge X-ray absorption spectroscopy (NEXAFS) were used to characterize the surfaces of halide salt – water mixtures above, at, and below the eutectic temperature.

INTRODUCTION

Ice plays a key role in the global ecosystem as a medium for storage of trace gases or as a catalyst for chemical reactions. The nature of halogen ions and its relation to the topmost, disordered layer on ice (so called quasi-liquid layer) are the topic of significant debate.

EXPERIMENTAL

The principle of the ambient pressure photoemission spectrometer operated at the Advanced Light Source (ALS) is described elsewhere [1]. 0.3 mg of NaCl were dissolved in a low amount of water on a Peltier cooled sample holder, dried and transferred into the spectroscopy chamber. H_2O at a partial pressure of 0.973 Torr was introduced allowing the formation of a NaCl solution droplet at -17°C. Next, the sample was cooled to -21.2°C and the H_2O partial pressure reduced to 0.679 Torr resulting in an eutectic solution. Then, the H_2O partial pressure and the temperature were lowered to 0.26 Torr and -30°C, respectively. XPS and Auger electron yield NEXAFS spectra were measured at each state. Finally, spectra of a NaCl single crystal at 0.3 Torr H_2O were taken as reference.

RESULTS

The O1, Na2s, and Cl2p XPS spectra at different photoelectron kinetic energies (200-600 eV) were measured to obtain a depth profile of Na and Cl, relying on the fact that the electron escape depth is kinetic energy dependent. The photoelectron kinetic energy was varied by tuning the incident photon energy. The ratios of peak areas were calculated from the spectra of each element taken at the same kinetic energy and normalized to the atomic subshell photoionization cross sections and corresponding photon fluxes. Na/O and Cl/O ratios (Fig. 1) increase with increasing probing depth and are higher for the single crystalline NaCl sample than for the solutions, as much less water is associated with its surface, and this water is confined to the surface. For the solutions, the two ratios stay constant with probing depth. At -30°C, the phase state is not exactly defined: at equilibrium a mixture of ice, $NaCl{\cdot}2H_2O$ and NaCl is feasible. This is reflected in the increase of the Na/O and Cl/O ratios with probing depth.

This mixture of phases is also evident from the O K-edge NEXAFS spectra (Fig. 2) at -30°C, showing markedly different intensity distribution at 535, 539, and 542 eV for different experiments and locations on the sample surface. We also observed that phase changes occurred leading to transformation of the NEXAFS spectra among the ones shown. A 'salt cake' (re-crystallized salt) was often observed at the end and appeared to be almost entirely dehydrated, as warming it up led only to little increase in the water vapor pressure. On the other hand, the spectra from the two solutions at -17°C and -21°C were always reproducible and showed the features of a concentrated halide solution [2]. Note that the small feature at around 532 eV is likely due to carbonaceous contamination.

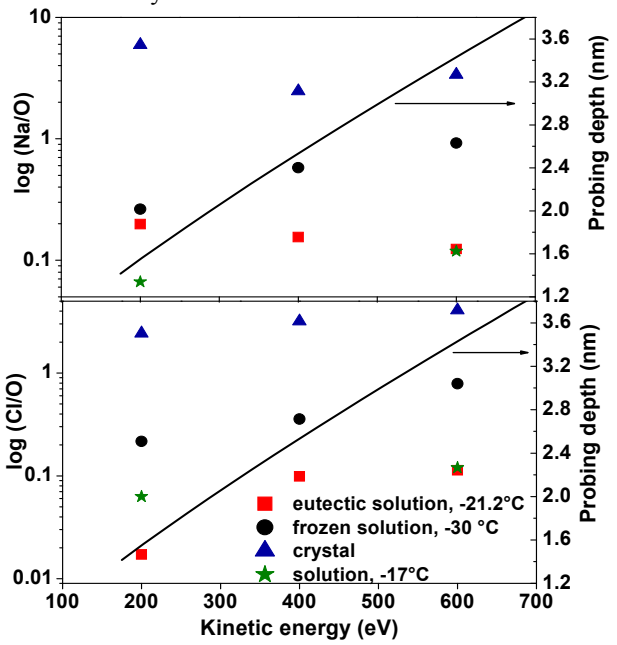

Fig. 1: Depth profiling: Na/O (top) and Cl/O (bottom) and electron escape depth as a function of electron kinetic energy.

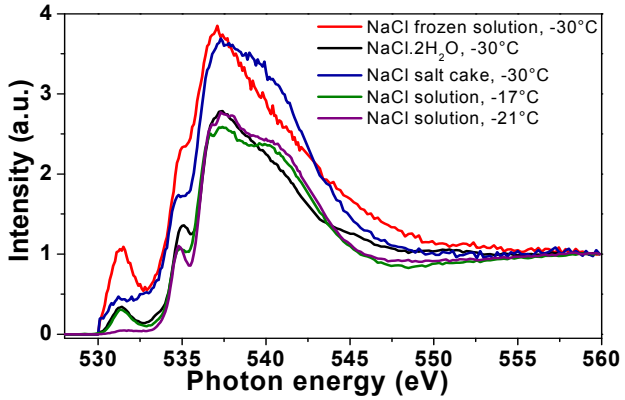

Fig. 2: Oxygen K-edge Auger electron yield NEXAFS spectra of NaCl solution at different temperatures.

ACKNOWLEDGEMENT

This work was funded by the PSI Research Commission.

REFERENCES

[1] D.F. Ogletree et al., NIMPR A., **601**, 151 (2009).
[2] C.D. Cappa et al., J. Phys. Chem. B, **109**, 7046 (2005).

ADSORPTION OF HCl ON ICE STUDIED BY X-RAY PHOTOELECTRON SPECTROSCOPY

A. Křepelová (PSI), J.T. Newberg, H. Bluhm (LBNL), T. Huthwelker, M. Ammann (PSI)

New X-ray photoelectron spectroscopy (XPS) and electron yield near edge X-ray absorption spectroscopy (NEXAFS) measurements were performed to study the impact of HCl adsorption on the surface premelting of ice.

INTRODUCTION

In this report, we continue our study of the impact of HCl on surface ice premelting [1]. XPS was applied to obtain local information of HCl adsorbed to ice. It has been reported that HCl affects the thickness of the disordered surface layer on ice [2].

EXPERIMENTAL

A stable ice film was grown on a Peltier cooled Cu substrate from water vapor and equilibrated at -41°C or -51°C. HCl was dosed directly as a mixture HCl/N_2 (20 ppm HCl) through a stainless steel tube towards the sample holder to improve the likelihood of HCl to reach the ice surface rather than reacting with the chamber walls (see Fig.1). The gas phase composition was monitored by a differentially-pumped mass spectrometer (MS). The measured N_2 pressure was used to obtain an upper limit of the HCl pressure in the chamber. O1s and Cl2p XPS and O K-edge NEXAFS spectra were recorded at constant temperature. Additionally, XPS of the Cu sample holder and MgO were measured for comparison.

Fig. 1: Cu sample holder with ice, HCl dosing tube, and electron sampling aperture.

RESULTS

Cl 2p XPS spectra of ice were measured during the dosing of HCl. The incident photon energy was 390 eV. However, no Cl signal on the ice surface was observed, even though the HCl pressure could have reached 10^{-6} Torr based on the N_2 measurement. Similar to our previous experiments, also O K-edge NEXAFS showed no difference between clean ice and ice with HCl (Fig.2). To be sure that HCl is dosed to the ice, the Cu sample holder and also an MgO sample were measured during dosing of HCl under identical conditions as described before for ice. In both cases, a measurable Cl signal was obtained and the spectra were consistent with Cl2p spectra in the literature [3] exhibiting two peak maxima at binding energies of 203.5 and 202 eV for $2p_{1/2}$ and $2p_{3/2}$, respectively (Fig.3). The reason for the lack of a chloride signal on the ice surface could be the too low HCl pressure due to its loss to the chamber walls and correspondingly too low surface coverage. Also, diffusion of HCl into the bulk of the polycrystalline ice sample might be a likely reason.

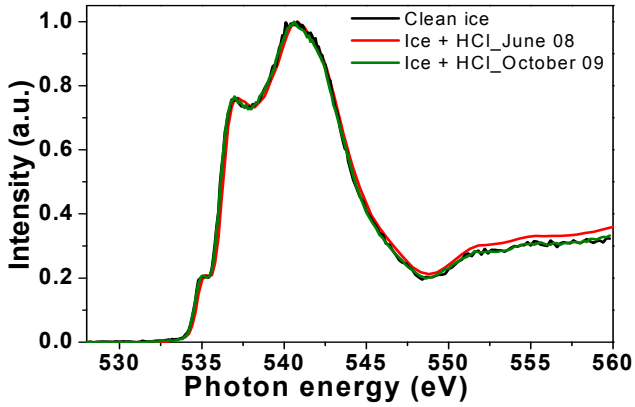

Fig. 2: Oxygen K-edge NEXAFS spectra of clean ice and ice in presence of HCl.

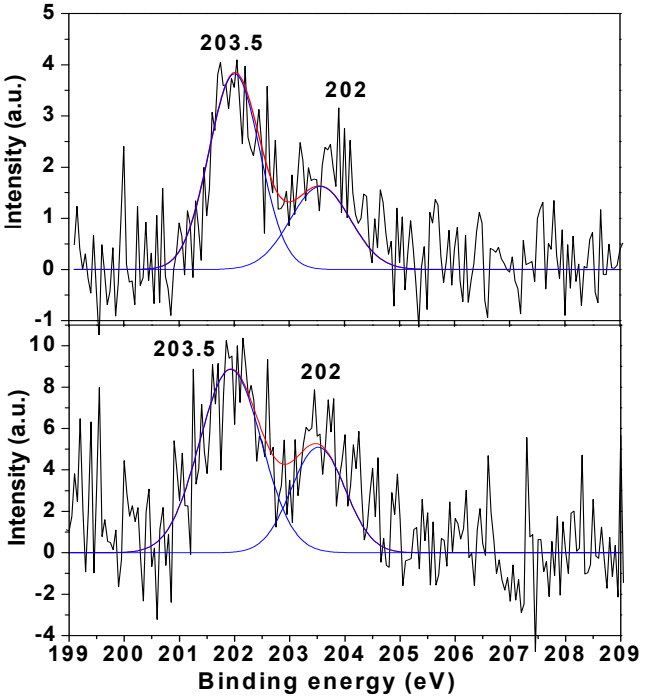

Fig. 3: Photoelectron spectra of Cl2p on the Cu sample holder (top) and on MgO (bottom).

ACKNOWLEDGEMENT

This work is part of our contribution to the EU FP6 project SCOUT-O3.

REFERENCES

[1] A. Křepelová et al., Ann. Rep. Lab. of Radio- & Environ. Chemistry, Uni Bern & PSI (2008), p. 16.
[2] V.F. McNeill et al., PNAS, **103**, 9422 (2006).
[3] B. Winter et al., J. Am. Chem. Soc., **130**, 7130 (2008).

BY-PRODUCTS OF THE HO_2NO_2 SYNTHESIS: QUANTIFICATION OF THE HONO CONCENTRATION

T. Ulrich (Univ. Bern & PSI), T. Bartels-Rausch (PSI), M. Ammann (PSI)

In preparation of experiments of the interaction of peroxynitric acid (HO_2NO_2) with ice we have developed a photochemical source of HO_2NO_2. Here, we quantify the formation of nitrous acid (HONO) as by-product.

INTRODUCTION

Nitrogen peroxides, such as peroxynitric acid (HO_2NO_2) act as reservoir for atmospheric NO_x and HO_x species and thus affect the oxidative capacity of the atmosphere. High concentrations of HO_2NO_2 in the range of 20 to 80 pptV occur in polar regions [1] and in the upper troposphere [2]. Little is known about the partitioning of HO_2NO_2 to ice and snow, even though ice may represent a major sink for HO_2NO_2 [3]. For uptake experiments in ice coated wall flow tubes, we have developed earlier an online photochemical source of HO_2NO_2. In the following we describe the synthesis and show first results of measuring HONO as a by-product.

EXPERIMENTAL

Central to the synthesis is a photolysis cell, where water is photolysed in the presence of CO, N_2, O_2, NO, NO_2 and O_3. Here, HO_2NO_2 is produced by reaction of NO_2 with HO_2. Also the by-product HONO may be produced, mainly by the reaction of NO with OH. The products were monitored using a chemical ionization mass spectrometer (CIMS). The initial NO mixing ratio was 363 ppb, which was quantitatively oxidized to NO_2 prior to entering the photolysis cell. The estimated HO_2NO_2 concentration was 121 ppb corresponding to a yield of 33 %.

We used the very sensitive Long Path Absorption Photometer (LOPAP) instrument to measure the HONO concentration [4]. It scrubs the gas samples into an acidic solution, where protonated HONO leads in two steps to an azo-dye, which is detected.

RESULTS AND DISCUSSION

Figure 1 shows the diluted mixing ratios, as measured by the LOPAP instrument. When NO_2 is switched on at 0 min, the absorption increases in both channels. These two channels operated in series allow correcting for interferences of the LOPAP signal. The same amount of NO_2 is sampled in the first and in the second channel, making a correction possible. This is opposite to the behavior when the light in the photolysis chamber is switched on. As soon as the light is switched on, HO_2NO_2 is produced and is quantitatively taken up by the stripping solution in the first stripping coil due to its high Henry coefficient. In this case a remarkable increase in channel 1 but not in channel 2 can be seen, giving evidence that both HONO and HO_2NO_2 are fully taken up in the first channel. HO_2NO_2 may result in dye formation through NO_2^+.

Fig. 1 shows that HONO can be measured in the synthesis gas very sensitively. The undiluted concentration of HONO in the synthesis is at typical settings 10.9 ppb at maximum. This is still a significant concentration compared to the 121 ppb of HO_2NO_2 at an initial NO concentration of 363 ppb. The yield of HONO is 3 % at maximum.

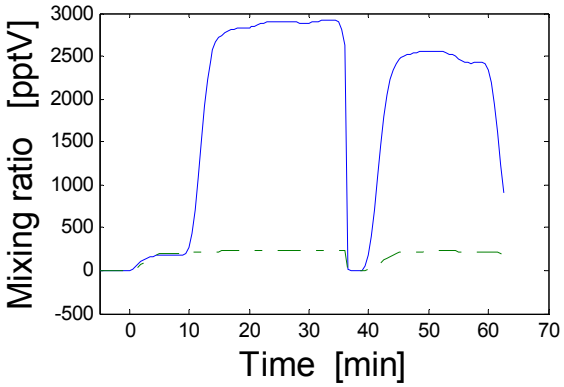

Fig. 1: Mixing ratios of the HONO and HO_2NO_2 signal as measured by the LOPAP instrument. The blue solid line is channel 1 and the green dash-dotted line is channel 2.

To decide, whether HO_2NO_2 contributes to the measured absorption, the gas flow was passed through a tube held at 80°C (residence time 0.3 s) at 38 min. HONO is thermally stable, while HO_2NO_2 is highly unstable [5] and should decay entirely during the available residence time at 80°C, if we neglect recombination. We observed a significantly lower mixing ratio. This test shows that the LOPAP signal is a combination of both: HONO and HO_2NO_2. The interference is at least 1.5 % to 10 % at maximum, related to the HO_2NO_2 mixing ratio. The first value is based on the assumption that only the difference of the two levels is due to interference by HO_2NO_2. The latter value represents the case, where no HONO would be present at all and the entire LOPAP signal would be due to HO_2NO_2 under the additional assumption that thermal decomposition of HO_2NO_2 was not complete. This means that mixing ratios of HONO in the environment may be 0.2 pptV to 8 pptV too high in the presence of significant amounts of HO_2NO_2.

ACKNOWLEDGEMENT

We appreciated funding by the Swiss National Science Foundation (grant number 200021_121857).

REFERENCES

[1] D.L. Slusher et al., Geophys. Res. Let., **29**, 2011 (2002).
[2] S. Kim et al., J. Geophys. Res., **112**, D12S01 (2007).
[3] Z. Li et al., J. Geophys. Res., **101**, 6795 (1996).
[4] J. Heland et al., Environ. Sci. Technol., **35**, 3207 (2001).
[5] T. Gierczak et al., J. Phys. Chem. A, **109**, 586 (2005).

A NEW SETUP FOR KINETIC UPTAKE EXPERIMENTS ON ICE UNDER NON EQUILIBRIUM CONDITIONS

S. Schreiber (ETH Zürich & PSI), M. Kerbrat (PSI), T. Huthwelker (SLS/PSI), M. Birrer, M. Ammann (PSI)

With a new low pressure setup presented here, uptake kinetics of trace gases (e.g. HONO) on ice surfaces under non-equilibrium conditions can be investigated for a wide range of ice growth rates.

INTRODUCTION

Adsorption of different trace gases on ice surfaces in equilibrium has been studied extensively. However, the mechanism for uptake on growing ice is not clear, although this may be relevant to both atmospheric ice particles and snow layers subject to often occurring temperature gradients. Kärcher et al. [1] suggested a theoretical model, which needs to be validated experimentally. So far, only little experimental data about this topic exists [2].

EXPERIMENTAL SETUP

A Knudsen reactor is a low pressure cell operated in the molecular flow regime, thus the mean free path length is on the order of the cell dimensions. Gas phase diffusion can therefore be neglected. The substrate, a vapor deposited ice film, can be either exposed to the gas flow or covered by using a moveable plunger. The new setup is designed in very compact form with typical dimensions of 10 mm, so it can be operated in the molecular flow regime up to a pressure of $5x10^{-2}$ mbar, allowing temperatures of up to 220 K relative to only 200 K of typical Knudsen cell setups. The tubes and the cell are made of chemically inert materials, mostly glass and PFA, in order to enable uptake measurements with reactive trace gases like HONO or HNO_3.

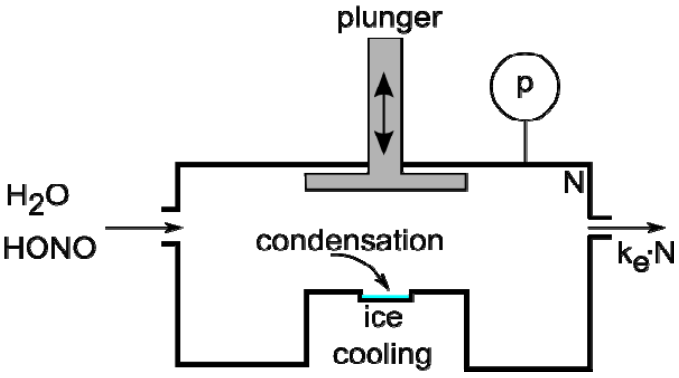

Fig. 1: Principle of a Knudsen cell: The number of molecules leaving the cell is proportional to the total number of molecules N. Once the plunger is lifted, the net H_2O adsorption onto the ice can be calculated from the decrease of pressure p. To measure the trace gas uptake, labelled $HO^{13}NO$ molecules and two coincident detectors (not shown) are used.

The ice growth rate is measured using the pressure difference from covered to exposed substrate, as indicated in Fig. 1. It can be adjusted over three orders of magnitude from $5x10^{14}$ to $5x10^{17}$ molecules $s^{-1}cm^{-2}$. Trace gas uptake is monitored using molecules labeled with radioactive ^{13}N atoms, which are provided by the PROTRAC facility. The decay of these positron emitters is detected with two detectors set up in coincident counting configuration [3].

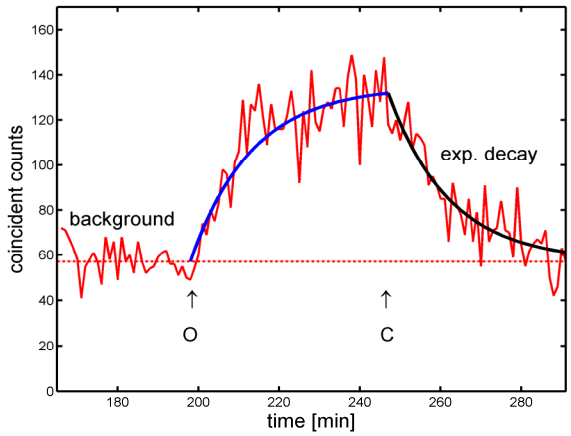

Fig. 2: Uptake of $HO^{13}NO$ on vapour deposited ice at T=205K at an ice growth rate of 1.4 nm/s. Ice growth and HONO uptake takes place between "O" and "C". The signal agrees well with the theoretical solution for a constant burial rate (blue line). After the ice is covered again, the buried tracer atoms decay with the lifetime of 10 minutes (black line).

So far, the geometrical property k_e needed for quantitative analysis was determined for different exit orifices. First uptake experiments have been performed, indicating that the setup is working. A typical experimental trace is shown in Fig. 2. The slow increase suggests clearly burial into the bulk rather than mere surface adsorption.

ACKNOWLEDGEMENT

This work is supported by the Swiss National Science Foundation and is part of a collaboration with the Snow and Avalanche Research Institute SLF/WSL in Davos.

REFERENCES

[1] B. Kärcher et al., J. Geophys. Res., 114, D13306 (2009).
[2] M. Ullerstam et al., Phys. Chem. Chem. Phys., 7, 359 (2005).
[3] M. Ammann, Radiochim. Acta, 89, 831 (2001).

PHOTOLYTIC REDUCTION OF MERCURIC COMPLEXES IN ICE

T. Bartels-Rausch (PSI), G. Krysztofiak (PSI/Univ. Orleans), A. Bernhard (Univ. Bern), M. Schwikowski, M. Ammann (PSI)

Mercury shows a very active photochemistry in aqueous solutions. Here we show first results demonstrating that similar processes also occur in the ice matrix at low temperatures. Better knowledge of this reactivity might help to improve our understanding of the cycling of the toxic mercury between the atmosphere, snow, ocean, and food web.

INTRODUCTION

Mercury is long-range transported in the atmosphere even to remote polar areas, where it can be transformed to more toxic halogen compounds that have a high affinity for the snow phase. During snowmelt the mercuric ions might then be released to the surface water from where they can enter the food web [1]. Yet, mercuric compounds in aqueous solution are known to be photoactive in the presence of organic as well as inorganic substances [2]. Here we describe first experiments in the ice phase to quantify the impact of common trace constituents in Arctic snow on the light-driven mercury release. This process is of importance because the product, elemental mercury, is released back to the atmosphere and consequently will not enter the aqueous phase during snow melting. Also, better knowledge of this loss pathway is important for paleoclimate research, e.g. for interpreting mercury profiles in ice cores.

ORGANIC COMPOUNDS

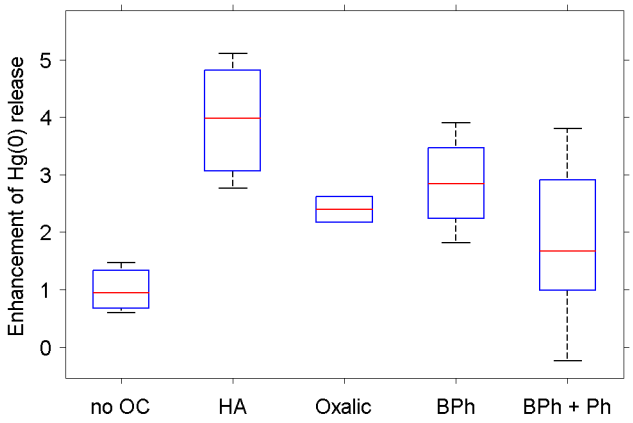

Fig. 1: Enhancement of the mercury loss from an irradiated ice film in the presence of organic matter relative to the loss from ice containing only $Hg(OH)_2$. This reference is denoted as "no OC", humic Acid as "HA", oxalic acid as "Oxalic", benzophenone as "BPh", and 2,6-dimethoxyphenol as "Ph".

Figure 1 illustrates the significant enhancement of the mercury loss during irradiation in the 300 – 420 nm range when different types of organics are present. Experiments were performed with an ultrathin ice film at -15 °C in a coated wall flow tube while nitrogen gas passed the ice surface to immediately remove the released mercury from the photo reactor. The ice matrix was dosed with 1 ppm humic acid and 300 ppb mercuric nitrate, and the released mercury was trapped from the carrier gas and quantified in an atomic fluorescence spectrometer. Alternatively, the ice film contained 10 ppb mercuric hydroxide and 100 ppb oxalic acid or benzophenone. The mercuric concentration was directly measured in the molten ice films after the experiment.

Interestingly, the addition of 10 ppb phenol to the ice matrix did not further enhance the reactivity of benzophenone towards mercuric ions, as it was observed for other reaction partners [3]. This might indicate that complex formation, a prominent property of mercuric ions, affects its photo reactivity [2].

HALOGENS AND OXYGEN

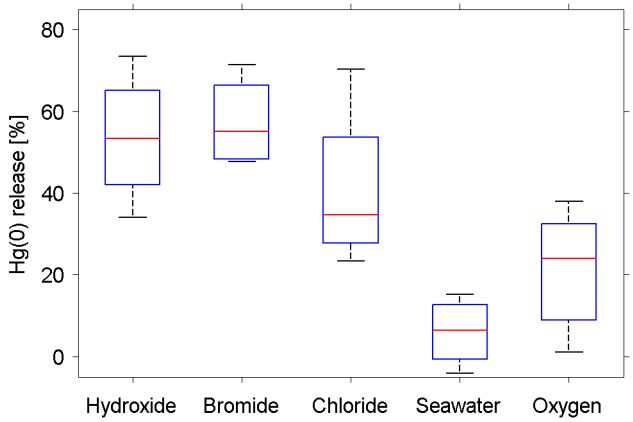

Fig. 2: Loss of mercury from irradiated ice films in the presence of benzophenone and different additional complexing ligands.

The polar mercury chemistry is most active close to the open sea where high concentrations of halogens are present in the snow [2]. Figure 2 shows that the mercury release in the presence of benzophenone is totally inhibited when the ice matrix was prepared from artificial seawater, as opposed to experiments with $Hg(OH)_2$ and BPh in ultrapure water. Also the use of oxygen as carrier gas significantly reduced the mercury release. Both observations point to the importance of re-oxidation of mercury. This does also explain why small amounts of chloride (10 ppb) show a stronger effect than the same amount of bromide. During photolysis of chloride ions stronger oxidizers are formed than with bromide.

REFERENCES

[1] A. Steffen et al., Atmos. Chem. Phys., **8**, 1445 (2008).
[2] H. Zhang et al., Recent Developments in Mercury Science (2006) p. 37-79.
[3] C. George et al., Faraday Discuss., **130** (2005).

A NEW DYE TO PROBE THE WATER-AIR AND ICE-AIR INTERFACE

T. Bartels-Rausch (PSI), H.M. Frey, S. Leutwyler (Uni Bern), D. Langenegger, L. Tiefenauer (PSI/BMR)
M. Ammann (PSI)

The uptake and chemistry of acidic gases on ice or snow surfaces is of considerable importance in air quality research and climate science. Both processes might be crucially influenced by the acidity on the surface, about which only little is known. Here, we present first results of acidity measurements on the top layer of water and ice.

INTRODUCTION

The acidity conditions on the uppermost layer of the air-water interface, and even more of the air-ice interface, are still heavily debated [1]. Tackling this open question is of fundamental importance, and also of great interest in the atmospheric science community [2]. As the acidity at this interface region may influence the uptake and chemistry of atmospheric trace gases, and consequently the air quality and climate forcing.

Here we present first results of a novel use of a pH indicator dye for measurements in the uppermost layers of an air-surface interface. High and well-defined spatial resolution is achieved by the surfactant properties of the phospholipid backbone to which a dye is coupled.

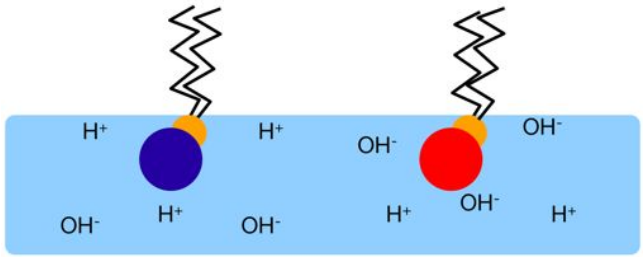

Fig. 1: Illustration of the high spatial selectivity of the dye (blue and red dot) for the upper layers of a water surface, which is a result of the phospholipid backbone (orange dot and black lines).

SPECTRA IN AND ON WATER OR ICE

The dye is a fluorescein derivative, the absorption spectrum of which shows a clear response to the acidity conditions in the bulk water phase (Figure 2). To get a sufficiently high concentration of the insoluble dye in water, it was embedded into 100 nm liposomes, the scatter of which is most probable responsible for the high absorption background at wavelength below 480 nm. Unaffected by this, a maximum absorption at alkaline conditions was observed at 507 nm.

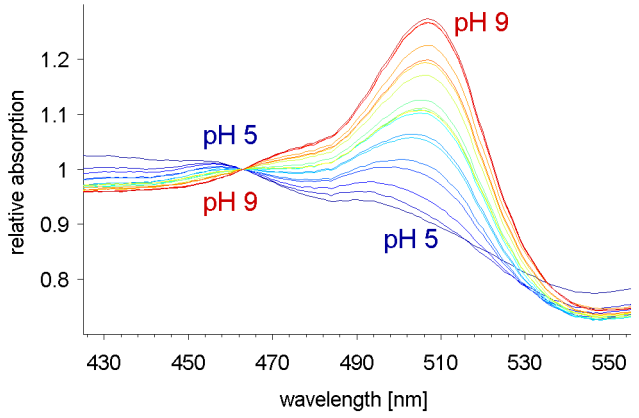

Fig. 2: Transmission spectra of liposomes that contain the fluorescence dye. Reddish lines denote alkaline pH of the aqueous solvent, bluish acidic conditions.

First experiments on ice and water surfaces in the absence of liposomes reveal that the maximum in the absorption spectrum at alkaline conditions is blue-shifted on the ice surface compared to the water surface (Figure 3) and to bulk water (Figure 2). This might indicate a shift in polarity. For the measurements on the surface a small amount of the dye in chloroform was added on a water film. After the solvent evaporated fluorescence was triggered using a tuneable laser between 430 nm and 550 nm. The fluorescence signal was collected above the surface and recorded by means of a photomultiplier. The ice film was prepared at -15°C by freezing a water droplet containing the dye and a high concentration of NaOH.

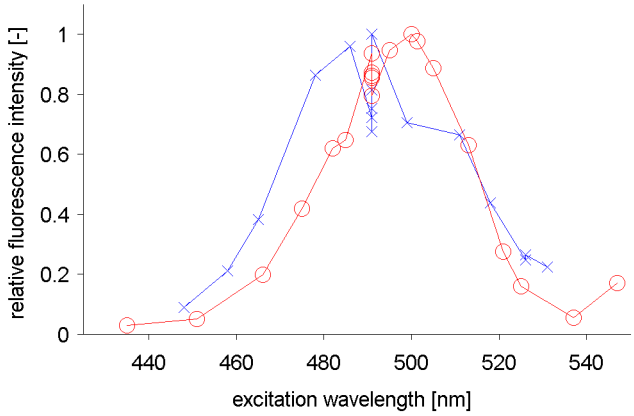

Fig. 3: Fluorescence excitation spectra of the dye -relative to the maximum intensity on water – (circles, red line) and on an ice surface (crosses, blue line).

These results show that the dye is well suited to monitor the acidic and possibly polarity conditions on ice surfaces. Further optimization of the laser-induced fluorescence set-up with focus on the high scatter in the data observed on ice at 490 nm, but not on water surfaces, is work in progress.

ACKNOWLEDGEMENT

Funded by the Swiss National Science Foundation (grant number 200021_121857).

REFERENCES

[1] R. Vácha, Phys. Chem. Chem. Phys., **9**, 4736 (2007).
[2] Th. Huthwelker et al., Chem. Rev., **106**, 1375 (2006).

1,000 YEAR OF SUMMER TEMPERATURES RECONSTRUCTED FROM AN ICE CORE DRILLED AT COLLE GNIFETTI, SWISS/ITALIAN ALPS

M. Sigl, M. Schwikowski (Univ. Bern & PSI), T.M. Jenk (CIC), D. Divine (NPI),
J. Gabrieli, C. Barbante (Univ. Venice & CNR Venice), C. Boutron (LGGE Grenoble)

We reconstructed summer temperatures from ice core stable isotope records ($\delta^{18}O$, d-excess) over the last Millennium by applying multiple linear regression to account for changes in moisture source contribution over time.

Ice cores are valuable archives for various climatic parameters of the past. Ice core stable isotope ratios, for instance, are commonly used as temperature proxies. Contrary to the high-latitudes, only few sites in the European Alps have the potential to obtain long-term records spanning more than 500 years. Those time-periods are especially valuable as the number of climate records available from other sources e.g. tree-rings, historical documentary data or lake sediments substantially decrease in number, spatial coverage, and quality. Besides, many of those archives are not well suited in reconstructing low-frequency components of climate variability. To answer the question if the last decades that were among the warmest since the start of meteorological monitoring, are unprecedented in the past, quantified reconstructions of the medieval temperature level are essential.

For the first time in the Alpine region, a 1,000 year $\delta^{18}O$ ice core record is evaluated for its palaeo-climatic significance. We found a significant positive correlation between instrumental summer air temperature (May-July) and mean annual $\delta^{18}O$ from Colle Gnifetti ice core (Swiss/Italian Alps, 4450 m a.s.l.) for AD 1900-2007 ($r=0.56$, $p<0.06$ for 5-yr filtered time series). This correlation is, however, not stable through time as indicated by instrumental data reaching back to AD 1760. This suggests influences from secondary processes such as moisture source region effects or changes in the seasonality of preserved snowfall. Analysis of the residuals revealed significant correlations ($r=0.39$, $p<0.08$ for 5-yr filtered time series, AD 1800-2007) to the deuterium excess ($d=\delta D-8*\delta^{18}O$). Thus, long-term changes in source regions and pathways as indicated by the d-excess are supposed to affect the $\delta^{18}O$ signal of the ice core. Alpine precipitation originating from the Atlantic, the Mediterranean, or from land-evaporation differs remarkably in isotopic composition. Changes in their relative contribution, related to circulation changes in the atmosphere or in the ocean system, therefore bias the $\delta^{18}O$/temperature relation.

A correction is proposed using multiple linear regression to account for this bias reflected in the d-excess record. Based on this technique, we quantitatively reconstructed May-July temperatures for the last 1,000 years (Fig. 1). During the calibration period (1760-2007) the reconstruction is significantly correlated with instrumental data [1] ($r=0.75$, $p<0.04$ for 21-yr filtered time series). Before the instrumental period, our data agree closely to independent reconstructions using documentary evidence (not shown, [2]) and natural archives (e.g. Alpine stalagmite $\delta^{18}O$ [3]) and to regional glacier fluctuations (not shown, [4]). The warmest periods in our reconstruction over the last 500 years are AD 1530-1550, 1720-1740, 1790-1805, 1940-1950 and 1980-2000. Time periods before AD 1500 are characterized by strong decadal scale variability. Short warm spells with values comparable to the 20th century occurred around AD 1400 and 1220. Short cool periods are recorded at AD 1180, 1250, 1350 and 1500. Persistently warm conditions prevailed from AD 980-1100 before temperatures gradually decreased.

REFERENCES

[1] I. Auer et al., Int. J. Climatol., **27**, 17 (2007).
[2] C. Casty et al., Int. J. Climatol., **25**, 1855 (2005).
[3] A. Mangini et al., Earth Planet. Sci. Lett., **235**, 741 (2005).
[4] H. Holzhauser et al., Holocene., **15**, 789 (2005).

ACKNOWLEDGEMENT

This work was supported by NCCR Climate of the Swiss SNF and the EU FP6 project MILLENNIUM.

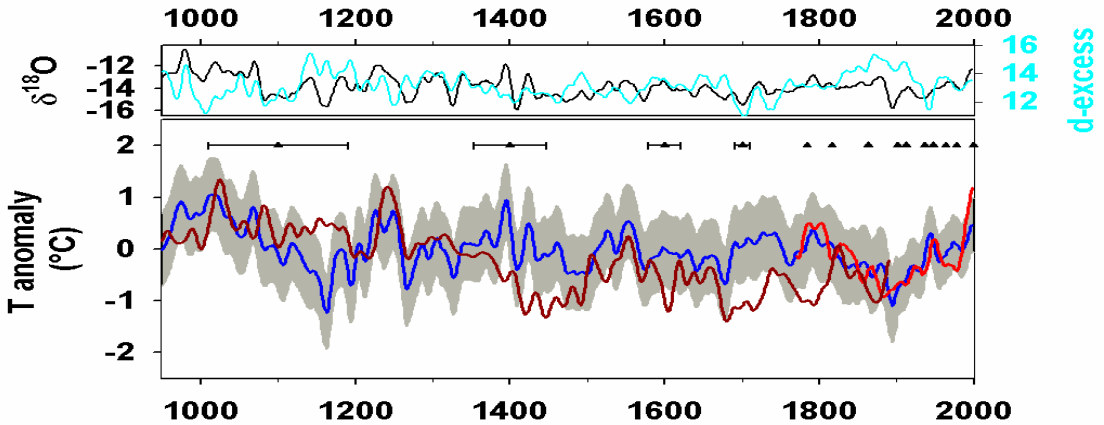

Fig. 1: (Top): 21-yr filtered time series of $\delta^{18}O$ (black) and d-excess (light blue) for the time period AD 950-2000. (Bottom): Reconstructed May-July temperature anomalies (°C wrt 1901-2000, blue line, shading is 2*RMSE as determined in the calibration) using $T=0.37*\delta^{18}O-0.32d+9.3$ ($r=0.75$; $p<0.04$). Red line is May-July instrumental data [1], dark red line is a temperature reconstruction from an Alpine stalagmite [3]. Triangles mark dating points. Age uncertainty is given by error bars.

1,000 YEAR HISTORY OF SAHARAN DUST RECORDED IN AN ALPINE ICE CORE

M. Sigl, M. Schwikowski (Univ. Bern & PSI), J. Gabrieli, C. Barbante (Univ. Venice & CNR Venice), C. Boutron (LGGE Grenoble)

During the last 200 years, annually resolved mineral dust records derived from Colle Gnifetti ice core show a strong link to the North Atlantic Oscillation and to North African drought conditions of the previous winter (January-April) season. On the millennial time scale, a recent increase in dustiness and the absence of pronounced long-term trends are the most prominent features of the dust records.

Mineral dust is a major component of atmospheric aerosols. Dust aerosols directly affect climate by scattering and absorbing solar radiation and outgoing thermal radiation [1] and indirectly by processes that change the physical properties of clouds such as brightness or lifetime [2]. Inter-annual variability of North African atmospheric dust is strongly linked to drought conditions in the Sahel and to the winter North Atlantic Oscillation (NAO) [3]. However, direct observations are limited to the last decades only.

Here, we present a highly resolved ice core record of mineral dust from the Swiss/Italian Alps, spanning for the first time in Europe the last 1,000 years. We focus thereby on concentrations of Ca^{2+} which is a typical element present in long-range transported Saharan dust.

We show that the mineral dust transport to the Southern Alps is primarily controlled by large-scale circulation by linking dust concentrations to NAO like patterns prevailing during winter and spring season (Fig. 1). The established correlations between Ca^{2+} concentrations and the winter NAO [7] ($r=0.41$, $p<0.1$) and droughts in Morocco [8] ($r=0.56$, $p<0.05$) are significant for the last 150-200 years.

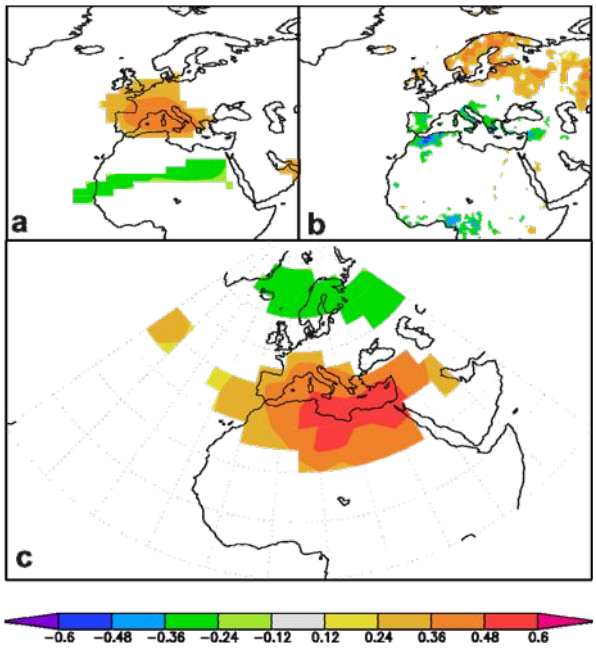

Fig. 1: Spatial correlations of annual, logarithmic, non-sea-salt Ca^{2+} concentrations with (a) NCEP/NCAR reanalysis JFMA (January-April) air temperatures at 500mbar height (1948-2005) [4], (b) CRU TS 3.0 JFMA precipitation (1948-2005) [5], and Northern Hemisphere JFMA sea level pressure (1940-2005) [6]. Only correlations exceeding the 90% significance level are displayed.

Mean dust concentrations and frequencies of major dust events show decadal-scale variability with enhanced dust levels at AD 1010-1060, 1230-1250, 1460-1470, 1640-1680, 1790-1800, 1900-1920 and 1970-2000 (Fig. 2). Low dust concentrations are recorded at AD 1080-1100, 1350-1390, 1570-1630, 1680-1710 and 1890-1900. Mean dust concentrations of the last 20 years are unprecedented in the context of the last 1,000 years. This increased Saharan dust deposition is consistent with the observed widespread increase in dustiness and dust storm frequencies over Northern Africa from direct measurements or from satellite based observations over the last decades.

In contrast, persistent arid conditions in the main source regions of dust in Northern Africa, as reconstructed between AD 1050 and 1400 [8], and a sustained positive state of the NAO over this time period [9], is not supported by the mineral dust records of Colle Gnifetti. The reason might be a low frequency bias of the tree-ring based reconstruction of Moroccan droughts [10].

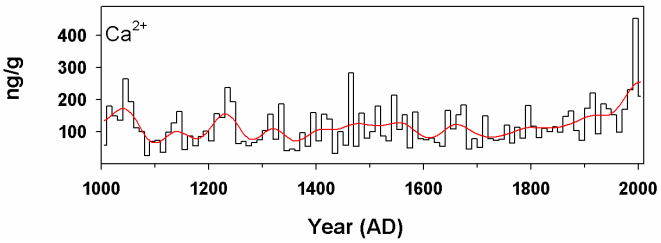

Fig. 2: Time series of Colle Gnifetti Ca^{2+} concentrations for the last millennium. 10-year averages (black) are filtered with a 5-point FFT filter (red line).

ACKNOWLEDGEMENT

This work was supported by NCCR Climate of the Swiss SNF and the EU FP6 project MILLENNIUM.

REFERENCES

[1] Z. Levin et al., J. Geophys. Res. **110**, (2005).
[2] N. Bellouin et al., Nature, **438**, 1138-1141 (2005).
[3] I. Chiapello et al., J. Geophys. Res. **110**, (2005).
[4] E. Kalnay, Bull. Am. Meteorol. Soc., **77**, 437-471 (1996).
[5] T. Mitchell, P. Jones, Int. J. Climatol. **25**, 693-712 (2005).
[6] K. Trenberth, D. Paolino, Mon. Weather Rev., **108**, 855-872 (1980).
[7] J.W. Hurrell, Science, **269**, 676-679 (1995).
[8] J. Esper et al., Geophys. Res. Lett., **34**, (2005).
[9] V. Trouet et al., Science., **324**, 78-80 (2009).
[10] K.J. Anchukaitis, Geophys. Res. Lett., in press.

POST 17th CENTURY CHANGES OF EUROPEAN PAHs EMISSIONS RECORDED IN THE COLLE GNIFETTI FIRN/ICE CORE

J. Gabrieli, C. Barbante (Univ. Venice & CNR Venice), C. Boutron (LGGE Grenoble), M. Sigl, H.W. Gäggler, M. Schwikowski, (PSI & Univ. Bern)

Concentrations of 12 Polycyclic Aromatic Hydrocarbons (PAHs) were determined at high resolution in the upper 58 m of a firn/ice core from Colle Gnifetti glacier (Monte Rosa, 4450 m a.s.l.). These palaeo-records document the history of atmospheric PAHs contamination over the last three centuries.

Polycyclic Aromatic Hydrocarbons (PAHs) are ubiquitous pollutants, originating mostly from incomplete combustion of organic matter and fossil fuels (e.g. diesel engines, domestic heating, industrial combustion) and for this reason very useful as tracers of anthropogenic combustion activities. The historical environmental burden of PAHs in remote areas as a consequence of human activities have essentially been obtained by analyzing lake sediments, in particular from high altitude sites. Snow deposited in the Alps documents the effect of anthropogenic emissions in Europe [1] and mountain glaciers can be used as natural archives of studying historical trends of pollution. Many efforts on Alpine glaciers have been devoted mainly to the reconstruction of the history of heavy metals pollution over the last centuries [2] but recently they have been used also for studying historical trends of Persistent Organic Pollutants [3,4]. The studies regarding PAHs in glaciological records are few and limited to Greenland and, only recently, to the Himalaya region.

The occurrence of organic pollutants in Alpine snow/ice has been reconstructed over the past three centuries using a new on-line extraction method for PAHs followed by chromatographic determination. The melt water flow from a continuous ice core melting system was split, with one aliquot directed to an ICP-QMS for continuous trace elements determinations and the second introduced into a solid phase C18 (SPE) cartridge for semi-continuous PAHs extraction. The cartridges were then eluted and the concentration of 12 PAHs determined by HPLC-FD. The recoveries obtained for spiked snow samples ranged from 71% to 93%, with a precision ranging from 12% to 32%. The depth resolution for PAH semi-continuous extractions ranged from 40 to 70 cm, corresponding to 0.7 to 5 years.

The PAHs pattern is normally dominated by Phenatrene (Phe), Fluoranthene (Fla) and Pyrene (Pyr), which represent 60-80% of the total PAH mass. Before 1875 the sum of PAHs concentrations (ΣPAHs) was very low with total mean concentrations lower than 2 ng/kg and 0.08 ng/kg for the heavier compounds (ΣPAHs*). During the first industrial revolution (1770-1830) the PAHs deposition showed a weak increase which became much greater from the start of the second industrial revolution at the end of 19th century. In the 1920s, economic recession in Europe depressed industrial production, halving PAHs emissions until the 1930's when they increased again and reached a maximum concentration of 32 ng/kg from 1945 to 1955. From 1955 to 1975 the PAHs concentrations decreased significantly reflecting improvements in emission controls especially from major point sources while from 1975 to 2003 rose again to values equivalent to those of 1910.

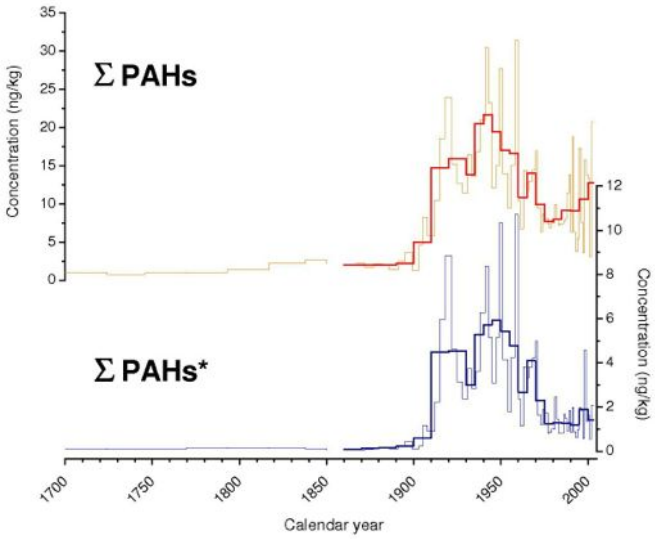

Fig. 1: ΣPAHs profiles for all the compounds analysed and heaviest compounds (ΣPAHs*) with more than 4 aromatic rings.

The ratio Fla/(Fla+Pyr), often used for source assignment, indicates an increase in the relative contribution of gasoline and diesel combustion with respect to coal and wood burning from 1860 to the 1980s. The increase of these values during the last two decades could be explained by the growth in the relative contribution of wood combustion which is very popular for domestic heating not only in alpine towns but also in many large cities.

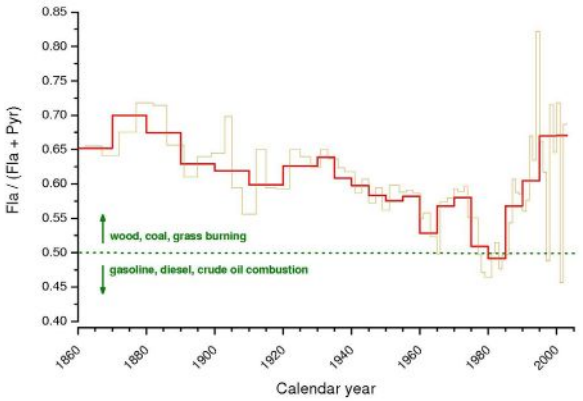

Fig. 2: Fla/(Fla+Pyr) ratio profile.

REFERENCES

[1] G.L. Dali and F. Wania, Environ. Sci. Technol., **33**, 385 (2005).
[2] C. Barbante et al., Environ. Sci. Technol., **38**, 4085 (2004).
[3] S. Villa et al., Ecotox. Environ. Safety, **63**, 17 (2006).
[4] P. Gabrieli et al., Environ. Sci. Technol., submitted.

750 YEARS OF SIBERIAN FOREST FIRE HISTORY

A. Eichler, S. Brütsch (PSI), S. Olivier (PSI & Univ. Bern), W. Tinner (Univ. Bern Plant Sci.), T. Papina (IWEP), M. Schwikowski (PSI & Univ. Bern)

A 750 years history of Siberian wildfires was reconstructed from trace species and charcoal concentrations in an ice core from the Siberian Altai. No long-term trend is found for the forest fire activity so far, but a period of strongly increased frequency around 1600-1670. The reasons are most probably exceptionally dry conditions in the period 1550-1600 and increased temperatures.

Emissions from biomass burning impact the radiation and CO_2 budget of the Earth and, hence, regional and global climate. In this study we reconstruct the fire history in Siberia during the past 750 years from trace species and charcoal concentrations in an ice core from Belukha glacier in the Siberian Altai.

Principal Component Analyses (PCA) on the decadal concentration means of all chemical species was performed in the time period 1250-1940 to investigate the main emission sources in the pre-industrial period [1]. PC1 and PC2 show high loadings of dust related ions (e.g. Ca^{2+}) and species released in the atmosphere by direct biogenic emissions (e.g. NH_4^+), explaining 50% and 23% of data variance, respectively. High loadings of K^+ and NO_3^- were observed in PC3 (11% of data variance explained). During forest fires, nitrogen oxides are formed that are rapidly converted into HNO_3 and NO_3^- aerosol [see e.g. 2,3]. Many studies have demonstrated that potassium is a tracer for biomass burning [e.g. 3-5].

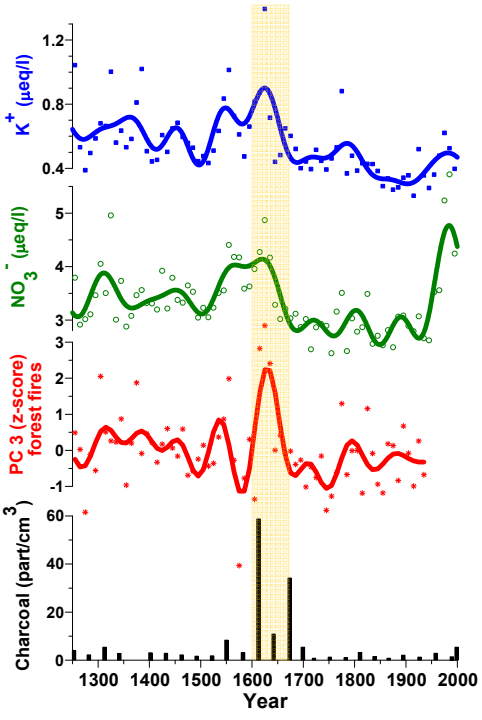

Fig. 1: Ice core records of K^+, NO_3^-, PC3 (10-year averages – individual symbols, 80-years lowpass filtered data – bold line), and charcoal (bars). The period of increased forest fire frequency is marked in yellow.

Records of K^+, NO_3^-, and PC3 in the preindustrial period reveal no long-term trend, but strong short-term variations and a maximum between about 1600 and 1670. The strong increase of the NO_3^- concentrations in the industrial period after 1940 is due to enhanced anthropogenic NO_x emissions in Eastern Europe and Russia mainly from traffic [1]. We relate the observed maximum 1600-1670 to a strongly enhanced fire activity in this period. An independent direct proxy for fires are microscopic charcoal particles in the ice. Indeed, markedly higher charcoal concentrations were measured in the samples taken from the ice core part that covers the period of geochemically-inferred higher forest fire frequency (Figure 1).

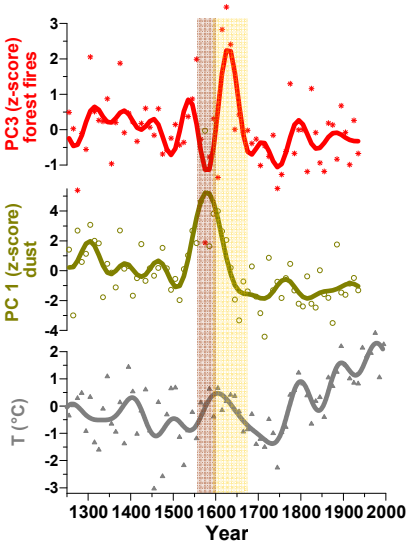

Fig. 2: Ice core records of PC3, PC1, and temperature (10-year averages – individual symbols, 80-years lowpass filtered data – bold line). The maxima in dust and forest fire frequency are marked in brown and yellow.

The cause of the strong increased frequency of forest fires 1600-1670 is most probably a preceding dry period 1550-1600 marked by a maximum in dust (PC1, Figure 2). Exceptionally dry conditions led to forest dieback (recorded in pollen records [6]) and the formation of dead biomass. The increased temperatures around 1600 may have initiated and favoured the expansion of forest fires. However, the increasing temperatures in the last 200 years did not cause an enhanced forest fire activity.

REFERENCES

[1] A. Eichler et al., Geophys. Res. Lett., **36**, doi: 10.1029/2009GL038807 (2009).
[2] R.M.B. Cerón et al., Atmos. Environ., **36**, 2367 (2002).
[3] C.H. Song et al., J. Atmos. Chem., **51**, 43 (2005).
[4] J. Paatero et al., J. Radioanal. Nucl. Chem., doi : 10.1007/s10967-009-0254-9 (2009).
[5] S. Owega et al., Atmos. Environ., **38**, 5545 (2004).
[6] A. Eichler et al., this report, p. 30.

ACKNOWLEDGEMENT

This work was supported by the SNF, Marie Heim-Vögtlin program, Grant no. PMPD2-110174.

PALEOECOLOGICAL ANALYSIS OF A SIBERIAN ALTAI ICE CORE

A. Eichler (PSI), W. Tinner (Univ. Bern Plant Sci.), T. Papina (IWEP), M. Schwikowski (PSI & Univ. Bern)

Pollen records of an ice core from Belukha glacier were used to reconstruct the vegetation history during the past 750 years in the high-altitude Siberian Altai region. Pollen data suggest the predominance of steppe and meadow vegetation. A distinct decline of trees (forest) and an advance of herbs and shrubs (steppes, semi-deserts) were observed in the period 1550-1670. This is in response to dry conditions 1550-1600 and a high fire activity 1600-1670. Our results are in good agreement with pollen and charcoal records from the 150 km distant lake Teletskoye.

Analyses of pollen in natural archives provide a unique tool to reconstruct the regional vegetation history. In our study we use an ice core from Belukha glacier to reconstruct vegetation changes during the past 750 years in the high-altitude Siberian Altai.

Pollen slides were prepared using 300-500 g ice core sample and the different pollen types and charcoal particles counted following standard procedures [1,2]. Altogether we analysed 26 ice core samples with one sample covering a time period of 2-5 years. Concentrations of the main pollen types (see Figure 1) range from 100 to 10 000 grains l^{-1}, which is in agreement with other ice core studies [3].

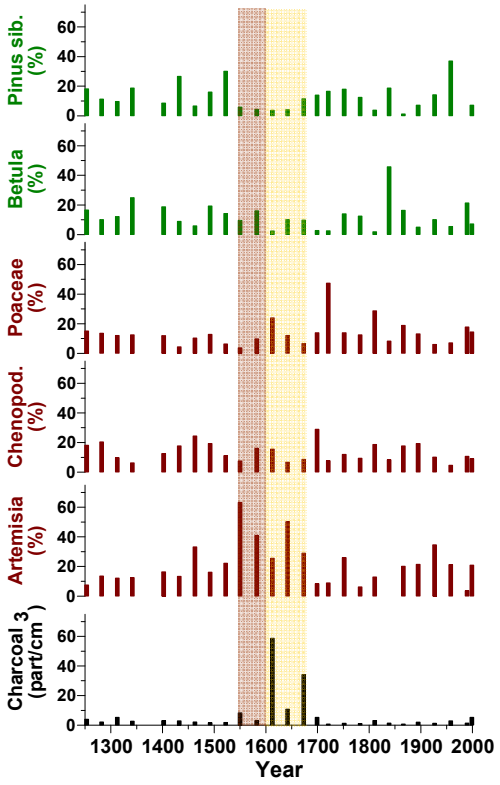

Fig. 1: Ice core pollen diagram (herbs and shrubs – brown, trees – green) and charcoal record (black). Periods marked by high dust content and strongly increased forest-fire frequency are marked in brown and yellow, respectively.

Pollen data suggest the predominance of steppe and meadow vegetation. The pollen diagram is characterized by a high percentage of *Artemisia*, Chenopodiaceae, and Poaceae pollen. Tree pollen are dominated by *Pinus sibirica* and *Betula* (Figure 1). This result is in agreement with pollen data from a 2.4 m Belukha [3].

Remarkable features in the pollen records are a distinct decline of *Pinus sibirica* and a strong advance of the *Artemisia* in the period 1550-1600. During this time maximum dust concentrations occurred [4]. After the exceptionally dry phase, the time period 1600-1670 revealed the highest forest-fire activity of the last 750 years. This lead to further decline of *Pinus sibirica* and *Betula* forests and an advance of steppic Poacea and *Artemisia*.

Belukha pollen and charcoal records were compared with sediment core data from the 150 km distant lake Teletskoye (Figure 2). Here, Siberian-pine (*Pinus sibirica*) taiga dominated the vegetation during the last millennium [5]. Distinct charcoal maxima between 1550 and 1700 confirm the regional scale of increased fire activity recorded in the Belukha core. In agreement, during the period of increased forest fire activity, forests (tree pollen) declined and steppic vegetation (herbs and shrubs) expanded also at lake Teletskoye.

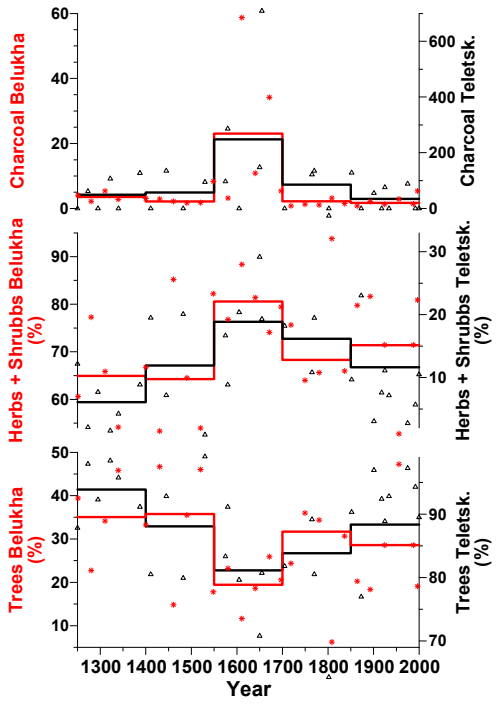

Fig. 2: Pollen diagram and charcoal record from Belukha glacier (red) and lake Teletskoye [5] (black). Shown are individual samples (symbols) and 150-year means (lines).

REFERENCES

[1] P.D Moore et al., Pollen Analysis (1991).
[2] W. Tinner and Hu, Holocene, **13**, 499 (2003).
[3] F. Nakazawa et al., J. Glaciol., **51**, 483 (2005).
[4] A. Eichler et al., this report, p. 29.
[5] A.A. Andreev et al., Quat. Res., **67**, 394 (2007).

ACKNOWLEDGEMENT

This work was supported by the SNF, Marie Heim-Vögtlin program, Grant no. PMPD2-110174.

FIRST ICE CORE FROM THE MONGOLIAN ALTAI

M. Schwikowski, H.W. Gäggeler, P.-A. Herren, B. Rufibach, M. Schläppi, M. Sigl (PSI), H. Machguth (Uni Zürich), T. Papina, N. Malygina, E. Mitrofanova, T. Uskov (IWEP)

In June 2009 an ice core was extracted from an ice cap in the Tsambagarav mountain range, Mongolian Altai. Due to the low precipitation rates in this area, this ice core is assumed to contain about 1000 years of climate information. The core is being analyzed at PSI in order to obtain climate records for the medieval and earlier periods and to verify the sensitivity of the temperature response in this region to changes in sun activity.

In order to place recent climate change in a longer term context the reconstruction of climatic variations on annual, interannual, and decadal time scales of the last 1000 years is a priority target in current climate research. A region with particularly poor data coverage is Central Asia, which experiences strong warming due to its high continentality. For the Siberian Altai a temperature increase of 3.2±1.7°C between the Maunder minimum and the end of the 20th century was reconstructed by our group using an ice core $\delta^{18}O$ record from Belukha glacier (49°48'N, 86°35'E) [1]. A major result from that core was that temperatures showed an exceptionally high correlation with reconstructed solar activity in the pre-industrial period 1250-1850 AD [1, 2].

The Altai is especially suited for finding a glacier which records temperature, since it is the northern most mountain range in Central Asia, experiencing highest continentality and a negligible monsoonal influence. This is in contrast to many other ice core sites in Central Asia, located on the Tibetan Plateau, where $\delta^{18}O$ is mainly controlled by precipitation amount. However, there are only very few glaciers in the Altai which might fulfill the requirements for ice core drilling, such as flat topography and sufficient altitude to prevent melt water influence. The most promising glaciers are located in the Mongolian Altai. Due to a pronounced West-East gradient in precipitation, accumulation rates in the Mongolian Altai reach only 50% of Belukha glacier 335 km to the west. Thus, glaciers might contain records covering a longer time period than Belukha ice core. The aim of our project was therefore to obtain an ice core, suitable for palaeo climate reconstruction, from the Mongolian Altai.

As drilling site one of the ice caps in the Tsambagarav range (4140 m asl, 48°39.338'N, 90°50.826'E) was selected (Fig. 1). From 20 June to 14 July 2009 our joint Swiss-Russian expedition (Fig. 2) extracted a 72 m ice core to bedrock and a 52 m parallel core. In addition, during the one week spent on the glacier (3-10 July), a detailed ice thickness survey with ground penetrating radar (GPR) was conducted, ice temperatures in the borehole were measured, and samples from a snow pit were collected. Ice cores were shipped to PSI in frozen condition where they are being analyzed for trace species concentrations and stable isotope ratios [3].

Fig. 2: Expedition team in front of the helicopter at base camp (3000 m asl, Photo H. Machguth).

REFERENCES

[1] A. Eichler, A. S. Olivier, K. Hendersen, A. Laube, J. Beer, T. Papina, H.W. Gäggeler, M. Schwikowski, Geophys. Res. Lett. **36**, L01808, doi:10.1029/2008GL035930 (2009).

[2] A. Eichler, S. Brütsch, S. Olivier, T. Papina, M. Schwikowski, Geophys. Res. Lett. **36**, L18813, doi:10.1029/2009GL038807 (2009).

[3] P.-A. Herren et al., this report, p. 32.

ACKNOWLEDGEMENTS

This project was supported by the Swiss National Science Foundation (200021_119743) and the Russian Academy of Sciences (Integration project No. 92 of SB RAS and project 16.12 of Presidium RAS). We are much indebted to Sergey Mironov, Chairman of the Council of the Federal Assembly of the Russian Federation for assistance in organizing our expedition and to the Federal Security Service of the Russian Federation for flying us safely to the glacier. The help of Dr Beket from the Social Economy Research Center in Bayan-Ulgii, Mongolia, and V. Morozova from IWEP is highly acknowledged.

Fig. 1: View from the drilling site to the camp and the ice capped mountains of the south-eastern part of the Tsambagarav range (Photo H. Machguth, http://itsfish.ch/selection.php?sel=0&put=8&sec=1).

FIRST RESULTS FROM AN ICE CORE OF THE MONGOLIAN ALTAI

P.-A. Herren, H.W. Gäggeler, B. Rufibach, M. Schläppi, M. Sigl, M. Schwikowski (PSI & Univ. Bern)
H. Machguth (Uni Zürich), T. Papina, N. Malygina, E. Mitrofanova, T. Uskov (IWEP)

The upper 12 m of the ice core from the Tsambagarav glacier in the Mongolian Altai show fluctuations in the ammonium concentration, which are attributed to seasonal variations. The resulting accumulation rate of 0.26 m weq per year agrees with previous estimations for this region and suggests that the ice core may contain climate information of the last millennium.

We analyzed the upper 12 m of the new Mongolian ice core [1] for major ions and stable isotopes ($\delta^{18}O$). Standard methods such as ion chromatography and stable isotope mass spectrometry were applied.

The abundance of ice lenses formed by refreezing of melt water in the upper 12 m is noticeable in the new core. With increasing depth their occurrence declines significantly. The irregular distribution of the ice lenses with depth indicates climatic changes during the last decades.

Concentrations of major ions reveal different characteristics with depth (Fig. 1). As shown by chloride, sulphate, potassium, magnesium, and calcium and expected from the occurrence of ice lenses, a relocation by melt water percolation of the ions is clearly visible. Ammonium is weakly affected by percolation and thus distinct seasonal variations are visible. It is best suited to evaluate the age of the ice by layer counting. Our first age estimation based on a five point moving average applied on the ammonium concentration is 21 years ± 2 years for the first 5.5 m weq of the ice core.

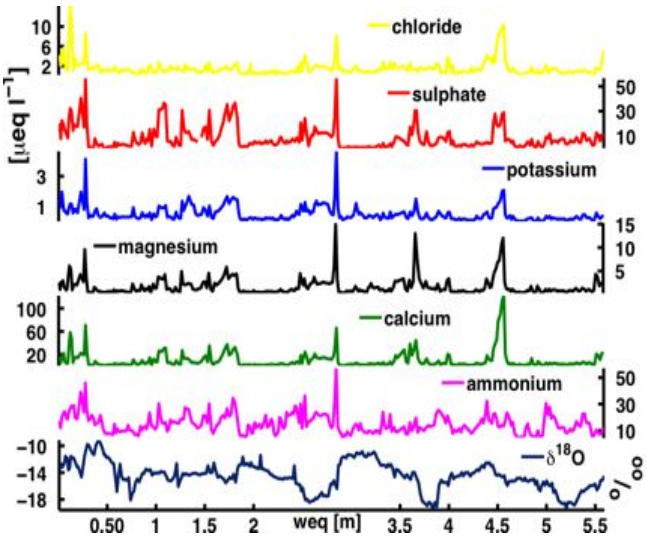

Fig. 1: Concentration of the major ions and evolution of $\delta^{18}O$ with depth of the ice core drilled in the Tsambagarav mountain range.

Dust layers have been recognized while processing the ice and are clearly seen in the ion concentrations at 2.89 m weq. The source of the dust will be inspected and a comparison with dust layers found on Belukha glacier will be done.

The stable isotope ($\delta^{18}O$) record does not show seasonal variations (Fig. 1). This indicates little winter precipitation and a smoothing of the signal by diffusion. Most of the accumulation is occurring in summer, since winter air temperatures are too cold due to the strong continental climate to transport water vapour. The amplitude and the mean value of the $\delta^{18}O$ record agree with values from a previous short core from the same mountain range. The two records have a similar evolution with depth [2].

Temperatures in ice are defined by mean air temperature, thermal diffusion, percolating melt water, and latent heat exchange processes. The temperature in the borehole is below -12°C, so percolating melt water refreezes within the top layers. Elevated temperatures between 8 and 20 m suggest the release of latent heat due to refreezing. Geothermal heat explains the increased temperature close to the bedrock (Fig 2).

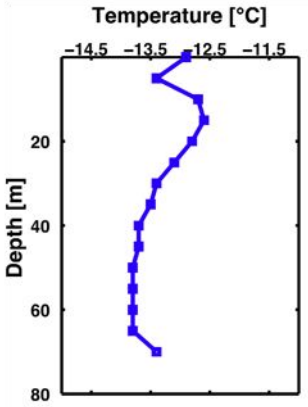

Fig. 2: Evolution of the ice temperature with depth.

Our accumulation based on the age estimation is 0.26 ± 0.01 m weq per year for the first 10 m of ice and agrees with values of a short core drilled in 1991 (0.25 m weq, [2]). This low accumulation let suppose that the ice core contains approximately one millennium of climate information.

For more precise dating, tritium will be analysed to locate the 1963 bomb peak and ^{210}Pb will be measured. Insects captured in the ice matrix will be used for ^{14}C dating.

Parallel to $\delta^{18}O$ temperature reconstruction, an additional temperature reconstruction based on the melt percent will be performed analogous to the Belukha ice core [3].

ACKNOWLEDGEMENT

This project was supported by the Swiss National Science Foundation (200021-119743).

REFERENCES

[1] M. Schwikowski et al., this report, p. 31.
[2] U. Schotterer et al., Clim. Change **36,** 519 (1997).
[3] K. Henderson et al., Geophys. Res. **111** doi: 10.1029/2005JD005819.

RECENT INCREASE IN BLACK CARBON CONCENTRATIONS FROM A MT. EVEREST ICE CORE SPANNING 1860-2000 AD

S. Kaspari (CWU & PSI), M. Schwikowski (PSI & Uni Bern), M. Gysel (PSI/LAC), P. Mayewski (Univ. Maine), S. Kang (ITP, China)

Black carbon increased threefold from 1970-2000 relative to 1860-2000 AD. This increase is likely associated with intensified atmospheric warming in this region, and may contribute to glacier retreat by reducing glacier albedo.

Black carbon (BC) produced by the incomplete combustion of biomass, coal and diesel fuels can significantly contribute to climate change by altering the Earth's radiative balance. BC in the atmosphere absorbs light and causes atmospheric heating, whereas BC deposited on snow and ice can significantly reduce the surface albedo, resulting in rapid melting of snow and ice [1]. Historical records of BC concentration and distribution in the atmosphere are needed to determine the role of BC in climate change. Reconstructing BC concentrations in Asia is particularly important because this region has some of the largest BC sources globally, which can negatively impact climate, water resources, agriculture and human health. Interest in BC in the Himalayas has recently increased due to concerns that BC is contributing to glacier retreat via atmospheric heating and BC deposition on glacier surfaces. We analyzed a 108 m ice core collected from the col of the East Rongbuk glacier located on the northeast ridge of Mt. Everest (28.03 N, 86.96 E, 6518 m) for black carbon using a Single Particle Soot Photometer (SP2) [2].

The high-resolution BC data demonstrates strong seasonality (Fig. 1), with peak concentrations during the winter-spring due to peak emissions from biomass burning and fossil fuel emissions and dry conditions that prolong the residence time of BC in the atmosphere. During the summer monsoon season BC concentrations are low due to wet removal of BC and lower BC emissions.

BC concentrations from 1975-2000 relative to 1860-1975 have increased approximately threefold (Fig. 2). The timing of this increase is consistent with BC emission inventory data from South Asia and the Middle East, however, the ice core record does not indicate a continual increasing trend since 1990 as seen in the emission inventory. It is notable that there is no increasing trend in iron (used as a proxy for dust) since 1860. This is significant because it suggests that if the recent retreat of glaciers in the region is due, at least in part, to the effect of impurities on snow albedo, the reduced albedo is due to changes in BC emissions, not dust.

The increase in BC concentrations since 1970 in the Mt. Everest ice core supports that BC from anthropogenic sources is being transported to high elevation regions of the Himalayas. The atmosphere in the Himalayas naturally has a high dust loading, resulting in deposition of dust on Himalayan glaciers. BC is estimated to be fifty times more efficient than dust in reducing the snow albedo [3]. Further work is needed to determine if BC deposition on Himalayan glaciers is substantial enough to alter the energy balance of glaciers and contribute to glacial melt.

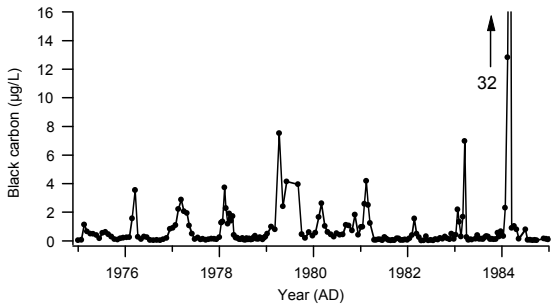

Fig. 1: High resolution BC from the Everest ice core.

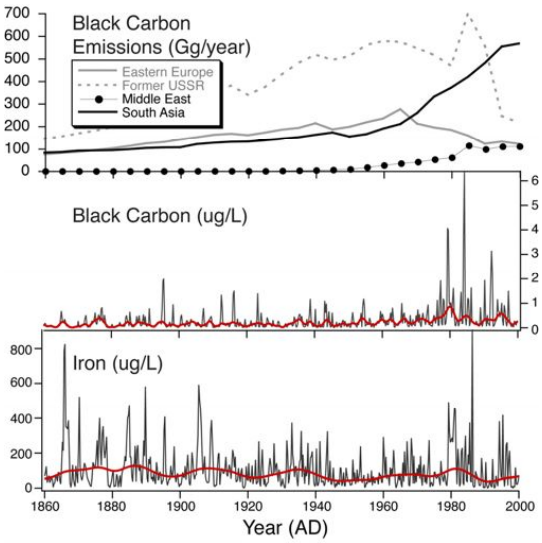

Fig. 2: BC emission data [4]; Everest ice core BC, and iron (used as a proxy for dust) [5]. The ice core data is resampled to 4 samples per year due to differences in sampling resolution, and smoothed with a robust spline.

ACKNOWLEDGEMENT

S. Kaspari is supported by the US NSF International Research Fellowship Program.

REFERENCES

[1] V. Ramanathan and G. Carmichael, Nature Geoscience **1**, 221-227, (2008).

[2] J. P. Schwarz et al., J. Geophysical Research **111**, doi:10.1029/2006JD007076, (2006).

[3] S. Warren and S. Wiscombe, Journal of Atmospheric Sciences **37**, 2734 (1980).

[4] T. Bond et al., Global Biogeochemical Cycles **21**, doi:10.1029/2006GB002840 (2007).

[5] S. Kaspari et al., Journal of Climate **22**, doi:10.1175/2009JCLI2518.1 (2009).

DATING OF THE ICE CORE FROM CERRO MERCEDARIO, CENTRAL ANDES

A. Ciric, H.W. Gäggeler, M. Schwikowski (PSI & Univ. Bern), L. Tobler, D. Piquet (PSI), J. Eikenberg (PSI), E. Vogel (Uni Bern), G. Casassa (CECS), R. Kipfer, M.S. Brennwald (EAWAG)

Dating was performed with annular layer counting supported by identification of reference horizons from volcanic eruptions and nuclear weapon test, resulting in a time span of 92 years (1913-2000) and a corresponding annual accumulation of 0.91 m weq.

For the climatic interpretation of ice cores an accurate dating is crucial. Several dating methods exist and are generally combined to reduce the dating uncertainty [1,2]. For the Mercedario ice core (104 m ice core, drilled on 6100 m a.s.l. in 2005, 31°58'S, 70°07'W [3]) a combination of annular layer counting (ALC) of seasonal varying parameters and reference horizons (volcanic and nuclear weapon test horizon) was applied. Major ions (Na^+, NH_4^+, K^+, Mg^{2+}, Ca^{2+}, F^-, $CH_3SO_3^-$, Cl^-, NO_3^-, SO_4^{2-}) were analyzed with ion chromatography, while tritium (T or ^3H) was indirectly determined via its decay product ^3He (^3He ingrowth method [4]).

All investigated major ions showed strong fluctuations, mostly in phase with the $\delta^{18}O$, indicating a pronounced seasonality at this site. The $\delta^{18}O$ signal and the concentrations of NH_4^+ showed strongest seasonal fluctuations over the entire ice core and were used for ALC (Figure 1). Minima (maxima) in the $\delta^{18}O$ signal and low (high) ion concentrations are assumed to correspond to austral winter (austral summer) and resulted in a time span of 92 years (1913-2004), yielding an annual accumulation of 0.91 m weq.

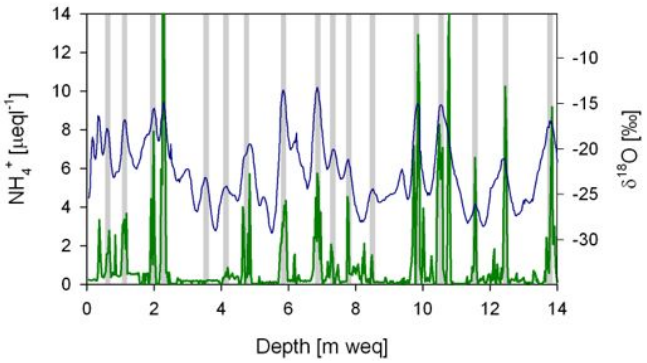

Fig. 1: NH_4^+ (green) and $\delta^{18}O$ (dark blue) profile of the upper 14 m weq of the Mercedario ice core. Attribution of annular layers is indicated by grey bars.

Volcanic layers of Pinatubo and/or Hudson (1991, Figure 2), El Chichón (1982) and Quizapu (1932) were identified using the concentrations of non-dust related excess SO_4^{2-} ($exSO_4^{2-}$), non-sea salt Cl^- (nss Cl^-) and F^-. Another stratigraphic marker is tritium originating from nuclear weapon tests. ^3H has widely been used in nuclear weapons for boosting a fission bomb or the fission primary of a thermonuclear weapon. The testing period in the 1950s and 1960s introduced large amounts of ^3H into the atmosphere, and hence into the water cycle. Figure 3 shows the obtained tritium record together with the attribution of the two Southern Hemisphere maxima 1960/61 and 1964/65.

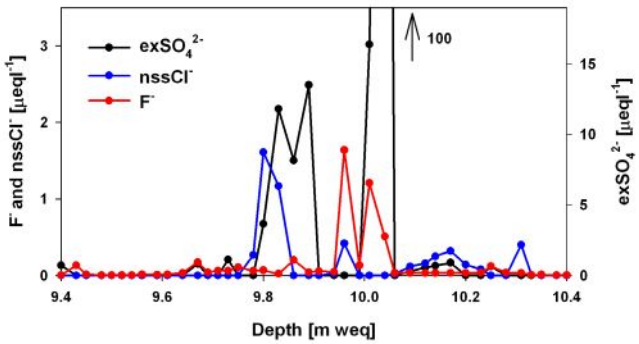

Fig. 2: Volcanic layer of Pinatubo and/or Hudson in 1991, indicated by increased concentrations of $exSO_4^{2-}$ (black), $nssCl^-$ (blue) and F^- (red).

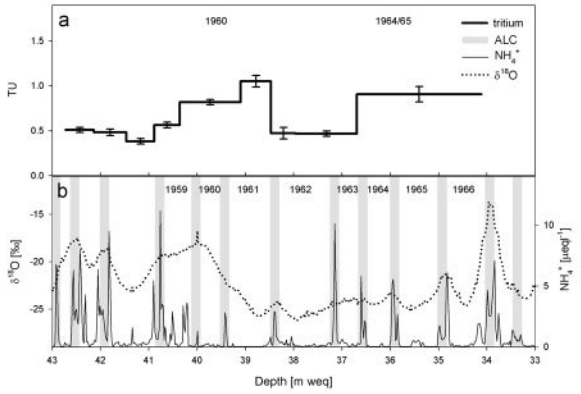

Fig. 3: a) Tritium profile of the Mercedario ice core between 33 and 43 m weq. b) Dating by annual layer counting using the NH_4^+ and $\delta^{18}O$ signal over the same depth interval.

All stratigraphic markers agree very well with the age-depth-relationship established by ALC of NH_4^+ and $\delta^{18}O$. By combining the ALC with the stratigraphic markers, the uncertainty is around ±1 years between the horizons, while at the bottom of the core; a maximum of ±3-5 years can be estimated.

ACKNOWLEDGEMENT

This work was supported by the Swiss National Science Foundation (200021-100289).

REFERENCES

[1] A. Eichler et al., J. Glaciol., **46**, 507 (2000).
[2] S. Knüsel et al., J. Geophys. Res. **108,** doi:10.1029/2001JD002028 (2003).
[3] A. Ciric, PhD thesis, University of Bern (2009).
[4] U. Beyerle et al., Environ. Sci. Tech., **34**, 2042 (2000).

ENSO RELATED ACCUMULATION VARIABILITY ON CERRO MERCEDARIO

A. Ciric, H.W. Gäggeler, M. Schwikowski (PSI & Univ. Bern)

Annual accumulation at La Ollada glacier on Cerro Mercedario is influenced by the El Niño Southern Oscillation and shows a similar year-to-year variability pattern as precipitation in Central Chile.

The climate of South America is irregularly altered by the El Niño-Southern Oscillation (ENSO), which is a climate phenomenon of the tropical Pacific having important consequences on climate and weather around the globe. The term "El Niño" was originally formed by fisherman from Peru and Ecuador (Spanish for "Christ child" or "Little Boy"), as they noticed an abnormal warming of the ocean current every few years, usually around Christmas.

In subtropical South America, between 28 and 35°S, El Niño events are associated with increased precipitation [1], which is probably due to a less pronounced anticyclone that allows the Westerlies to move further north. Figure 1 shows the rainfall anomaly of Santiago de Chile with major El Niño events of the recent past such as 1997, 1987, 1982 and 1972 [2].

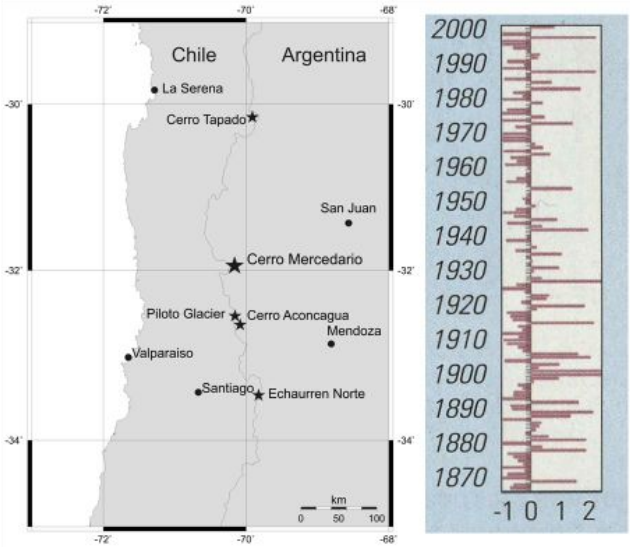

Fig. 1: Left: Map of Central Chile and Argentina with main cities (dots) and mountains/glaciers (stars). Right: Rainfall anomaly of Santiago [2].

In 2005, a 104 m ice core was recovered from Glaciar La Ollada on Cerro Mercedario (31°58'S, 70°07'W, 6100 m a.s.l.), covering 92 years (1913-2004) [3]. Accumulation at Cerro Mercedario varies between 0.3 and 1.8 m weq, with a mean accumulation of 0.91 m weq. This is high compared to Santiago de Chile (0.32 m, Central Valley), but as already pointed out by Schwerdtfeger [4] the amount of precipitation in the high elevation Andes can usually be of the order of three or four times the amount over the Central Valley at the same latitude. Nevertheless, the year-to-year fluctuation agrees well (r=0.42) and years with high accumulation generally corresponds to El Niño events (Figure 2). The ice core from Cerro Tapado (30°S, 5500 m a.s.l., 200 km north of Mercedario) revealed a net-accumulation between 0.1 and 1.03 m weq per year (mean 0.32 m weq per year, 1963-1999), but this glacier is located much closer to the South American Dry Diagonal and strongly influenced by sublimation. During some years, sublimation resulted in a loss of 84% of the total accumulation [5]. Mass balance data from Piloto Glacier at Cajón del Rubio (32°S, 4500 m a.s.l.) support the observed accumulation rate on Cerro Mercedario. There, mean total accumulation was 0.96 m weq yr^{-1} for the time period 1979-2002 [6]. Echaurren Norte (33°S, 3800 m a.s.l.), a glacier 50 km east of Santiago de Chile, shows even higher accumulation rates of 2.7 m weq yr^{-1} in the period 1975-2009 (data by World Glacier Monitoring Service, WGMS and G. Barcaza, personal communication). Both glaciers have high ablation rates as they are located at a lower altitude. As they are systematically monitored since 1975 and 1979, respectively, the accumulation history can be compared to the obtained accumulation record of Cerro Mercedario (Figure 3). Similar to Santiago the year to year fluctuation agrees well (Piloto Glacier: r=0.41), Echaurren Norte: r=0.33). In addition, Piloto Glacier and Mercedario show a decreasing trend since the mid 1980s, which is unincisive in the Santiago record.

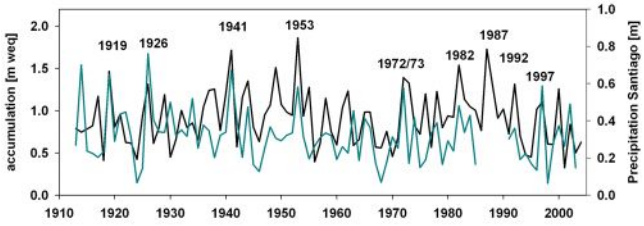

Fig. 2: Accumulation at Cerro Mercedario (black) in comparison to precipitation in Santiago (cyan).

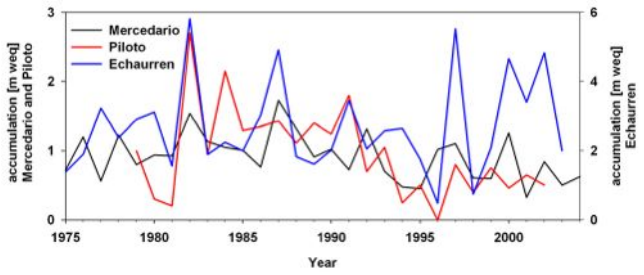

Fig. 3: Mercedario accumulation record in comparison to accumulation at Piloto Glacier (32°S, 4500 m a.s.l.) [6] and Echaurren Norte (33°S, 3800 m a.s.l.).

REFERENCES

[1] P. Aceituno, Mon. Wea. Rev., **116**, 505-524 (1988).
[2] L. Ortlieb et al. Pages News **10**, 14 (2002).
[3] A. Ciric et al., this report, p. 34.
[4] W. Schwerdtfeger, Climates of Central and South America, Elsevier Scientific Publishing Company (1976).
[5] P. Ginot et al., Clim. Past, **2**, 21 (2006).
[6] Leiva et al., Glob. Planet. Chang., **59**, 10 (2007).

ACKNOWLEDGEMENT

This work was supported by the Swiss NSF (200021-100289).

ENSO INFLUENCE ON MAJOR ION CONCENTRATIONS IN THE MERCEDARIO ICE CORE

A. Ciric, H.W. Gäggeler, M. Schwikowski (Univ. Bern & PSI), A. Eichler (PSI)

Temporal variability in major ion concentrations is strongly related to the El Niño-Southern Oscillation, as indicated by a high negative correlation between the Southern Oscillation Index and major ion concentrations.

The El Niño-Southern Oscillation (ENSO) is the most important coupled ocean-atmosphere phenomenon, which causes global climate variability on inter-annual timescales. Cerro Mercedario is located in subtropical South America, where El Niño events are associated with increased precipitation (between 28 and 35°S, [1]). In 2005, a 104 m ice core was extracted from Glaciar La Ollada on Cerro Mercedario (31°58'S, 70°07'W, 6100 m a.s.l.), covering 92 years (1913-2004) [2]. Ice core sections were processed in a cold room using well established decontamination techniques and analyzed for major ions (Na^+, NH_4^+, K^+, Mg^{2+}, Ca^{2+}, F^-, $CH_3SO_3^-$, Cl^-, NO_3^- and SO_4^{2-}).

A principal component analysis (PCA) was performed on the major ion dataset and revealed five factors, explaining 90% of the variability [3]. Factor 1 was dominated by Na^+, Cl^- and NH_4^+, and was attributed to a marine source, while factor 2 was dominated by mineral dust related ions such as Ca^{2+}, SO_4^{2-} und Mg^{2+} (hereby referred to PC1 and PC2). Each factor explained 28% of the variability, while factors 3 to 5 made only minor contributions and are not discussed. Although the PCA based on the single values revealed a clear separation of the ions according to their different sources, annual mean data are highly correlated and show a connection to ENSO (Figure 1). High ion concentrations correlate well with El Niño events when the Southern Oscillation Index (SOI) is negative (r=-0.73 and -0.71), but the correlation is weaker between 1913 and 1935, which is probably related to a higher dating uncertainty at the bottom of the ice core, but the SOI shows as well a low variability.

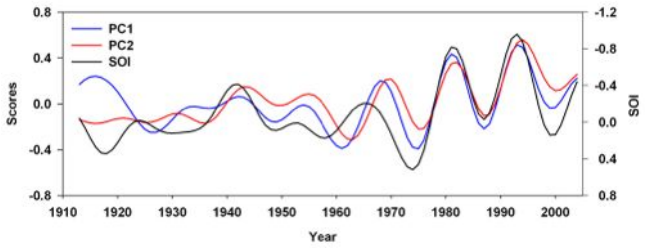

Fig. 1: SOI (black, reverse scale) in comparison to PC1 (blue) and PC2 (red) of the Mercedario ice core for the time period 1913-2004. Annual means smoothed with a 10-year lowpass filter.

During El Niño, the high pressure system located in the east Pacific Ocean is weakened, which in return allows the Westerlies to move further north, leading to higher precipitation amounts in Central Chile [1] and at the Mercedario site [4]. Increased precipitation generally results in depletion of aerosols in the atmosphere due to scavenging and to overall lower concentrations of trace components in precipitation. The observed inverse relationship might be explained by an enhanced transport of aerosols to the glacier, due to higher wind speeds (meridional and zonal) and deeper convection at high elevations (tested with the Climate Explorer of the Royal Netherlands Meteorological Institute (KNMI, http://climexp.knmi.nl)). This transport behavior may also explain the similarity between the records of PC1 and PC2.

ENSO does not have a single well-defined period, but instead occurs every 3-7 years [5], with an average of 3-4 years. A wavelet analysis was performed on PC1 and PC2 to investigate the stability of the periodicity over time and compared to the SOI (Figure 2). The wavelet power spectra are very similar and the frequencies between 3 and 6.4 (classical ENSO bandwidth) are relatively stable in time. The long-term frequency of 9-16 years between 1960 and 2004 is very well represented in both PCs and seems to be more intense than in the SOI. Wang et al. [6] associated the longer frequency with El Niño (12 year cycle) and La Niña (16 year cycle) activity (via spectral analysis of El Niño and La Niña indices), but this frequency might also result from the solar cycle (11 years).

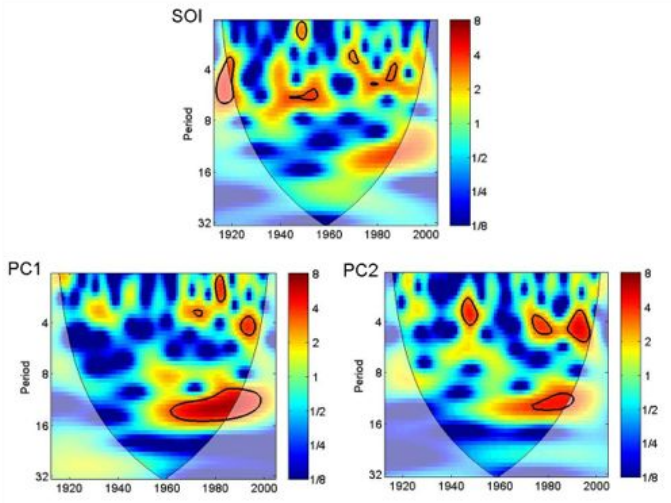

Fig. 2: Wavelet power spectrum of the annual means of SOI in comparison to PC1 and PC2 of the Mercedario ice core, together with a 95% confidence level (black line).

ACKNOWLEDGEMENT

This work was supported by the Swiss National Science Foundation (200021-10289).

REFERENCES

[1] P. Aceituno, Mon. Wea. Rev., **116**, 505 (1988).

[2] A. Ciric et al., this report, p. 34.

[3] A. Ciric, PhD thesis, University of Bern (2009).

[4] A. Ciric et al., this report, p. 35.

[5] P.J. Webster & T.N. Palmer, Nature, **390**, 562 (1997).

[6] X. Wang et al., Geophys. Res. Lett., **36** (2009).

ENSO INFLUENCE ON STABLE ISOTOPE RATIOS OF MERCEDARIO ICE CORE

A. Ciric, H.W. Gäggeler, M. Schwikowski (Univ. Bern & PSI), A. Eichler (PSI)

The stable isotope ratio $\delta^{18}O$ does not show a clear local temperature signal, instead, a connection to sea surface temperatures in the moisture source area and the Southern Oscillation Index during warm phases of the Pacific Ocean.

The El Niño-Southern Oscillation (ENSO) is a coupled ocean-atmosphere system rooted in the Pacific Ocean having important consequences on the South American continent (periodicity of 3-7 years) [1]. The Pacific Decadal Oscillation (PDO) and Inter-decadal Pacific Oscillation (IPO) are a long-lived pattern of Pacific climate variability with a mean periodicity of 20-30 years. PDO and IPO are often described to be ENSO-like, because the spatial fingerprint of the cold and warm phases is similar to those of El Niño and La Niña [2].

In 2005, a 104 m ice core was recovered from Glaciar La Ollada on Cerro Mercedario (31°58'S, 70°07'W, 6100 m a.s.l.), located in a El Niño sensitive region. The core covers 92 years (1913-2004) [3]. The ice core sections were processed in a cold room and analyzed for the stable isotope ratios $\delta^{18}O$ and δD.

The isotopic composition of water is commonly used as a proxy of local temperature. In Antarctica, a robust relationship exists between surface temperatures and the isotopic composition of snow [4]. When comparing annual mean $\delta^{18}O$ of the Mercedario ice core and temperature in Pudahuel (33°S, Santiago airport) the overall long-term pattern seem to be similar. However, the correlation is weak (r=0.14) and the year to year fluctuations in the $\delta^{18}O$ are too strong for being only local temperature controlled. The stable isotope composition is also affected by depletion during transport and washout (the so-called "amount effect", visible as by trend high annual accumulation is associated with lower $\delta^{18}O$ values in the Mercedario ice core) and by atmospheric convection ($\delta D/\delta^{18}O$ slope=8.38 and observation of convective clouds in the afternoon during the field campaigns in austral summer 2003, 2004 and 2005 [5]). Thus, no simple interpretation of the stable isotope ratios is possible.

However, ENSO generally combines these mentioned effects. Bradley et al. [6] reported a strong link between sea surface temperatures (SSTs) across the Equatorial Pacific, ENSO and the stable isotope ratio in ice cores from the tropical Andes and the Dasuopu Glacier in the Himalayas. For Mercedario this is only partly true, as the stable isotope ratio seems to be triggered by warm and cold phases in the Pacific (Figure 1,2). During the warm phase (reddish shaded period in Figure 1) a positive connection exists between El Niño events (SOI negative) and $\delta^{18}O$ (Figure 1) and between the $\delta^{18}O$ and SSTs in the moisture source area (along the Pacific shore, mainly approaching from southwest, Figure 2c, 1977-2004). During the cold phase this correlation breaks down (Figure 2b), or even the opposite correlation prevails. This is not caused by changes in the moisture source area (tested with air mass back trajectories) and therefore probably caused by massive changes in SSTs across the Pacific.

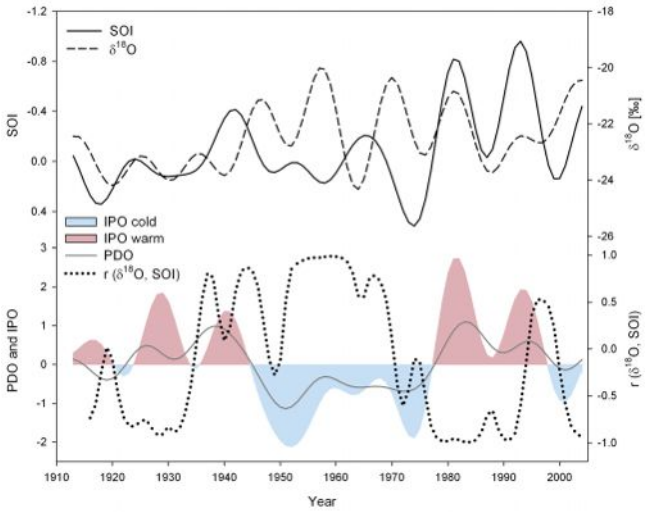

Fig. 1: Top: Mercedario $\delta^{18}O$ profile in comparison to the SOI. Bottom: 9-point moving correlation between SOI and $\delta^{18}O$ in comparison to the PDO and IPO (annual mean data smoothed with a 10 year lowpass filter). Cold (blue shaded) and warm (red shaded) phases of the Pacific Ocean are indicated (using the IPO index).

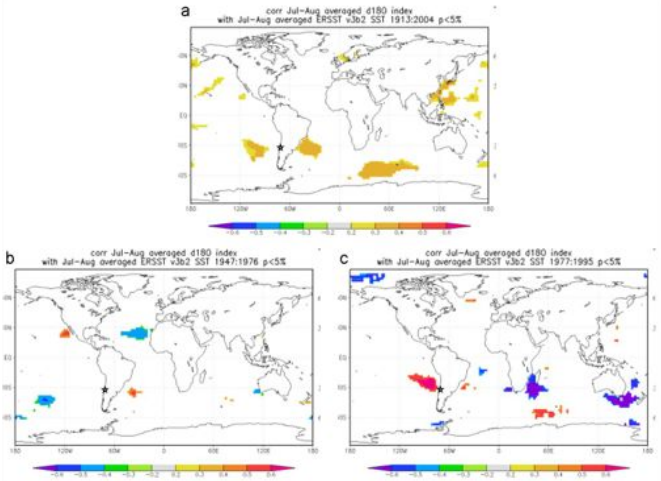

Fig. 2: Spatial correlation analysis of annual $\delta^{18}O$ values and July/August sea surface temperatures: a) for the time period 1913-2004, b) 1947-1976 (cold phase) and c) 1977-1995 (warm phase). Cerro Mercedario is marked with a star.

REFERENCES

[1] P.J. Webster & T.N. Palmer, Nature, **390**, 562 (1997).
[2] R.D. Garreaud & D.S. Battisti, J. Clim., **12**, 2113 (1999).
[3] A. Ciric et al., this report, p. 34.
[4] J. Jouzel et al., J. Geophys. Res., **108** (2003).
[5] D. Bolius et al., Ann. Glaciol., **43**, 14 (2006).
[6] R.S. Bradley et al., Geophys. Res. Lett., **30** (2003).

IDENTIFICATION OF TRACE ELEMENT SOURCES BY FACTOR ANALYSIS IN AN ICE CORE FROM CERRO MERCEDARIO

L. Tobler (PSI), A. Ciric, M. Schwikowski (PSI & Univ. Bern)

*Concentrations of trace elements were determined with the **C**ontinuous **I**ce **M**elting (CIM) **I**nductively **C**oupled **P**lasma **S**ector **F**ield **M**ass **S**pectrometry (ICP-SF-MS) in an ice core from the La Ollada glacier on Cerro Mercedario, Argentina. Factor analysis was applied to the data set of 34 elemental concentrations determined in this ice core in order to extract and interpret the factors causing the variability.*

INTRODUCTION

Factor analysis is a multivariate statistical method for the purpose of describing the relationships among many variables in terms of a few underlying and unobservable random quantities, called factors. It can be considered as an extension of Principal Components Analysis (PCA). Factor analysis provides a comprehensive view of complex interactions.

METHOD

Ice core segments from La Ollada glacier on Cerro Mercedario were analyzed for their elemental concentrations by CIM-ICP-SF-MS (Element1, Finnigan MAT) [1, 2, 3]. Concentrations of 34 elements from 2732 data points, corresponding to a depth resolution of about 0.8 cm, were used as input data for the factor analysis. Initial inspection of the data showed that the concentrations were lognormally distributed. Therefore, the concentrations were first transformed to their logarithmic values and standardized ($z_{ij}=(c_{ij}-C_j)/s_j$; c_{ij}: log concentration, C_j: log average concentration, s_j: log standard deviation of element j and data point i). Factor analysis by the principal components method with subsequent varimax-rotation was applied, using the statistical toolbox of the MATLAB® program. The goal of factor rotation is to find a parameterization in which each variable has only a small number of large factor loadings. That is, each variable is affected by a small number of factors, preferably only one.

RESULTS

Three factors were retained, which explain 86.6% of the variance. Additional factors would only give minor contributions to the explained variance. Factor 1 explains 49.6%, factor 2 22.3%, and factor 3 14.7% of the variance. The communality for a given element, which can be interpreted as the proportion of variation in that element explained by the three factors, is for most of the elements larger than 80%. Only for the two elements Cr and Ba, the communality is less than 70%. The loadings of factor 1 and factor 2 are shown in Fig. 1A. Elements with high loadings in factor 1 (i.e. Rb, Al, Cs, Zr, Th, U, Sc, Tl, Fe, V, and the rare earth elements; red circle) are attributed to soil-derived crustal material. Fig. 1B gives the loadings for factor 2 and 3. Factor 2 shows the highest loadings for Na, Cu, Sr and Ca in the range from 0.84 to 0.74 (blue circle), which is an indication for a contribution from sea water, due to the fact that Na, Ca, and Sr belong to the most abundant elements in sea water [4]. Mg, also abundant in sea water, shows the next highest loading (0.57) in factor 2. However, Mg, Ca, and Sr are also found in factor 1, hinting to a soil-derived origin. The higher loading for Cu in factor 2 is not clear at the moment. One possible explanation could be the transport of Cu from copper mines together with Na, Sr, and Ca from nearby saline lakes and salt crusts (called salars). The elements with higher loadings in factor 3 (green circle) might be influenced by anthropogenic activities or by volcanic activity. The remaining elements cannot be attributed to a single factor and are distributed among all three factors.

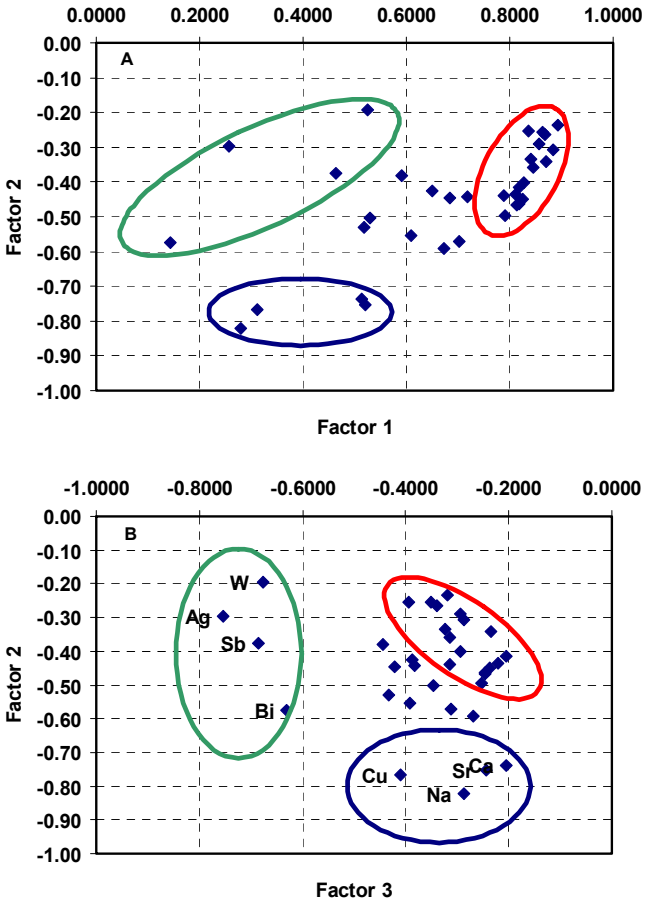

Fig. 1: Factor loadings of the elements for factor 1 and factor 2 (A), respectively factor 3 and factor 2 (B).

REFERENCES

[1] A. Ciric, PhD thesis, University Bern (2009).

[2] T. Kellerhals et al., Environ. Sci. Technol., in press, DOI: 10.1021/es902492n.

[3] L. Tobler et al, Ann. Rep. Lab. of Radio- & Environ. Chemistry, Uni Bern & PSI (2008), p. 29.

[4] B. Mason and C.B. Moore, Principles of Geo-chemistry, J. Wiley & Sons, 1982.

ANCIENT ICE IN THE ARID CENTRAL ANDES?

M. Schwikowski, A. Ciric, T. Kellerhals, M. Schläppi, (PSI & Univ. Bern), M. Buchroithner, A. Kleber (TU Dresden)

Ice discovered underneath a volcanic ash layer in the Valle de Barrancas Blancas (27°S) in the arid Central Andes of Chile was analyzed for its stable isotope composition to test the hypothesis that it is perennial, ancient ice.

The arid Central Andes are located in the transition zone between the tropical and extratropical circulation systems. Today, the core area of the mountain desert known as Arid Diagonal crosses the Andean range between 24°S and 26°S from northwest to southeast. Annual precipitation is in the range of 100 mm. Due to the lack of moisture, perennial snowfields and glaciers are basically absent in the area between about 20°S and 27°S even in the continuous permafrost belt above 5600 m. Precipitation on the western side of the Andes at 4000 m increases from 100 mm a^{-1} at 26°S to 400 mm a^{-1} at 30°S, and winter precipitation with Pacific moisture related cyclone activity becomes dominant [1 and references therein]. Equilibrium line altitudes (ELA) decrease from 5900 m at 27°S to 5300 m at 30°S.

During field work for mapping in the Valle de Barrancas Blancas in the area of Nevado Ojos del Salado (6893 m), El Solo (6190 m), and Nevado Tres Cruces (6748 m) at 27°S, ice was discovered at altitudes between 4900 and 5200 m (Fig. 1), underlying volcanic tephra. No historical eruptions are confirmed for these volcanoes. One sample of overlying pumice yielded preliminary Ar-Ar ages of 0.44±0.10 and 0.62±0.15 Ma (thanks to Johann Genser, Salzburg University). Thus, the question arose if the ice is ancient.

In order to test this hypothesis, samples were collected from ice and snow layers in March 2008, and from snow layers, penitents, melt water, and surface water in February 2009. Samples were analyzed for $\delta^{18}O$ and δD using stable isotope mass spectrometry.

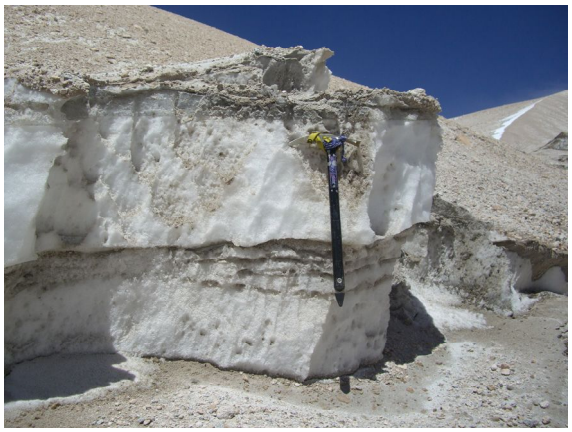

Fig. 1: Ice underneath ash layer in the Valle de Barrancas Blancas.

Results are presented in Fig. 2 in a plot of δ^2H versus $\delta^{18}O$. Samples from the Valle de Barrancas Blancas (BB) were classified into snow/ice and surface waters and compared to the Global Meteoric Water Line (GMWL) and to annual averages from Mercedario ice core (6100 m a.s.l., 32'S) over the time period 1913-2004 [2]. BB surface waters show the displacement of the isotopic composition from the GMWL typical for evaporative loss in arid areas (lower slope), see schematic in Fig. 3. BB snow/ice samples have a similar slope as the GMWL, but a higher y-axis intercept, indicating an arid water vapour source. Slope and intercept of BB snow/ice and Mercedario annual averages are the same, with generally lower values at Mercedario. This is reasonable since Mercedario samples are from higher altitude and higher latitude, both favouring cooler conditions, resulting in more negative δ^2H and $\delta^{18}O$ values. The similarity in the isotopic composition of ice and snow samples from Valle de Barrancas Blancas and Mercedario is an indication of a modern age of the ice, since glacial ice has more negative δ^2H and $\delta^{18}O$ values. A possible mechanism is that winter snow is immediately covered by tephra, which is redistributed by strong winds. The tephra layer prevents evaporation and seasonal snow is preserved. Partial melting and compression enhances snow to ice metamorphosis.

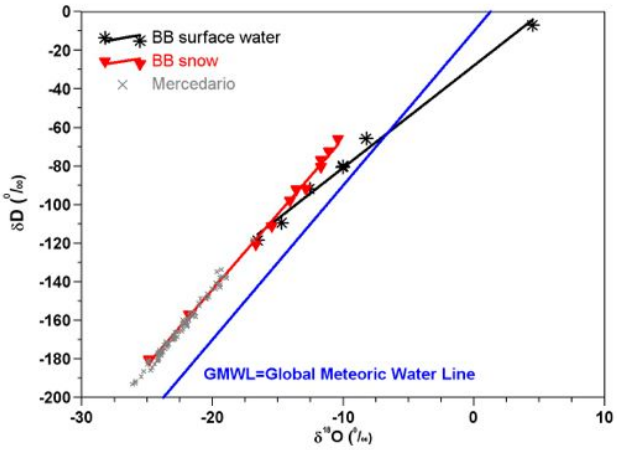

Fig. 2: Plot of δ^2H versus $\delta^{18}O$ of snow/ ice samples from Valle de Barrancas Blancas (BB), surface waters, and annual means from Mercedario ice core.

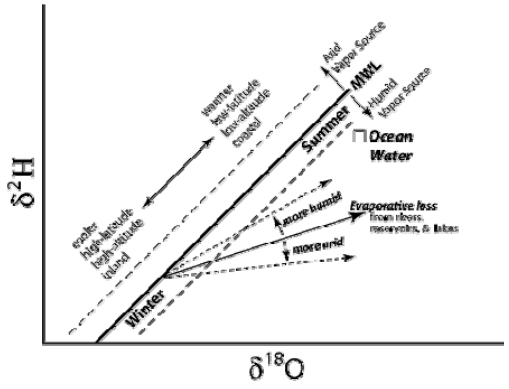

Fig. 3: Schematic plot of δ^2H and $\delta^{18}O$ variations and related processes, adapted from [3].

REFERENCES

[1] C. Kull et al., Climatic Change **52**, 359 (2002).
[2] A. Ciric, PhD thesis University of Bern (2009).
[3] J.J. Gibson et al., In: J.B. West et al. (eds.), Isoscapes: Understanding movement, pattern, and process on Earth through isotope mapping, DOI 10.1007/978-90-481-3354-3_18, Springer (2010).

BLACK CARBON CONCENTRATION IN PIO XI ICE CORE, SOUTHERN PATAGONIAN ICE FIELD

M.Schläppi (Univ. Bern & PSI), G. Casassa, A. Rivera (CECS), M. Gysel (PSI, LAC), M. Schwikowski (PSI & Univ. Bern)

Black Carbon (BC) from fossil fuel and biomass burning strongly influences global climate. Here, first results of BC concentration in snow/ice from the Southern Hemisphere outside Antarctica are presented, showing very low concentration levels ranging from 10 ngL^{-1} to 75 ngL^{-1}.

INTRODUCTION

Black Carbon (BC) is a byproduct of incomplete combustion of biomass and fossil fuels and contributes direct to global warming due to absorption of sunlight [1]. In addition there is an indirect effect on climate due to its impact on snow albedo when black carbon is deposited on glacier surfaces [1]. Despite its importance concerning climate forcing little is known about global concentration distribution and emission histories especially from the Southern Hemisphere. We therefore analyzed BC concentrations in the upper part of Pio XI ice core [2]. To our knowledge this are the first BC in ice data from the Southern Hemisphere outside Antarctica.

METHOD

For determination of BC concentration a single particle soot photometer (SP2) was used. Central component in SP2 is a Nd:YAG laser which hits a dry aerosol flow. The resulting laser induced incandescence and light scattering of particles is detected by four avalanche photodiode detectors which are focused on the intersection of the aerosol jet and the laser beam (Fig. 1). Distinguishing between scattered light and light from incandescence allows determining size and mass of BC particles [3].

To analyze BC concentration in Pio XI ice core, samples were acidified with HNO_3 to 0.5 M. After sonification for 15 minutes samples were nebulized (CETAC, U5000AT$^+$). The produced dry aerosol was transferred with a particle free carrier gas to the SP2.

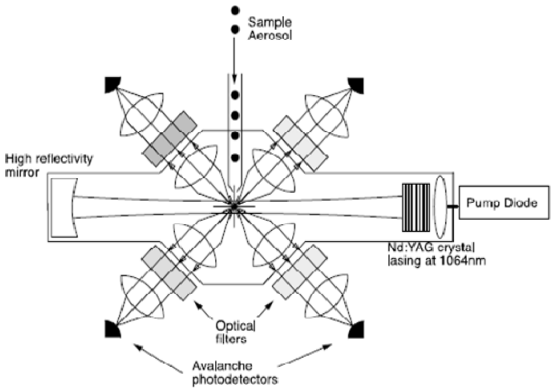

Fig. 1: Schematic of optical head of SP2 measurement system with laser components and detector optics (from [3]).

RESULTS

In Fig. 2 BC concentrations in Pio XI ice core are presented. Concentrations range from 10 ngL^{-1} to 75 ngL^{-1}, which is extremely low compared to other ice core studies. From Greenland concentrations of surface snow between 2.1 µgL^{-1} and 2.6 µgL^{-1} were reported [4], whereas ice cores showed concentrations between 1.1 µgL^{-1} [4] and 2.3µgL^{-1} [1]. In Antarctica average concentrations ranged from 0.2 µgL^{-1} near Amundsen-Scott South Pole Station [5] to 2.5 µgL^{-1} at Ross Ice Shelf [4]. Unfortunately, results are not directly comparable due to different methods used for analyzing BC concentrations [6].

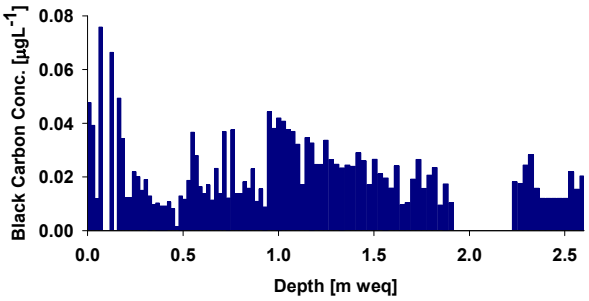

Fig. 2: Black carbon concentration of Pio XI ice core from 0 to 2.5 m weq.

BC concentrations in Pio XI ice core do not show seasonality and do not correlate to any ionic species (main source: sea spray [2]). The extremely low BC concentrations reflect the large distance to BC sources and a dilution of the atmospheric signal by heavy snowfalls. The preliminary BC in ice data represents clean Southern Hemisphere background conditions.

REFERENCES

[1] J. R. McConnell et al., Science **317**, 1381 (2007).
[2] M. Schläppi et al., Ann. Rep. Lab. of Radio- & Environ. Chemistry, Uni Bern & PSI (2008), p. 30.
[3] J. P. Schwarz et al., J. Geophys. Res. **111**, 16207 (2006).
[4] P. Chylek et al., J. Geophys. Res. **92**, 9801 (1987).
[5] S.G. Warren and A. Clarke, J. Geophys. Res. **95**, 1811 (1990).
[6] S. Kaspari et al., Ann. Rep. Lab. of Radio- & Environ. Chemistry, Uni Bern & PSI (2008), p. 24.

TRACE ELEMENT ANALYSIS IN FIRN CORES FROM PIO XI

L. Tobler, N. Millius (PSI), M. Ernst (Kantonsschule Olten), M. Schläppi, M. Schwikowski (PSI & Univ. Bern)

*The melting head used for the determination of trace elements in ice by **C**ontinuous **I**ce **M**elting (CIM) **I**nductively **C**oupled **P**lasma **S**ector **F**ield **M**ass **S**pectrometry (ICP-SFMS) was tested for melting and analyzing firn cores, because results from former experiments with a special firn melting head did not satisfy the requirements. For firn with densities above 0.65 g/cm^3 the ice melting head performed well.*

INTRODUCTION

The study of trace elements in ice cores provides a unique possibility to obtain information on changes of the atmospheric aerosol concentrations in the past. Continuous ice melting coupled to an ICP-SFMS (CIM-ICP-SFMS) is applied for trace element analyses in ice cores [1, 2]. However, the upper part of ice cores retrieved from glaciers consists mostly of firn for which this method is questionable and was not applied until now. Due to capillary forces in the porous firn, meltwater could be soaked up into upper layers of the firn above the melter and decrease the spatial resolution of the analyses. Furthermore, contaminated water from the core surface could reach the inner part of the firn core. Results obtained with a special firn melting head [3], which should avoid the above-mentioned problems, were not satisfying [4].

EXPERIMENTAL

The performance of the ice melting head for firn was tested by melting and analyzing firn cores from PIO XI [5]. Densities of the PIO XI firn cores were between 0.65-0.72 g/cm^3. Bars of 2.3 x 2.3 cm^2 cross section and a length of about 70 cm were cut out of the firn cores. The firn bar was placed in a plexiglas holder onto the melting head which was heated to 55°C. The produced melt water from the inner part of the core was acidified (~ 0.25 mol HNO_3) and taken up by a self-aspiring nebulizer of the APEX sample introduction system (Elemental Scientific Inc., Omaha, USA). The polyethylene filter normally put onto the inner outlet of the melting head was omitted, due to problems with the self-aspiration of the water, caused by the air bubbles trapped in the firn. The generated dry aerosol was analyzed in the ICP-SFMS (Element1, Finnigan MAT, Bremen, Germany) [2]. Mean resolution between data points was about 1.25 cm.
Parallel firn core segments were already analyzed by ion chromatography (IC) with a resolution of 4 cm [5].

RESULTS

The comparison of concentrations of Na, Mg, and Ca analysed with CIM-ICP-SF-MS and IC shows an excellent agreement (Fig.1). Smearing of the signal was not observed as the record of Na shows. The larger deviation for Ca between 29.1- 29.2 m can be explained by the fact that the end piece of this core section was badly positioned on the melting head. Furthermore, it has to be taken into account that the parallel cores used for the analyses are not real aliquots.
Na shows by far the highest concentrations, followed by Mg and Ca with values about one order of magnitude lower. These elements are also the most abundant cations in sea water (Na 30.6% Mg 3.7%, Ca 1.2%, Sr 0.03%) [6], which points to the dominance of sea spray as a source of impurities in this core. Sr, the next abundant cation in sea water, correlates very well with Mg (r=0.934, P<0.001, n=263), indicating the sea spray origin. Mg shows equal concentrations for both methods. This was not the case for other ice cores, where the CIM-ICP-SFMS results were higher due to the acidification of the samples, implying the dissolution of soil-derived particulates. Therefore, Mg in the PIO XI core was highly soluble, which further supports its sea spray origin. All other trace elements analysed in this core have very low concentrations, which confirm the remoteness of this site from anthropogenic sources.
Considering these results, the application of the ice melting head for firn analyses seems to be promising.

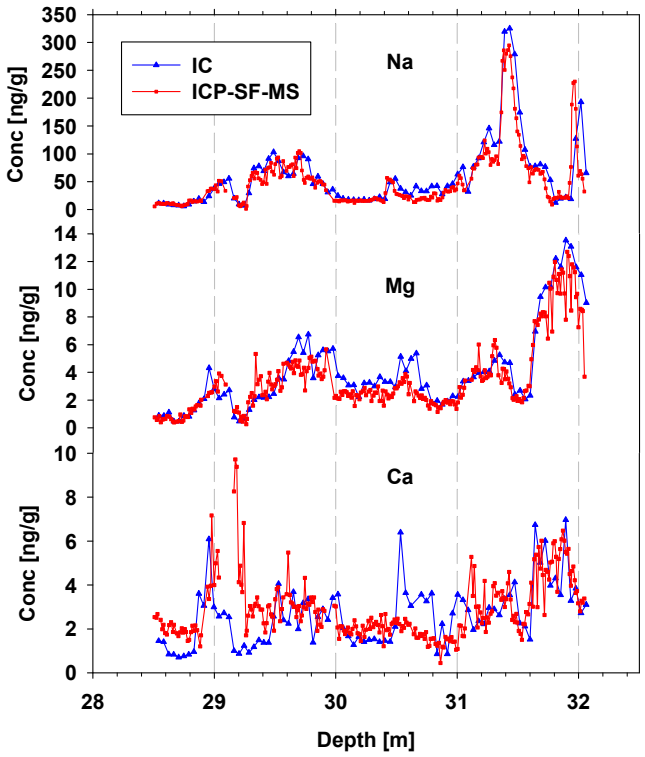

Fig. 1: Comparison of the IC (blue curve) and ICP-SF-MS (red curve) analyses for a firn core section from PIO XI.

REFERENCES

[1] S. Knüsel et al., Environ. Sci. Technol., **37**, 2267-2273 (2003).
[2] T. Kellerhals et al., Environ. Sci. Technol., in press, DOI: 10.1021/es902492n.
[3] R. Röthlisberger et al., Environ. Sci. Technol. **34**, 338-342 (2000).
[4] M. Schläppi et al., Ann. Rep. Lab. of Radio- and Environ. Chemistry, Uni Bern & PSI (2008), p. 32.
[5] M. Schläppi et al., Ann. Rep. Lab. of Radio- and Environ. Chemistry, Uni Bern & PSI (2007), p. 39.
[6] B. Mason and C.B. Moore, Principles of Geochemistry, J. Wiley & Sons, 1982.

A NEW SVALBARD ICE CORE

M. Schwikowski (PSI & Univ. Bern), A. Eichler, B. Rufibach (PSI), D. Stampfli (FS INVENTOR), C. Vega (UU), M. Björkman, G. Rotschky, E. Isaksson (NPI)

In March this year a new ice core was drilled at Lomonosovfonna, Svalbard. The goal is to reconstruct the development of black carbon in this part of the Arctic. Black carbon is an aerosol component assumed to be responsible for a large fraction of the Arctic warming and a faster retreat of glaciers.

Svalbard, which consists of a group of islands, is located in the north of Norway surrounded by the Arctic Ocean, Barents Sea, and North Atlantic. The archipelago ranges from 74 to 81°N and from 10 to 35°E. The islands comprise an area of 61,022 km², of which about 60% is covered by glacier. Three large islands are populated: Spitsbergen (37,673 km²), Nordaustlandet (14,443 km²) and Edgeøya (5074 km²).

The first ice core studies in Svalbard were conducted by groups from the Soviet Union (e.g. [1]) and Japan (e.g. [2]) on various parts of the islands. Even though several ice cores were drilled, very few have been studied in detail. The main problem with most of these previous Svalbard ice cores was determining how much of the original record had been altered by melting [3]. In general the results from these cores suggested similar major climatic trends as recorded in other ice cores from the Arctic, but many questions remained concerning the timing of events and shorter time scale changes. In many cases the dating was insufficient due to a combination of melting, crude sampling and few analyzed chemical species. However, one of the highest glaciers, Lomonosovfonna, indicated better preserved stratigraphy than the other sites on Svalbard, suggesting less influence from melting [4]. At this glacier a 121 m long ice core was drilled in 1997 by an expedition organized by the Norwegian Polar Institute (NPI). This core has been analyzed in great detail, giving insight into many aspects of the pollution and climate history of Svalbard (e.g. [5-7]). The assumption was confirmed that the Lomonosovfonna ice cap is less affected by melting.

Recently, Black carbon (BC) was suggested to be responsible for a large fraction of the Arctic warming and a faster retreat of glaciers (e.g. [8, 9]). Since no ice was left from the 1997 Lomonosovfonna core, and no ice core BC record exists from Svalbard, an ice coring expedition was conducted in March 2009 to drill a new core from that ice cap. The initial goal was obtaining an archive to study the development of black carbon in the Arctic.

During the 10-day expedition we drilled two new ice cores of 149 m and 37 m depth, respectively, at the Lomonosovfonna (1202 m asl, 78°49'24.4" N; 17°25'59.2"E) (Fig. 1). At 149 m the drill got stuck and was released by applying antifreeze. It is therefore not clear if bedrock was reached. A ground penetrating radar survey to measure glacier thickness is planned for spring 2010. Ice temperatures ranged from -1.8°C at 12 m depth to -2.2°C at 42 m depth, the deepest point were temperature was measured.

The 149 m ice core was shipped to PSI and is being analyzed for BC concentration and a variety of other components related to climate variability and pollution [10]. We estimate that it covers roughly the last 1000 years.

REFERENCES

[1] A. Tarrusov, In: R.S. Bradley, P.D. Jones, (Eds.), Climate since A.D. 1500. Routledge, pp. 505 (1992).
[2] Y. Fujii, et al., Ann. Glaciol. **14**, 85 (1990).
[3] R. Koerner, J. Glaciol. **43**, 90 (1997).
[4] F.G. Gordiyenko et al., Polar Geogr. Geol. **5**, 242 (1981).
[5] E. Isaksson et al., The Holocene **15**, 501 (2005).
[6] T. Kekonen et al., J. Geophys. Res. **110**, doi:10.1029/2004JD005223 (2005).
[7] D.V. Divine et al., J. Geophys. Res. **113**, doi:10.1029/2008JD010076 (2008).
[8] D. Shindell & G. Faluvegi, Nature Geosci. **2**, 294 (2009).
[9] J. R. McConnell et al., Science **317**, 1381 (2007).
[10] A. Eichler et al., this report, p. 43.

ACKNOWLEDGEMENT

The drilling was a collaborative campaign between the PSI and the Norwegian Polar Institute (NPI), Tromsø, Norway. We are much indebted to the NPI logistics, especially to Jörg Lenk.

Fig. 1: The camp with left the ice core drilling tent on Lomonosovfonna (Photo G. Rotschky).

FIRST RESULTS FROM A NEW SVALBARD ICE CORE

A. Eichler (PSI), B. Wyler (PSI & Univ. Bern), T. Martma (Univ. Tallinn), E. Isaksson (NPI), M. Schwikowski (PSI & Univ. Bern)

The upper 5.7 m (2.6 m w.eq.) of a new Svalbard ice core were sampled and analyzed. This core part was found to cover about four years. The $\delta^{18}O$ record shows a pronounced seasonal cycle with higher values attributed to summer snow, whereas concentration records of the chemical species tend to peak in winter/early spring. Average ion concentrations compare well with long-term records deduced from earlier studies at the Lomonosovfonna.

A new ice core was drilled at the Lomonosovfonna in Svalbard in March 2009 [1]. In this study we sampled the upper 5.7 m (2.6 m weq.) of this ice core and determined the concentrations of the water soluble ions in 97 samples using ion chromatography and the $\delta^{18}O$ ratio with isotope ratio mass spectrometry.

Due to the geographic location of Svalbard, the ice core chemistry is mostly influenced by sea-salt species (about 80%). Based on correlation analyses using the ion concentrations, chemical species were classified into four groups corresponding to their main sources:

(1) sea salt: Na^+, Cl^-, K^+, Mg^{2+}, SO_4^{2-};
(2) anthropogenic: NH_4^+, NO_3^-, SO_4^{2-};
(3) dust (transport with dust): Ca^{2+} ($HCOO^-$, $C_2O_4^{2-}$);
(4) marine biogenic: $CH_3SO_3^-$ (MSA^-).

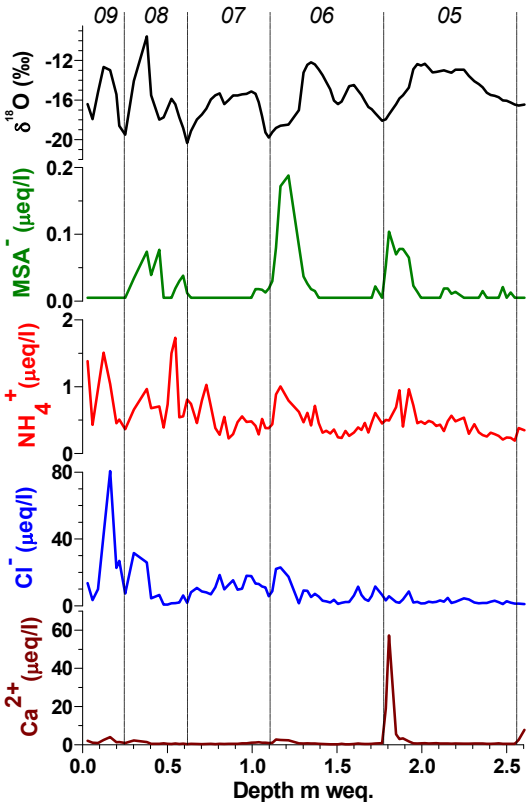

Fig. 1: Ice core records of $\delta^{18}O$ (black), MSA^- (green), NH_4^+ (red), Cl^- (blue), and Ca^{2+} (brown) together with a tentative dating (period 2005-2009).

The record of $\delta^{18}O$ shows distinct variations (Figure 1). Previous studies using another ice core from Lomonosovfonna [2,3] suggest that the long-term $\delta^{18}O$ record at this site can be related to temperature on a multiyear basis. Highest correlations were observed with temperature data from Longyearbyen and Vardø. Thus, we relate the $\delta^{18}O$ variations to seasonal fluctuations attributing high values to summer and low values to winter/early spring snow. However, this has to be proven by comparing the $\delta^{18}O$ record with atmospheric temperatures on a seasonal basis. We used the seasonal $\delta^{18}O$ signal for a first tentative dating, revealing that the investigated ice core part covers the period 2005-2009. The resulting annual accumulation rates of 0.4–0.75 m weq. compare well with mean accumulation rates for previous Svalbard ice cores (0.36-0.45 m weq. [3]). Concentration records of all chemical species tend to peak in winter/early spring (Fig. 1). This was already observed for ambient aerosols in Svalbard (e.g. sea-salt species, SO_4^{2-}) and explained by a higher frequency of storms, an enhanced transport efficiency, and Arctic haze pollution in the cold season [4]. However, MSA aerosol clearly peaks in summer [4]. Here, ice core maxima in winter can most probably be explained with percolation effects during melting processes [5].

The average concentrations of sea-salt and mineral-dust related ions deduced in this work (period 2005-2009) correspond very well with long-term values [6] (Figure 2). Trace species with anthropogenic sources (e.g. NO_3^-) and MSA reveal the same low level compared to the period 1990-1997.

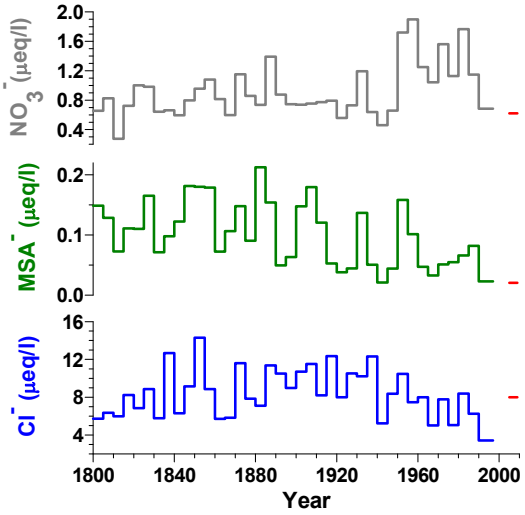

Fig. 2: Long-term records of NO_3^- (grey), MSA^- (green), and Cl^- (blue) (period 1800-1997) [6] together with the average of the period 2005-09 obtained in this work (red).

REFERENCES

[1] M. Schwikowski et al., this report, p. 42.
[2] E. Isaksson et al., J. Glaciol., **47**, 335 (2001).
[3] E. Isaksson et al., The Holocene, **15**, 501 (2005).
[4] J. Heintzenberg et al., Tellus B, **46**, 52 (1994).
[5] V.A. Pohjola et al., J. Geophys. Res., **107**, No. D4, 4036, 10.1029/2000JD000149 (2002).
[6] T. Kekkonen et al., J. Geophys. Res., **110**, D07304, doi: 10.1029/2004JD005223 (2005).

RADIOCARBON DATING OF ICE CORES FROM A DARK REGION IN THE WESTERN MELT ZONE OF THE GREENLAND ICE SHEET

I.G.M. Wientjes (IMAU), M. Schläppi (Univ. Bern & PSI), S. Fahrni, S. Szidat (Univ. Bern), M. Schwikowski (PSI & Univ. Bern), L. Wacker (ETHZ), R.S.W. van de Wal, J. Oerlemans (IMAU)

On satellite images a dark region can be seen in the western part of the Greenland ice sheet, which is thought to originate from outcropping layers of old dust. To confirm this hypothesis, ice cores were drilled in this dark region and carbonaceous aerosols in this ice were dated. The carbon concentration in most of the samples was too low for accurate dating. Samples that contained ice from directly below the ice surface were found to have high concentrations of modern aerosols. However, one sample taken at some depth below the surface was dated to an age of about 1000 to 2000 years, confirming our hypothesis.

INTRODUCTION

Satellite images show a region in the western part of the Greenland ice sheet that is darker than the surrounding ice, probably caused by higher concentrations of dust in the ice. During colder periods, more dust settles on the higher parts of the ice sheet. This dust travels through the ice sheet by the ice flow and crops out in the ablation zone, causing the dark region [1]. To confirm this hypothesis, carbonaceous particles in ice cores from this dark region were dated.

SAMPLES

The longest ice core (about 2 m) from the dark region, obtained at 66˚59.31' N, -49˚08.19' W (site 7), was divided into two samples, samples 3 and 4. Two smaller ice cores (about 0.8 m) from this region, both drilled at 67˚00.16' N, -48˚52.02' W (site 8), were treated as separate samples 1 and 2. Because the upper 15 cm of sample 2 contains cracks and holes, it was not further analysed. Therefore, only sample 1 and 3 contain ice from directly below the surface.

Another four samples were taken from ice that was drilled in brighter ice located closer to the ice sheet margin than the dark region. Sample 5 and 6 were obtained at 67˚05.15' N, 50˚14.09' W (site 1) and sample 7 and 8 at 67˚09.16' N, 49˚58.41' W (site 3). These samples contained ice situated at several meters depth and were used as reference samples.

The $^{14}C/^{12}C$ ratios from both organic carbon (OC) and elemental carbon (EC) from the samples were determined [2].

RESULTS AND DISCUSSION

For most of the samples the concentration of carbonaceous particles in the ice was found to be very low. Table 1 shows the carbon concentration in nanogram per gram of ice. Samples 1 and 3, the two samples that contain ice from the surface, have high concentrations of organic carbon. Two samples from a core near the ice margin (samples 5 and 6), also show higher concentrations of organic carbon.

The analyses indicated that only 6 ^{14}C measurements gave reliable results, see Table 2. Sample 5 seems to be older than the other samples, maybe because it was located closer to the margin. The ages of the elemental and organic carbon in sample 1 and of the organic carbon in sample 3 are equal within their uncertainties, and are modern to over modern. The elemental and organic carbon in sample 2 has an older age, probably because the uppermost part, containing modern carbon, was not used for the analyses. Therefore, this last result confirms the hypothesis that old dust is outcropping in this area. The melting out of this old dust, containing nutrients, may stimulate cyanobacteria and algal growth. This would explain the high concentrations of organic carbon and the modern age found for the samples containing dust from the surface.

Tab. 1: Carbon concentration in the ice samples.

Sample	C (ng/g)	+-
Sample 1 (OC)	75.94	1.69
Sample 1 (EC)	4.21	0.12
Sample 2 (OC)	3.94	0.13
Sample 2 (EC)	3.05	0.13
Sample 3 (OC)	76.53	1.74
Sample 3 (EC)	2.92	0.07
Sample 4 (OC)	1.28	0.06
Sample 4 (EC)	1.77	0.06
Sample 5 (OC)	15.76	0.34
Sample 5 (EC)	1.99	0.05
Sample 6 (OC)	19.44	0.42
Sample 6 (EC)	0.65	0.05
Sample 7 (OC)	0.56	0.05
Sample 7 (EC)	0.46	0.05
Sample 8 (OC)	1.01	0.04
Sample 8 (EC)	0.58	0.04

Tab. 2: Calibrated date of samples, with respect to 0 BC.

Sample	Date (68.2% probability)	
Sample 1 (OC)	1956 to 1957	17.8%
	1998 to …	50.4%
Sample 1 (EC)	1434 to 1706	41.6%
	1720 to 1820	14.5%
	1833 to 1883	6.7%
	1914 to 1952	5.4%
Sample 2 (OC)	-510 to -436	5.0%
	-426 to 218	63.2%
Sample 2 (EC)	250 to 1190	67.6%
	1196 to 1207	0.6%
Sample 3 (OC)	1956 to 1957	68.20%
Sample 5 (OC)	-1688 to -1056	68.20%

REFERENCES

[1] I.G.M. Wientjes and J. Oerlemans, to be submitted to The Cryosphere.

[2] T.M. Jenk et al., Nucl. Instrum. Meth. B, **259**, 518 (2007).

BIOGENIC SILICA: A POWERFUL TOOL FOR QUANTITATIVE CLIMATE RECONSTRUCTIONS FROM LAKE SEDIMENTS

M. Trachsel, M. Grosjean (Univ. Bern, NCCR Climate and Oeschger Center), A. Blass (Univ. Bern & EAWAG), S. Köchli (PSI), M. Schwikowski (PSI & Univ. Bern), M. Sturm (EAWAG)

Current research in annually laminated Lake Silvaplana, Engadine (NCCR Climate VIVALDI project, PI M. Schwikowski) shows that biogenic silica bSi has a great potential as a climate proxy in remote lakes and for time periods, when anthropogenic eutrophication played a minor role.

High-resolution, quantitative long-term climate reconstructions are essential to place the recent, probably anomalous climate changes into a longer perspective. One particular quality of lake sediments is (i) the potential for very long records, and (ii) the presence of multiple biological (e.g., diatoms, chrysophytes etc.), physical and bio-geochemical proxies (e.g. grain size distribution, mineralogy, stable isotopes, alkenones, and many others) within the same palaeoenvironmental archive. A particular challenge in current palaeolimnology is calibration and quantification of the proxy data. A major obstacle with biological proxies is that taxa identification and preparation of the data set is very time-consuming and expensive. This makes the search for rapid physical and bio-geochemical methods in lake sediments a very active field of investigation. The disadvantage here is that many of these proxies are controlled by the site-specific lake basin and lake catchment configuration (climatic zone, vegetation, geology, topography, etc.), which requires genuine calibration between a proxy and related environmental variables at every new site. This phenomenon is partly also known from ice cores. BSi is present in lake sediments as diatom opal, phytoliths and chrysophyte cysts, among others. Following the method by Mortlock and Froehlich, BSi is leached from the lake sediments with 1 M NaOH for 3 hrs at 90°C. In order to account for Si leached from inorganic alumino-silicates, BSi concentrations are corrected using the Al concentration in the leachate [1]. This method has been validated by absolute diatom valve counts on standardized samples. The Al correction is the reason why ICP-OES is the preferred analytical technique. Annually laminated (varved) cores of Lake Silvaplana were dated using varve counting, ^{137}Cs, ^{210}Pb, and event stratigraphy. Annual laminae were sampled year by year back to AD 1177. Annual biogenic silica flux to the sediments calibrated against instrumental (June-August) to warm season (June-November) temperatures (AD 1864-1949) revealed a very high and significant correlation ($r=0.7$, $p<0.01$; Fig. 1). This correlation is stable in time. Comparison with (i) early instrumental data back to 1760 AD, and (ii) two fully independent temperature reconstructions for the same area (based on dendro and documentary data) back to 1177 AD is consistent [2, 3]. During the second part of the Little Ice Age (1600-1850) bSi concentration is in good accordance with glacier length fluctuations. Figure 2 shows the comparison of bSi concentration with two glacier reconstructions based on historical documents. The bSi record shows a lead between 8 and 15 years compared to glacier length changes. bSi concentration is depending on the (summer) temperatures of the actual year whereas glacier length changes are lagged behind temperatures.

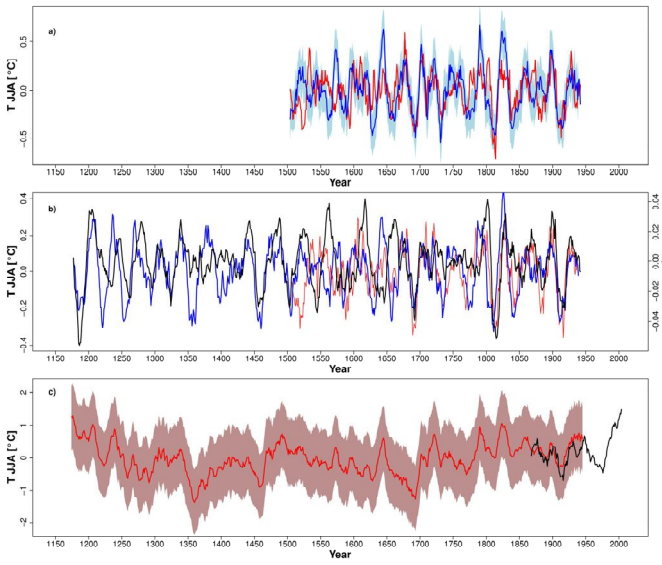

Fig. 1: (a) 100-year high-pass filtered and 9-year smoothed (9-100 years band-pass filtered) bSi flux-based T reconstruction (blue, light blue indicating the RMSEP) and multi-proxy summer T reconstruction [3] (red; data filtered in the same way). (b) 15-100 years band-pass filtered bSi T reconstruction (blue), JJA T reconstruction [3] (red) and tree ring based Alpine summer T reconstruction [4] (black). (c) Combined chironomid and bSi flux-based summer T reconstruction (9-year running mean, red, light red indicating the uncertainty) and 9-year running mean of summer (JJA) T from adjacent station Sils Maria (black). All anomalies are given with respect to 1961 – 1990).

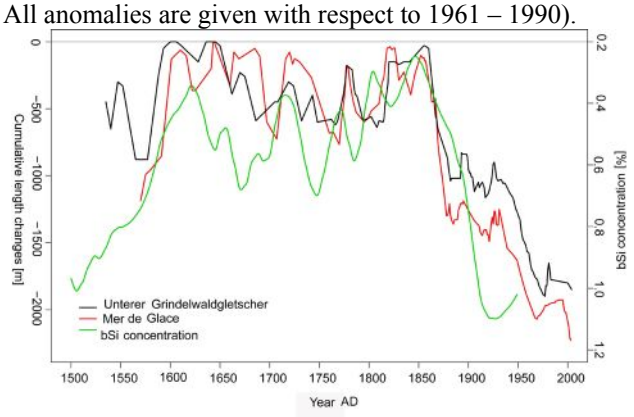

Fig. 2: Comparison of glacier length changes [3] and bSi concentration in Lake Silvaplana [2].

REFERENCES

[1] C. Ohlendorf, M. Sturm, J. Paleolim. **39**, 137 (2008).
[2] M. Trachsel et al. submitted to Quat. Sci. Rev.
[3] C. Casty et al., Int. J. Clim. **25**, 1855 (2005).
[4] U. Büntgen et al., J. Climate 19, 5606 (2006).
[5] S.U. Nussbaumer et al. Z. f. Gletscherkunde u. Glazialgeologie **40**, 141 (2007).

NEW MEASUREMENT OF THE ^{60}Fe HALF-LIFE

D. Schumann, R. Weinreich (PSI), N. Kivel, I. Günther-Leopold (PSI/AHL), M. Wohlmuther (PSI/ABE), G. Rugel, T. Faestermann, K. Knie, G. Korschinek, M. Poutivtsev (TU Munich)

A new determination of the half-life of ^{60}Fe using γ-measurements and ICP-MS was performed. The new value is $(2.62\pm 0.04)\cdot 10^6$ yr, significantly above the previously reported value of $(1.49\pm 0.27)\cdot 10^6$ yr.

INTRODUCTION

Radioactive nuclei produced by astrophysical processes are a key for understanding the development of our universe. The half-life of ^{60}Fe plays an important role in different astrophysical investigations. Most prominent examples are the nucleosynthesis in the current galaxy as observed through γ-rays, the history of the early solar system as observed through meteoritic inclusions and deposits of supernova ejecta on earth as indicated in ocean-crust material.

Up to now, only two measurements of the half-life of ^{60}Fe had been reported: 3·105 yr (uncertain by a factor of 3) [1], and $(1.49\pm0.27)\cdot10^6$ yr [2], which was the currently accepted value. A more accurate determination of the 60Fe half-life might have significant impact on astrophysical data and their interpretation.

In general, half-life determinations can be performed by measuring the two components of equation (1): A - ^{60}Fe activity and N - number of ^{60}Fe atoms:

$$T_{1/2} = \frac{N}{A}\cdot \ln 2 \qquad (1)$$

The ^{60}Fe sample material had been separated by the RadWasteAnalytics group at PSI from 3.86 g of a copper beam dump irradiated with high-energetic protons. Details of the sample preparation are described earlier [3]. The work is part of the ERAWAST initiative at PSI (Exotic Radionuclides from Accelerator Waste for Science and Technology).

ACTIVITY - MEASUREMENT

The activity A of the ^{60}Fe sample was determined at TU Munich by the in-growth of the daughter isotope ^{60}Co via the two prominent γ-ray lines of 1.17 and 1.33 MeV. In Fig.1 the in-growth of the two lines with the fit is shown for almost 1000days.

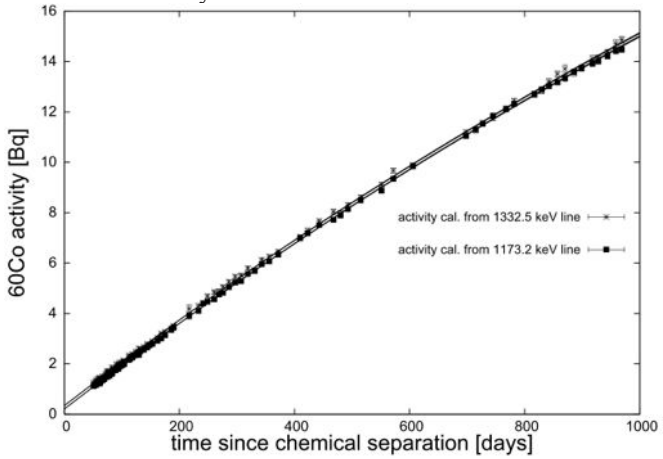

Fig. 1: Activity of the two ^{60}Co-lines as a function of time.

The precondition for an accurate and precise measurement is the almost complete separation of ^{60}Co contaminations from the ^{60}Fe before starting the γ-measurements. Our sample contained 0.2 Bq. The measurement of both lines yielded a value of A_{60Fe} (49.19±0.11) Bq.

NUMBER OF ATOMS - MEASUREMENT

The number of ^{60}Fe atoms has been determined in the Hotlab of PSI using a multicollector inductively coupled plasma mass spectrometer (MC-ICP-MS, Neptune, Thermo Fisher Scientific, Bremen, Germany). Stable Fe carrier was added in order to measure isotopic ratios.

Unfortunately, spallation reactions produce the entire spectrum of radionuclides and stable isotopes with masses equal and lower than the target mass. Therefore, natural isotopic ratios cannot be expected in the 60Fe sample for the Ni contaminations.

Therefore, an additional chemical treatment was necessary to determine the ^{60}Ni background at mass 60 correctly by adding stable Ni carrier, followed by repeated chemical separation.

The iron content in the sample was determined to be (2.662±0.009) mg of iron with a non-natural abundance using an enriched ^{57}Fe standard as reference material. The ratio N_{60Fe}/N_{Fe} has been determined to be $(2.0483\pm0.0035)\cdot10^{-4}$. The number of N_{60Fe} in the sample is therefore $(5.873\pm0.020)\cdot10^{15}$.

RESULT

With Eq. (1) we obtain a half-life of ^{60}Fe of $(2.62\pm0.04)\cdot10^6$ yr [4]. This new value is much more precise and significantly higher than previously accepted. The contributions to the uncertainty can be seen in Table 1.

Tab. 1: The various contributions to the uncertainty (1σ).

	rel. uncertainty [%]	
	stat.	syst.
^{60}Co standard		1.5
γ-measurement fit	0.23	
N_{Fe} sample weighting		0.18
N_{Fe} ICP-MS	0.28	
N_{60Fe}/N_{Fe}ICP-MS	0.18	
total	**0.4**	**1.51**

REFERENCES

[1] J. Roy et. al., Can. J. Phys. 35, 649 (1957).
[2] W. Kutschera et al., NIM B 5, 430 (1984).
[3] D. Schumann, et al., J. Phys. G 35, 014046 (2008).
[4] G. Rugel et. al., PRL 103, 072502 (2009).

REMOTE CONTROLLED SYSTEM FOR PRODUCTION OF ^{26}Al, ^{59}Ni, ^{53}Mn, ^{44}Ti, AND ^{60}Fe FROM A PROTON IRRADIATED COPPER BEAM DUMP

M. Ayranov, D. Schumann (PSI)

A remote controlled system for separation of exotic radionuclides from a proton irradiated copper beam dump was designed. The system is installed in a hot cell for handling high radioactive materials. First separations from gram amounts of a copper target demonstrated the functionality and reliability of the installation.

INTRODUCTION

A conceptual scheme for radiochemical separation of exotic radionuclides from a proton irradiated beam dump was developed. In principal it is a combination of selective precipitation of the copper matrix as CuS and ion exchange for separation of the elements of interest from the high ^{60}Co activity. The procedure was tested with indicative activity levels and proved to be selective with high radiochemical yield [1].

Based on the developed radiochemical procedure a remotely controlled system for separation of exotic radionuclides from a proton irradiated beam dump was set up.

DESIGN OF THE SEPARATION SYSTEM

Generally the system is composed of two parts. In the first one (Figure 1) the copper sample is dissolved in 7M HNO_3 and diluted to 0.5 M. Then the copper matrix is selectively precipitated as CuS by saturation of the solution with H_2S. Solid CuS is separated by filtration and the precipitation with H_2S repeated until quantitative separation of copper is obtained.

Further the liquid sample is evaporated and the residue dissolved in 8 M HCl. In order to avoid the contact of corrosive acid vapors with the hot cell, the evaporation is performed with the help of a rota-evaporator.

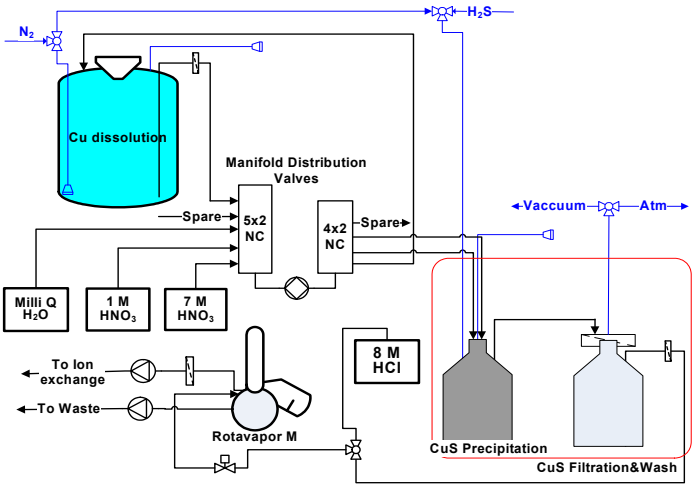

Fig. 1: Scheme of the copper dissolution and precipitation part of the system.

The ion exchange separation of exotic radionuclides is processed in the second part of the system – Figure 2. The sample in 8 M HCl is loaded on the strong basic anion exchanger Dowex 1x8 [2]. ^{26}Al, ^{59}Ni, ^{53}Mn, and ^{44}Ti are leaving the column as a single fraction with the load

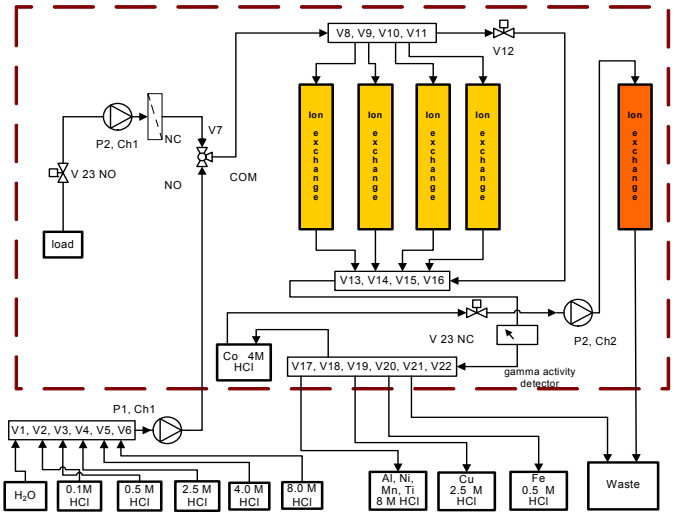

Fig. 2: Scheme of the ion exchange part of the system.

solution and the following wash with 8 M HCl. The Co is eluted with 4 M HCl, Cu with 2.5 M HCl and finally Fe with 0.5 M HCl. Further, additional ion exchange and liquid extraction steps are applied for the separation of ^{26}Al, ^{59}Ni, ^{53}Mn, and ^{44}Ti as well as for better decontamination from ^{60}Co.

The full scale remotely controlled ion exchange system is installed in a hot cell where high activity levels are allowed to be handled.

FIRST RESULTS OF THE SYSTEM OPERATION

In order to evaluate the reliability and functionality of the system extensive tests have been done. During the test period 13.86 g in total of the proton irradiated copper beam dump were processed for separation of ^{26}Al, ^{44}Ti, ^{53}Mn, ^{59}Ni, and ^{60}Fe. The results showed that the system is operational and the radionuclide separation is selective with high chemical yield. The procedure manages the generated liquid wastes containing high levels of ^{60}Co activity as well, thereby reducing drastically their volume.

To make the separation system fully operational, work for the optimization of the selective copper matrix precipitation with H_2S is ongoing.

REFERENCES

[1] M. Ayranov et al., Ann. Rep. Lab. of Radio- and Environ. Chemistry, Uni Bern & PSI (2008), p. 38.

[2] G. Svehla ed., Comprehensive Analytical Chemistry, Vol XIV, Wilson and Wilson's, 1982.

PREPARATION OF A ^{7}Be STANDARD FOR ^{10}Be HALF-LIFE MEASUREMENTS

M. Ayranov, D. Schumann (PSI), N. Kivel, I. Günther-Leopold (PSI/AHL)

A cation exchange chromatographic separation procedure for purification of ^{7}Be, produced in the cooling system of the SINQ facility, has been developed. The separated ^{7}Be fraction is sufficiently pure to be used as calibration standard for a precise ^{10}Be half-life determination.

SCIENTIFIC BACKGROUND

^{10}Be and its daughter products have been used to examine soil erosion, soil formation from regolith, the development of lateritic soils, as well as variations in solar activity and the age of ice cores. One of the "hot topics" is the half-life of ^{10}Be, where the literature values differ from 1.34 to 1.51 Ma [1, 2]. Two very recent measurements support the lower value: 1.388 Ma [3] and 1.386 Ma [4]. Additional measurements are, therefore, urgently needed.

One possibility is the use of liquid scintillation counting (LSC) for the determination of the activity and inductively coupled plasma mass spectrometry (ICP-MS) for measuring the number of atoms. The calibration of the ICP-MS requires at least two isotopes in known amounts. Since Be has only one stable isotope (^{9}Be), ^{7}Be can serve as the second marker.

^{7}Be is produced in considerable amounts in the cooling water (D_2O) of the SINQ facility at PSI by spallation reactions on ^{16}O with the generated fast neutrons. By-products can be nearly neglected, thus this cooling water establishes an ideal source for highly active ^{7}Be-samples [5]. ^{7}Li, the decay product of ^{7}Be, interferes with the ICP-MS determination of ^{7}Be. The only possibility to overcome this interference is a complete separation of Li from Be and correction of the interference by calculating the ^{7}Li increase over time.

SEPARATION OF ^{7}Be

In order to study the separation of Li from Be on a Dowex 50x8 – HNO_3 system two experiments were performed. The first was implemented at trace level concentrations of ^{7}Be, stable Li and ^{22}Na and the separation was determined by gamma spectrometry. The differences in the distribution coefficients (D_g) [6] of Be and Li (Fig. 1) allow the efficient separation of the analytes on a Dowex 50x8 100x7 mm column (Fig. 2). Na has a similar D_g and was used as marker.

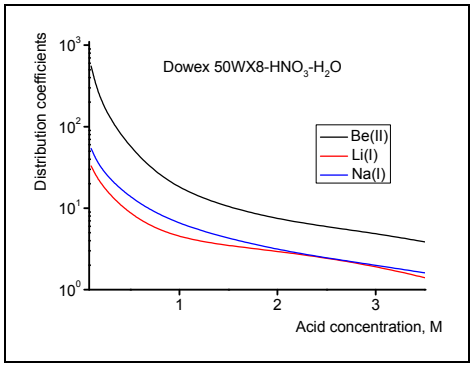

Fig. 1: D_g of Be, Li and Na in Dowex 50x8–HNO_3 system.

The second separation experiment was performed on a Dowex 50x8 100x7 mm column with ppb concentration levels of stable Li, Be, and B. B may be present as impurity

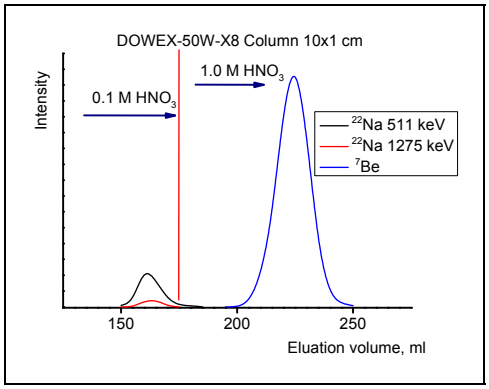

Fig. 2: Separation of ^{22}Na from ^{7}Be on a Dowex 50x8 column – gamma spectrometric results.

in the SINQ cooling water and may cause serious interference for the ICP-MS determination of ^{10}Be. The distribution of elements was determined by ICP-MS (Fig. 3).

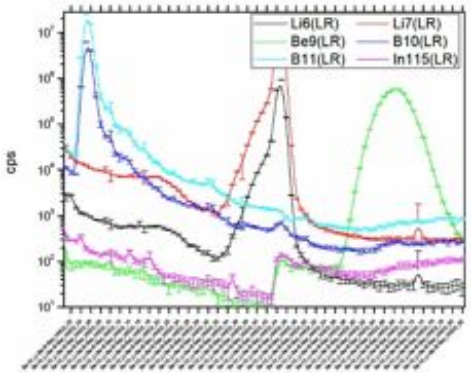

Fig. 3: Separation of stable Li, Be and B on a Dowex 50x8 column – ICP-MS results.

RESULTS

Chromatographic separation of Be from Li and B by cation exchange on Dowex 50x8 in HNO_3 media is highly selective and efficient. The isobaric interferences of Li and B in the ICP-MS measurements can be corrected and the purified ^{7}Be sample can be used as a second standard for the ^{10}Be half-life determination.

REFERENCES

[1] R. Middleton et al., Nucl. Instr. Methods B **82** p. 399-403 (1993).
[2] D. Fink et al., Nucl. Instr. Methods B **172** p. 838-846 (2000).
[3] G. Korschinek et al., doi:10.1016//j.nimb.(2009).09020.
[4] J. Chmeleff et al., doi:10.1016/j.nimb.(2009).09012.
[5] D. Schumann et al., Ann. Rep. Lab. of Radio- and Environ. Chemistry, Uni Bern & PSI (2008), p. 36.
[6] G. Svehla ed., Comprehensive Analytical Chemistry, Vol XIV, Wilson and Wilson's (1982).

PROTON IRRADIATED STAINLESS STEEL AS A SOURCE OF ^{44}Ti

M. Ayranov, D. Schumann (PSI)

First experiments for radiochemical separation of ^{44}Ti from proton irradiated stainless steel have been implemented. The preliminary results demonstrated that the stainless steel is a valuable source for production of ^{44}Ti, but nevertheless further efforts to develop an optimal separation procedure are necessary.

INTRODUCTION

^{44}Ti is an isotope of great interest for research domains as nuclear medicine and astrophysics. Its decay product, positron emitting ^{44}Sc, has an interesting physical half-life of 3.92 h and the radioisotope generator system ^{44}Ti/^{44}Sc is attractive for PET diagnostics. However, the long-lived mother radionuclide ^{44}Ti is difficult to obtain [1]. Furthermore, the nucleosynthesis of ^{44}Ti occurs predominantly in the explosive environment of all types of supernovae and recently a measurable ^{44}Ti γ-ray flux has been observed from the Cas A supernovae remnant [2].

Direct production of ^{44}Ti at high-flux cyclotrons is an option, but low yields and high cost are major drawbacks. In this context, the existence of ^{44}Ti in waste materials at PSI, such as a copper beam dump irradiated with high energy protons, and stainless steel, offers an excellent resource [3].

The samples of the stainless steel material were collected from the former PIREX gas chamber [4] by drilling in a hot cell (Figure 1). The material with a weight of 12 kg contains about 100 MBq ^{44}Ti with the main impurity being about 2 GBq ^{60}Co.

Fig. 1: Stainless steel sample collection.

FIRST ANALYTICAL AND SEPARATION EXPERIMENTS

The stainless steel (SS 316L) composition is: Cr-17.9 %, Ni-12.9 %, Mo-2.5 %, Mn-1.4 % and Fe-65.3 %. This complex matrix requires a multistep separation procedure, which should be capable on the one hand to separate micro amounts of titanium with high selectivity and chemical yield, and on the other hand to be maintained in appropriately shielded hot cells due to the high ^{60}Co radiation. Taking into account the general chemical properties of titanium and the elements of the stainless steel matrix, model separation experiments were performed [5, 6]. Based on the preliminary results a separation scheme was proposed in Fig. 2.

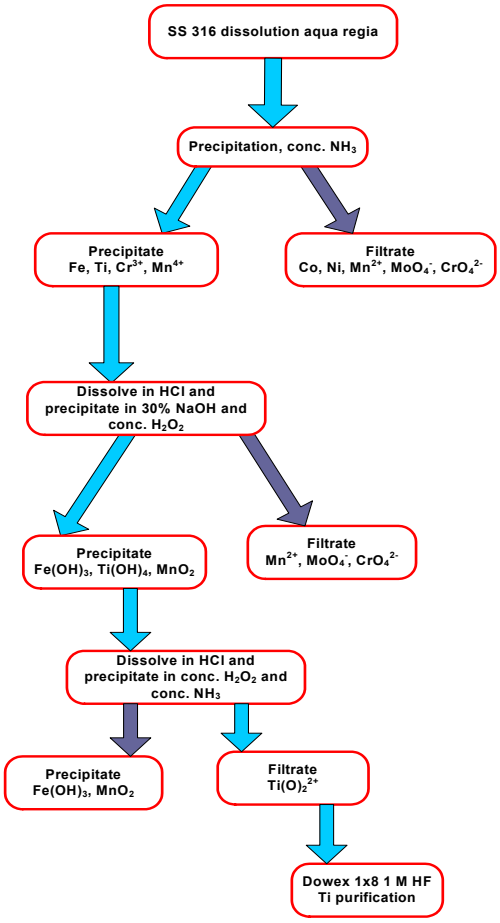

Fig. 2: Flowchart of the proposed separation procedure.

Experiments aimed at evaluating the separation capabilities of the procedure are ongoing.

REFERENCES

[1] F. Rösch et al., "Radionuclide Generators", Handbook of Nuclear Chemistry Vol.4, Kluwer Academic Publishers, The Netherlands (2003).

[2] M. Pierrick et al., New Astr. Rev., 52, 7-10, 401 (2008).

[3] D. Schumann et al., Ann. Rep. Lab. of Radio- and Environ. Chemistry, Uni Bern & PSI (2006), p. 40.

[4] M. Wohlmuther private comm.; PSI memorandum 31.8.2006.

[5] Ch. Baes et al., "The Hydrolises of Cations", John Weley & Sons (1976).

[6] A. Mizuike, "Enrichnemt Techniques for Inorganic Trace Analysis", Springer-Verlag (1983).

^{14}C AND ^{3}H DETERMINATION IN GRAPHITE FROM THE TARGET E STATION PART I: COMPARISON WITH OLD DATA

D. Schumann, T. Stowasser, S. Lüthi (PSI), D. Kiselev, S. Teichmann (PSI/ABE)

The ^{3}H and ^{14}C content of several old samples from graphite wheels of the target E station was determined. The results were compared with previous values, which were obtained using another chemical separation technique. The present results are generally higher than the older data by a factor 2-3 and do not agree well with theoretical predictions.

INTRODUCTION

For the safe disposal of the graphite targets used for meson production at PSI's target E station, data on the radionuclide inventory are mandatory. Former determinations of the ^{14}C and ^{3}H content of several targets showed large discrepancies compared to theoretical predictions [1,2]. A mix-up of sample naming was suspected in some cases. Some of the measurements have been repeated using the same samples and a different chemical dissolving procedure. The results are compared with the previous values and predictions from calculation codes.
In Fig.1, a scheme of the rotating target wheel and incident proton beam is shown.

EXPERIMENTAL

While the authors in [2] used combustion in an oxygen flow at 900°C, we applied wet digestion to decompose the graphite. In a two-neck-vessel, about 20 mg of graphite were boiled with a mixture of H_2SO_4/HNO_3/$HClO_4$ 2:1:1 under reflux for 15 min. Nitrogen flow is used to transport the gases into two adsorption vessels (the first one contained 1M HCl to avoid acidification of the 1M NaOH for ^{14}C). Tritium remains in the dissolving solution. The chemical yield of the entire procedure was determined using known amounts of standard material.
Nuclide measurements were carried out using Liquid Scintillation Counting technique with the scintillation cocktail Ultima Gold LLT (^{3}H) and Aquasafe 500 plus (^{14}C).

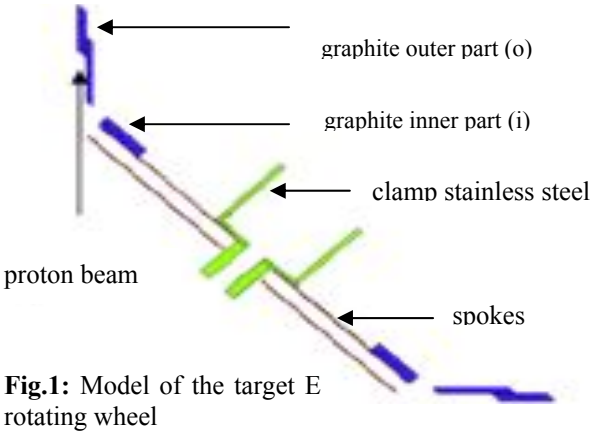

Fig.1: Model of the target E rotating wheel

CALCULATION CODES

For the calculation of the nuclide inventory the particle transport Monte Carlo Simulation MCNPX2.5.0 [3] in combination with decay- and build-up codes was used. For the results cited in Table 1, Cinder'90 version 06 [4] was coupled to the MCNPX output via a Perl script.

RESULTS

Tab. 1: comparison of previous and new measurements of ^{14}C and ^{3}H from samples of graphite targets; [Bq/g]; i - inner part; o - outer part.

sample	^{3}H new	^{3}H old	^{3}H calc.	^{14}C new	^{14}C old	^{14}C calc.
E70i	$4.6\cdot10^{5}$	$1.6\cdot10^{5}$		< 500	<1	
E70o	$7.7\cdot10^{8}$	$3.8\cdot10^{8}$	$1.6\cdot10^{9}$	$1.0\cdot10^{3}$	$3.6\cdot10^{2}$	2.7
E71i	$5.9\cdot10^{5}$	$2.2\cdot10^{5}$	-	< 500	<1	-
E71o	$4.8\cdot10^{8}$	$1.8\cdot10^{8}$	$2.4\cdot10^{9}$	$1.1\cdot10^{3}$	$6.3\cdot10^{2}$	3.5
E72i	$4.7\cdot10^{5}$	$7.0\cdot10^{5}$	-	< 500	<1	-
E72o	$1.4\cdot10^{9}$	$5.8\cdot10^{7}$	$1.9\cdot10^{9}$	$2.4\cdot10^{3}$	$5.2\cdot10^{2}$	2.7
E78i	$1.5\cdot10^{6}$	$5.2\cdot10^{5}$	-	< 500	10.3	-

The new data obtained for the old samples E70, E71, E72, E78 are compared with the previous ones and with the predictions coming from the calculations (Table 1). With exception of E72i for ^{3}H, the new values are higher than the former ones by a factor of 2-4.

Since we find a general tendency for higher values with the new chemical determination technique for both isotopes, we suppose that the combustion technique leads to losses of activity due to an incomplete absorption or during the following purification operations [2]. The comparison with the theoretical predictions [1] shows a general underestimation for ^{14}C and an overestimation for ^{3}H. The discrepancy for the latter can be explained by the fact, that due to the high temperature of the target wheel (~1700°C) an unknown amount of tritium is expected to evaporate. Part of the tritium is found in the exhaust air. A rough estimate leads to 30 % but the uncertainty of this estimate is high. The disagreement for the carbon values cannot be explained at the moment. A possibility would be a larger amount of nitrogen present in the target wheel. The cross section for ^{14}N(p,n)^{14}C reaction is large.

REFERENCES

[1] D. Kiselev, private communication 2007.
[2] M. Argentini et.al; Ann. Rep. Lab. of Radio- and Environ. Chemistry, Uni Bern & PSI (2000), p. 41.
[3] D. Pelowitz, ed., MCNPX User's Manual, Version 2.5.0, LA-CP-05-0369.
[4] W.B. Wilson et al., Proc. GLOBAL'95 Int. Conf. on Evaluation of Emerging Nuclear Fuel Cycle Systems, Versailles, France (Sept. 1995).

^{14}C AND ^{3}H DETERMINATION IN GRAPHITE FROM THE TARGET E STATION PART II: NEW SAMPLES AND RADIAL DISTRIBUTION

D. Schumann, T. Stowasser, S. Lüthi (PSI), D. Kiselev, S. Teichmann (PSI/ABE)

The ^{3}H and ^{14}C content of new samples from graphite wheels of the target E station have been measured. The distribution of these two radionuclides perpendicular to the beam direction was determined by cutting the samples into small slices and performing a separate digestion procedure for every slice.

INTRODUCTION

After reproducing the old measurement data [1,2] for the tritium and carbon-14 content of old samples from target E, more efforts were put into the question, why the data are not consistent with the theoretical predictions [3]. One of the possible reasons is that there could be a radial distribution relative to the beam direction. If this would be the case, then the values depend strongly on the sample taking position. This influence has been studied by sawing samples perpendicular to the beam direction from the outer part of the target wheels . The nuclide measurement results are compared with predictions from calculation codes.

EXPERIMENTAL

Three targets E have been used to prepare new samples: E79, E83, and E92. To get information on the radial nuclide distribution, samples from the outer part of the target wheels were sawn into slices perpendicular to the beam direction. In Fig. 1, a schematic view of the sample taking is depicted. Between three and five "sub-samples" were obtained from each sample. The radial thickness of the graphite wheels is 6 mm. These "sub-samples" were chemically treated as described before in [1].

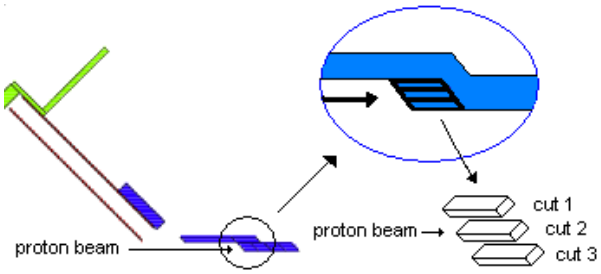

Fig. 1: Scheme of the sample cutting.

RESULTS

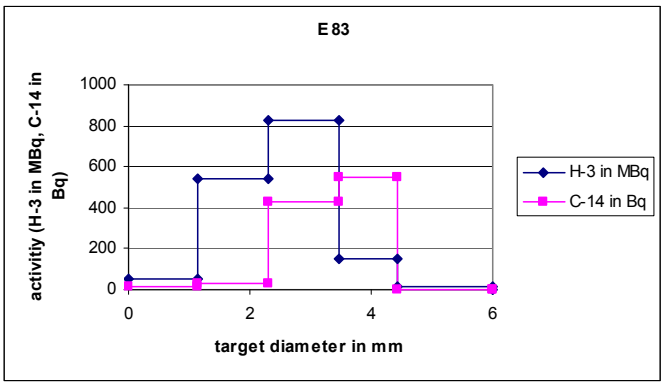

Fig. 2: Radial distribution of ^{3}H (left scale) and ^{14}C (right scale) in the graphite target No. E79.

Figure 2 shows the results for each slice of the target E79 sample. A clear dependence of the radionuclide content on the distance perpendicular to the beam axis is observed. The investigations of the other targets have given similar results.

Tab. 1: Measured data for all 3 targets: ^{3}H [MBq/g]; ^{14}C [Bq/g]; beam dose in Ah; max. - highest measured value; Ø - average value from all cuts; calc. - predicted value.

	Beam dose	^{3}H max.	^{3}H Ø	^{3}H calc.	^{14}C max.	^{14}C Ø	^{14}C calc.
E79	6.64	2039	694	2710	6788	2041	11
E83	1.84	824	319	883	548	205	3
E92	28.79	815	360	15600	18465	9401	53

Table 1 shows the maximum, average and calculated activities for all 3 targets, as well as the corresponding beam doses. Calculations have been carried out as described in [1]. It turns out that the tritium content is again generally overestimated, corresponding to former results [1]. It is conspicuous, that the measured tritium content does not correspond to the received beam dose. Obviously, tritium evaporation during operation seems to depend on several factors, e.g. operation time or temperature. An influence could be material deterioration of the graphite due to radiation, leading to modified gas storage properties. In particular all three targets were made out of different grades of graphite. Due to these uncertainties, a prediction of the ^{3}H content in these graphite targets does not seem to be reasonable.

The measured ^{14}C is underestimated by a factor of ~ 100, which corresponds to the earlier finding [1]. For the beam centre positions, this deviation is even higher. Therefore, the disagreement of measured and calculated values cannot be explained by the sample taking position. The strong radial dependence of the activity found in the measurement is an indication that ^{14}C is mainly produced by direct proton reactions and to a lesser amount by neutron capture on carbon. This would require the presence of nitrogen which is not taken into account yet in the calculations.
These results show that our measurements are reliable. Due to the radial dependence, a deviation factor of 2-3 for the former and present ^{14}C measurements presented in [1] seems to be reasonable.

REFERENCES

[1] D. Schumann et. al., this report p 50.
[2] M. Argentini et. al; Ann. Rep. Lab. of Radio- and Environ. Chemistry, Uni Bern & PSI (2000), p. 41.
[3] D. Kiselev, private communication 2008 (PSI-memorandum).

GREEN DIAMOND COLOUR IDENTIFICATION PROBLEM TACKLED WITH NEUTRON-, ELECTRON-, AND GAMMA-IRRADIATIONS

G. Bosshart (Horgen ZH), R. Dressler, S. Lüthi, D. Schumann, A. Vögele (PSI)

The possibilities to colour white diamonds using several kinds of radiation (neutron, electron, gamma) were studied. For neutron irradiation, the activation system of the SINQ facility at PSI was used.

Introduction: Pure diamond is "white" (colourless). However, in nature, other colours co-exist, actually an entire rainbow. In the jewellery sector, top qualities of such fancy colours command exorbitant carat prices, if the authenticity of these colours has been certified by professional gem-testing laboratories. For several reasons, natural green colour in polished diamonds is very rare. The large majority of green specimens on the market have routinely been coloured by physical laboratories under neutron or electron beams. They are most difficult to distinguish from their naturally coloured counterparts. The first author's Green Diamond Research Project (GDRP) aims at solving the identification problem by direct juxtaposition of the characteristics of natural and artificial green colours [1,2,3].

Any type of high-energy radiation ejects carbon atoms from diamond lattice sites (binding energy 7.3 eV), entailing the vibronic GR1 absorption in the red-orange spectral area and resulting in green hues. It is well known that α-, β-, and γ-radiation of natural radio-isotopes can change the colour of diamonds. The question arose whether or not neutron radiation could be another natural cause of colour alteration. The only known fossil nuclear reactors (critical 1.7 billion years before present) are located at Oklo (Gabon). But the nearest diamond occurrences are far outside the km range. In addition to nuclear fission processes, however, neutrons can be produced in sufficient amounts via secondary reactions of high-energetic α-particles impinging on the surrounding materials, so-called (α, xn)-reactions. The overall neutron yield in (α, xn)-reactions due to the natural radioactivity of Th or U (natural abundance 12 ppm and 3 ppm, respectively) is 2.4×10^{10} neutrons per cm^2 and per 10^6 years.

Results: Neutron, electron and γ irradiation tests are being carried out in parallel on non-irradiated diamond specimens, laser-cut into two slabs, in order to study their respective optical behaviour and to compare it to that of naturally irradiated, pre-analysed reference material. Analytical methods applied are colourimetry, MIR and UV-Vis-NIR absorption, Raman PL, α- and γ-spectrometry, LA-ICP-MS. About 50% of the GDRP study samples still await analysis and virtually all require spectral evaluation. At this stage, firm conclusions are premature. Nevertheless, the following can be stated:

Natural green: α-particles destroy diamond down to approximately 20 µm below the surface, irregularly staining it with intense green to black haloes. β-ray damage reaches to depths of 1.5 mm to 2.0 mm, yet γ-photons will not lead to discernible coloration unless acting over very long time periods (as, e.g., in the case of the famous 41 ct Dresden Green Diamond [3]). Residual radioactivity of some 140 natural green specimens was determined to be less than 5 mBq for ^{210}Po and less than 20 mBq for ^{210}Pb.

Artificial green: α-irradiation, first applied by Sir W. Crookes in 1904, produced strong and evenly green surface colouration of diamond crystals and lasting residual radioactivity which in 2004 still was 3.8 Bq for one of these samples. Recently, faceted Russian diamonds showed hazardous α-activities of up to 20 kBq. After two years of diamond exposure to a strong ^{60}Co gamma source, faint green tinges evidence that this is not an efficient method for industrial greening. One-hour electron irradiation yields pleasant bluish to yellowish-green colours if temperature is well controlled. Although not colouring the entire body of a multi-mm faceted diamond, the colour distribution appears to be homogeneous, e.g. after rotated sample irradiation.

Neutron activation: Neutron irradiation is second in terms of handling ease. Fig. 1 depicts the colour alteration of a natural diamond after repetitive irradiations of 2 hours at the preparative neutron analysis facility at PSI. During these irradiations a colour change from white over yellowish-green to green was observed. The optimal dose to modify the colour of a white diamond to green of 1.73×10^{15} epithermal n/cm^2 reported in [4] appears somewhat high compared to the total epithermal neutron dose of 8.1×10^{14} n/cm^2 applied in our experiments.

Fig. 1: Natural diamond sample n3C22:
a) before irradiation; b) after a epithermal neutron dose of 4.3×10^{14}n/cm^2;c) after an additional dose of 3.8×10^{14} n/cm^2.

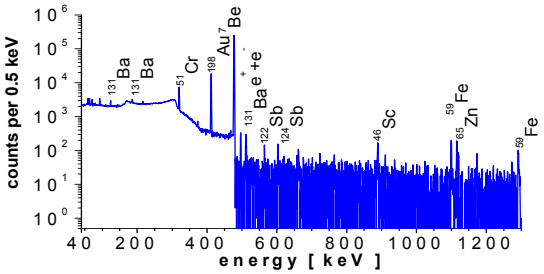

Fig. 2: Gamma-spectrum of neutron-irradiated diamond sample n3C22-c after an acquisition time of 93.5 h

The γ-spectrum (Fig.2) reveals a high chemical purity of the diamond. Besides ^{7}Be, induced by spallation of C, other elements activated, are present in traces only. They stem from polishing residues and minute inclusions,

Conclusion: α-irradiated and most electron-irradiated diamond colours can be separated from their natural counterparts. Green body colours of diamond resulting from natural γ-ray exposure and artificial neutron irradiation are expected to become distinguishable by means of characteristic UV-Vis-NIR absorption and Raman PL bands, FWHM values and in particular with normalised GR1 intensity depth profiles specific for each radiation type.

REFERENCES

[1] G. Bosshart: 29th Int. Gem. Conf. 2004 Wuhan (PRC).
[2] G. Bosshart: 30th Int. Gem. Conf. 2007 Moscow (RUS).
[3] G. Bosshart: J.Gemm. 21(6), 351 (1989).
[4] S. Sahavat, et al.: Kasetsart J. 43, 216 (2009).

FEASIBILITY STUDY FOR THE EXTRACTION OF MEDICALLY INTERESTING RADIONUCLIDES IN EURISOL

D. Schumann, J. Neuhausen, R. Dressler (PSI)

Extracting medically interesting radionuclides from a future EURISOL facility was found to be not cost-effective.

As a part of EURISOL [1], on-line extraction of medical interesting nuclides from Hg was proposed. The idea seemed to be prospective, but a detailed yield and cost estimation had never been done. In the present report, we give an assessment of the expected yield of radiopharmaceuticals based on the radionuclide production rates given in [1].

Isotopes for medical treatment are required with very high radiochemical purity, i.e. for radionuclides produced directly in spallation reactions a mass separation is mandatory. For generator nuclides the situation is better, because only the daughter nuclide is used. The conditions have to be checked for every desired radionuclide. The sole medically interesting α-emitter which can be produced in spallation reactions with mercury is ^{149}Tb - a radionuclide which counts as candidate for cancer treatment [2]. Due to its half-life of 4.1 h, also decay losses have to be considered here.

Basic assumptions and boundary conditions:

Volume of Hg 500 l; beam current 5mA; E_p 1GeV; 5 l/h by-pass extraction; operation time 40 years; 250 d/y.

Losses due to separation and processing time:

Adsorption of activity on the loop walls ~50%; Extraction yield (first step: Multi-element extraction from mercury) 50%; Chemical separation of the desired radionuclide 50%; Mass separation 95%; Labelling 30%; Removing from adsorber and separation from other radionuclides (lanthanide fractionation, final purification) 6h; Mass separation 4h; Labelling 3h; Quality control, shipping 3h

On-line extraction:

The mercury flows through a by-pass (~ 1% according to the basic assumptions) which contains an adsorption device sensitive for all interesting radionuclides. This adsorption material has to be removed frequently (dependent on the half-life of the wanted nuclide) for the follow-up chemical processes.

Off-line extraction:

The facility is driven for a certain period (dependent on the half-life of the desired radionuclide). Then, the mercury is pumped into a separation device, or adsorption materials are put into the flow. The activity can be extracted from the entire mercury volume. In the case of very high wall absorption, the mercury can be pumped into a storage tank or a second loop and the activity is then eluted from the loop walls by leaching with diluted HNO_3.

The on-line and off-line production yields are summarized in Tab.1. For offline-production, the extraction rate is replaced by the parameter extraction time (t-extr.). This is caused by the fact, that the activity is accumulated within the mercury.

From Tab.1. it can be seen, that off-line technology is in all cases more effective than on-line extraction. This is of special importance when one considers the probably very high wall adsorption, which leads to a drastical drop-down of the available activity. Moreover, it does not seem to be economical to extract long-lived and short-lived radionuclides simultaneously, because the required cycle times for the radionuclides are very different.

The possible production of ^{149}Tb will be sufficient for 1-3 patients per day. Larger amounts of activity can be obtained for radionuclides, which serve as generator systems. This could be the case for ^{44}Ti (100 MBq/y), ^{188}W (460 GBq/y), ^{178}W (212 TBq/y) and ^{68}Ge (188 GBq/y).

Considering the prices for cancer therapy (50k€) or commercial available generators (^{188}W/^{188}Re 18.5 GBq 10 k€) and taking into account the total costs for the production and purification, the method does not seem to represent a profitable alternative to other production routes (dedicated cyclotrons or nuclear reactors) [3].

REFERENCES

[1] The EURISOL Report, Appendix C, Ganil Report (2003).
[2] Beyer, G. J. et. al., E. J. Nucl. Med Mol. Imag. 31 (4) 547 (2004).
[3] J. Neuhausen et. al., EURISOL final report 2009.

Tab.1: Radionuclide production in an Hg target in on-line and off-line production mode (extr. rate: 5 l/h and 50% wall absorption; tcycle: duration of production cycle, i.e. for on-line mode: collecting time, for off-line mode: time for one cycle (3 -5 half-lives); overall chemical efficiency 0.00375; overall separation time 57600 s.)

Nuclide	$T_{1/2}$	Prod.rate	tcycle	On-line production		Off-line-production		Availability
				extr.rate	final activity	t_extr.	final activity	
		[1/s]	[d]	[1/s]	[GBq]	[s]	[GBq]	
Tb-149	4.1 h	3.50E+13	0.5	1.39E-06	0.154	36000	1.41	twice per day
Lu-177	6.7 d	2.40E+12	30	1.39E-06	4.14	36000	7.68	monthly
Ir-192	74 d	1.00E+14	250	1.39E-06	310	36000	336	per year
Sn-117m	13.6 d	7.00E+12	60	1.39E-06	16.6	36000	23.7	every second month
Sr-89	50.5 d	2.10E+13	250	1.39E-06	67.5	36000	75.1	per year
W-178	22 d	3.10E+14	90	1.39E-06	835	36000	1060	every third month
W-188	69 d	2.70E+12	250	1.39E-06	8.46	36000	9.20	per year
Ge-68	288 d	3.60E+12	750	1.39E-06	11.0	36000	11.3	every third year
Ti-44	60 y	7.00E+10	2500	1.39E-06	0.02	36000	0.02	every 10th year

ANALYSIS OF MERCURY IRRADIATED WITH HIGH ENERGY PROTONS USING γ-SPECTROSCOPY

J. Neuhausen, D. Schumann, R. Dressler (PSI)

The chemical behavior of nuclear reaction products in mercury samples irradiated with high energy protons was studied within the project EURISOL-DS using γ-spectroscopy. This report discusses the peculiarities of measurement and evaluation procedures arising from the complexity of the sample composition and presents selected results.

INTRODUCTION

The project EURISOL-DS deals with the design of a next-generation radioactive beam facility. One component of this planned facility comprises a 4 MW mercury spallation target. For this mercury target, a chemical separation of the radionuclides induced by irradiation was proposed to mitigate safety issues during operation, target disposal and also for nuclide production purposes. In this context, we studied mercury samples that were irradiated with high energy protons (1.4 GeV) using γ-spectroscopy.

GENERAL CHARACTERISTICS OF SAMPLES

High power proton irradiated Hg samples contain a vast range of nuclear reaction products ranging from atomic number Z = 1 to 81, giving rise to extremely complicated γ-spectra. Most radionuclides show inhomogeneous distribution within the samples. Furthermore, Hg shows very strong γ-ray absorption effects for low energy γ-rays. The combination of complex composition, inhomogeneous distribution of radionuclides and strong absorption effects leads to difficulties in the quantitative analysis.

EXPERIMENTS AND EVALUATION

Three irradiated samples were obtained from CERN. These samples were measured on HPGe-detectors after various decay times for nuclide identification and were subsequently used for studies of radionuclide distribution in the samples and their removal using a variety of chemical methods (for details see [1]). For the evaluation of γ-spectra the program GENIE2000 (Canberra) was used. For nuclide identification a special library was created, containing 134 nuclides that can be formed by nuclear reactions induced by high energy protons and have half-lives ≥ 1d. Using this library, a first automatic identification was performed, but because of the complexity of the spectra, extensive manual interactions were necessary for reliable nuclide identification. For the assessment of self-adsorption effects of the sample, the efficiency calibrations for the detectors were compared with calculated efficiencies obtained using the (ISOCS/LabSOCS)-tool of GENIE2000. Fig.1 shows such a comparison for homogeneous distribution of the activity in water (measurement using ^{152}Eu) and in Hg (calculation) for similar geometries, demonstrating strong self-absorption effects of mercury for low energy γ-rays.

RESULTS AND DISCUSSION

Over 60 radionuclides were identified in newly irradiated samples. Tab. 1 gives an excerpt of the results for measurements taken 4 weeks and 18 months after irradiation. Detailed studies revealed that the distribution of most of the nuclides in the sample is strongly inhomogeneous, making a quantitative absorption correction impossible. Therefore, the results given in Tab.1 should be regarded as semi-quantitative, especially for those nuclides with only low energy γ-rays. Naturally, short-lived nuclides dominate the spectra taken after short decay time, while long-lived nuclides are in many cases only detected after several months of decay. Apart from its use for EURISOL-DS, the experience gained can be used e.g. in the extensive γ-analyses planned for the MEGAPIE Post Irradiation Examination program (PIE).

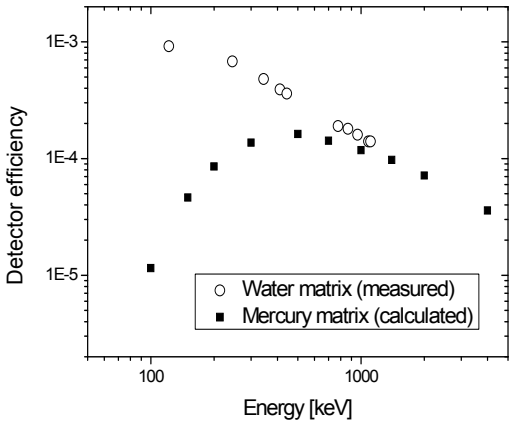

Fig. 1: Detector efficiency for a homogeneous activity distribution in water (circles; measured) and in mercury (squares, calculated).

Tab. 1: Selected results of γ-analyses of a proton-irradiated Hg-sample, decay corrected, no self-absorption correction.

Nuclide	date	22.05.2006	14.11.2007
	geometry	horizontal	horizontal
	Half-Life [d]	Activity [Bq]	Activity [Bq]
Ag-110m	2.50E+02		2.96E+02
Sn-113	1.15E+02	2.68E+03	2.19E+03
Ba-131	1.18E+01	1.05E+04	
Ba-133	3.84E+03		8.80E+01
Ce-139	1.38E+02	2.13E+03	2.94E+03
Pm-143	2.65E+02		3.78E+03
Eu-145	5.93E+00	1.11E+05	
Eu-146	4.59E+00	1.86E+06	
Gd-151	1.24E+02		4.42E+03
Hf-172/Lu-172	6.83E+02		2.88E+03
Lu-172	6.70E+00	9.39E+04	
Lu-173	5.00E+02		6.43E+03
Lu-177	6.71E+00	3.56E+04	
Re-183	7.00E+01	3.34E+04	3.31E+04
Os-185	9.36E+01	3.79E+04	7.19E+04
Pt-188/Ir-188	1.02E+01	2.82E+05	
Ir-190m	1.18E+01	7.85E+03	
Ir-192	7.38E+01	1.21E+03	
Au-195	1.86E+02		1.82E+03
Au-196	6.18E+00	2.04E+05	
Au-198	2.69E+00	9.21E+05	
Au-199	3.14E+00	9.13E+05	
Tl-202	1.22E+01	1.48E+04	
Hg-203	4.66E+01	1.37E+04	1.99E+04

REFERENCE

[1] J. Neuhausen et al., EURISOL-DS Task 2 Deliverable 2 (2009). http://www.eurisol.org.

SEPARATION OF RADIONUCLIDES FROM MERCURY BY ACID LEACHING AND DISTILLATION

J. Neuhausen, D. Schumann, S. Lüthi (PSI)

Chemical extraction of radionuclides from p-irradiated mercury was proposed for the spallation target unit of a future EURISOL radioactive beam facility. In this context, we studied the application of conventional leaching and distillation techniques for the removal of tracer-level radioactive impurities from p-irradiated mercury samples.

INTRODUCTION

Mercury purification by leaching with oxidizing aqueous solutions and distillation is an industrial standard procedure for the production of high purity mercury. Depending on the number of distillation stages, purities up to 9N can be reached. However, for the removal of impurities from mercury used as spallation target material one has to deal with a different and very complex variety of impurities compared to ordinary mercury which are formed in the mercury in very low concentrations as "no carrier added" contaminations. Therefore, we studied the applicability of these standard purification methods for the removal of traces of radionuclides from p-irradiated mercury.

EXPERIMENTAL

A part of an Hg sample irradiated with 1.4 GeV protons at CERN was leached with 2 M HNO_3 at ambient conditions for 3 hours. Subsequently, the two liquid phases were separated and the mercury was distilled at 200°C under a pressure of about 20 mbar. γ-spectra were recorded for the sample before the separation, the two liquid phases after the leaching process, the distillation residue and the distilled mercury.

RESULTS AND DISDUSSION

Fig. 1 illustrates the results of the 2 purification steps. After the leaching procedure, most of the less noble elements are extracted to the HNO_3-solution and are not detectable in the mercury anymore. For ^{185}Os, ^{139}Ce, and ^{121m}Te the major part is extracted to the acid, while a small amount of these nuclides can still be found in the liquid metal. For ^{110m}Ag, the transfer to the acid is less complete, leading to an approximately equal distribution between the acid and the mercury. The ^{106}Ru/Rh couple remains in the liquid metal and is not detected in the HNO_3-solution. Gold is also not transferred to the acid solution. With a few exceptions (Ru, Ag) this behaviour is in agreement with the electrochemical potential series. After the distillation, most of the activity is found in the distillation residue. The ^{194}Au-activity found in the distilled Hg arises from reproduction from ^{194}Hg. However, a very small amount of ^{195}Au was carried over with the mercury. Osmium and ruthenium partly remain in the residue, but are also in part transported in the gas phase with the mercury. It is known that these elements form volatile tetroxides when heated in air. A sufficient amount of oxygen for the formation of these oxides is present while performing the distillation. According to the higher stability of the osmium tetroxide, the majority of the ^{185}Os is distilled, while for ruthenium, which forms a less stable tetroxide, the majority of ^{106}Ru is detected in the distillation residue. In conclusion, the applicability of mercury purification by oxidizing acid leaching and distillation of samples contaminated with no carrier added radionuclides is demonstrated.

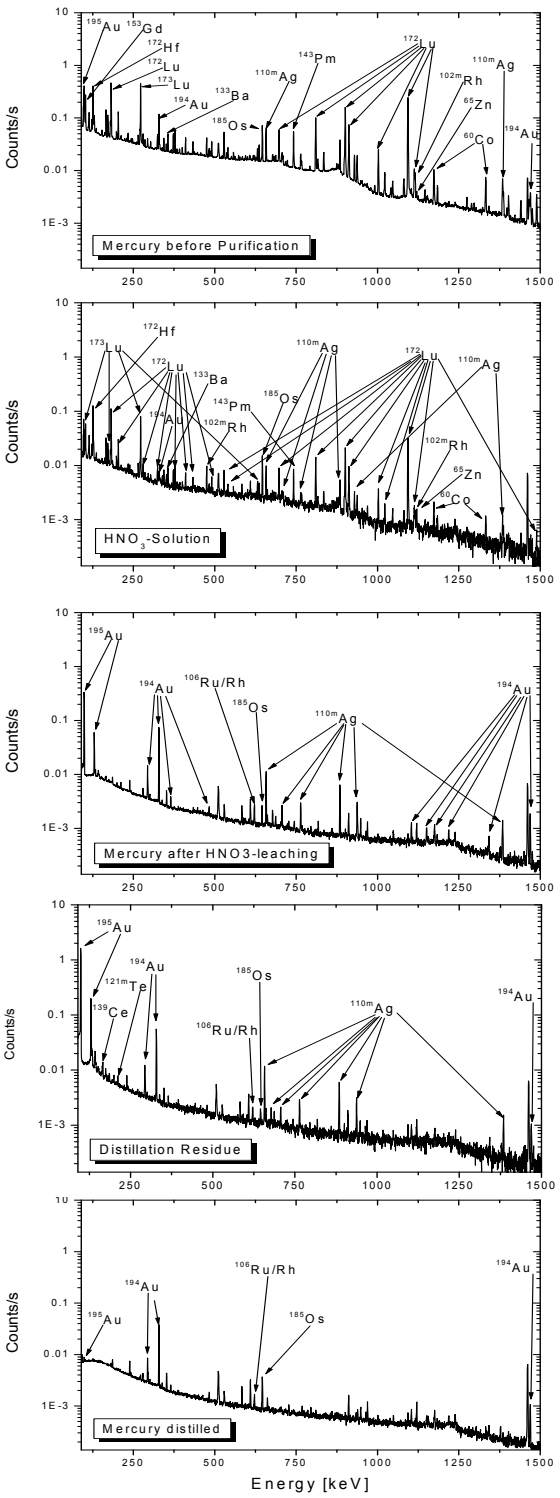

Fig. 1: γ-spectra of mercury before and after the individual separation steps.

REFERENCE

[1] J. Neuhausen et al., EURISOL-DS Task 2 Deliverable 2 (2009). http://www.eurisol.org.

DETERMINATION OF ^{210}Pb AND ^{210}Po IN WATER SAMPLES

M. Ayranov, D. Schumann (PSI), Z. Tosheva, A. Kies (Univ. Luxembourg)

In order to develop a simple, fast and sensitive method for sequential radiometric determination of ^{210}Po and ^{210}Pb in water samples, we examined the combination of spontaneous electrochemical deposition, co-precipitation and extraction chromatography.

INTRODUCTION

Lead-210 and Polonium-210 are naturally occurring members of the Uranium-238 decay series. They are found in various environmental samples, such as groundwater, fish and shellfish, contributing an important component of the human's natural radiation background [1]. For this reason the development of a fast, reproducible and sensitive method for determination of ^{210}Pb and ^{210}Po is of a great concern [2]. The aims of our study were to adopt procedures for radiochemical separation of these radionuclides and radioanalytical methods for their determination.

EXPERIMENTAL

The combination of spontaneous deposition, co-precipitation and extraction chromatography gives the opportunity for fast and effective radiochemical separation of the analytes (Figure 1).

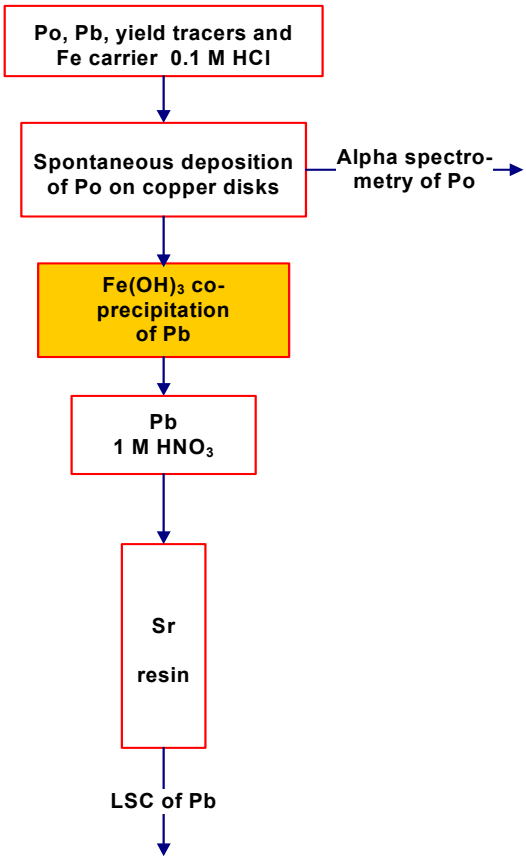

Fig. 1: Flowchart of the separation procedure.

Polonium was spontaneously plated on a copper disk from the stock solution. Lead was pre-concentrated by co-precipitation with $Fe(OH)_3$ and further purified by extraction chromatography on Eichrom Sr columns [3,4]. Alpha spectra of polonium were collected on Canberra PIPS detectors with 900 mm^2 active surface. The activities of lead were determined by LSC (Gardian Wallac Oy). Electro-thermal atomic absorption spectrometry (ET-AAS) was used for the determination of the concentration of stable lead carrier.

RESULTS AND DISSCUSSION

The obtained minimum detectable activities for a sample size 1000 ml are 0.2 Bq/m^3 and 2.3 Bq/m^3 for ^{210}Po and ^{210}Pb and with a chemical yield of 88 and 85%, respectively. The method was applied for analyses of numerous surface water samples from Luxembourg, Table 2, providing efficient isolation of ^{210}Po and ^{210}Pb, and enabling their rapid, simple, highly sensitive and quantitative determination at environmental levels.

Tab. 2: ^{210}Po and ^{210}Pb activity concentrations in waters samples originating from Luxembourg.

Sampling location	Nuclides concentration, mBq/l	
	^{210}Pb	^{210}Po
Rosport-Viva	-	10.4±1.6
Dudelange	-	15.1±2.2
Pedras	-	17.5±2.2
Hovelingerbaach - 1	39.2±0.1	15.0 ± 2.1
Hovelingerbaach - 6	< 13.0	11.6 ±1.9
Hovelingerbaach - 8	30.4±3.6	10.9 ±1.5
Hovelingerbaach - 22	46.8±0.1	5.4±1.0
Hovelingerbaach - AB	24.8±4.2	8.1±1.1
Source Hinkel, Born	-	102.6±7.1
Source salee, Born	-	434.1±19.9
Sourse salee, Echternach	-	27.6±3.7
Rosport	-	33.5±4.2

Under appropriate conditions the proposed procedure could be easily adapted for separation and radiometric analyses of ^{210}Po and ^{210}Pb as part of the radiochemical analyses of the ^{238}U decay series radionuclides from a variety of water samples.

REFERENCES

[1] H. Surbeck, The Sci. Tot. Environ. **173/174**, 91 (1995).
[2] C. Kralik et al., J. Environ. Radioact. **65**, 233 (2003).
[3] T. Tokieda et al., Talanta **12**, 2079 (1994).
[4] Eichrom Technologies Inc. http://www.eichrom.com/products/tech/srresin.cfm.

EVAPORATION STUDIES OF POLONIUM IN LEAD BISMUTH EUTECTIC (LBE): EXPERIMENTAL DESIGN STUDIES

S. Chiriki, J. Neuhausen, S. Heinitz, D. Schumann (PSI)

The contamination of spallation target facilities to be expected when an irradiated LBE (as a target material) surface is exposed to vacuum at high temperatures is of major concern for the design of windowless target systems. We report here in detail about an experimental set- up for studies of Po release into vacuum from free LBE surfaces.

INTRODUCTION

Liquid eutectic lead-bismuth alloy (LBE) is considered to be used as target material in future high power spallation targets for neutron production. PSI examined for the first time the feasibility of a LBE target system in the MW range, MEGAPIE. One of the important issues is the generation and accumulation of polonium (^{210}Po) in LBE since it is an alpha emitter and evaporates from a liquid LBE pool to cover gas region and deposit on structural material surfaces. This might cause radiological hazards during normal operation, facility maintenance procedures, or abnormal situations like accidental scenarios. The evaporation of polonium is of even higher importance for windowless targets, where the LBE free surface is exposed to the vacuum of the proton beam line. Therefore, it is important to understand mass transfer of Po in LBE target systems. Neuhausen et al., [1] investigated the evaporation behaviour of ^{206}Po from LBE under Ar/7%H_2 at ambient pressure over the temperature range of 500 - 1200°K. However, similar experiments using vacuum conditions failed because of irreproducibility caused by surface oxidation effects. This study focuses mainly on an experimental setup design to improve the reproducibility of evaporation experiments under dry gas (continuous flow of Ar/H_2) and vacuum.

EXPERIMENTAL

An experimental setup was constructed where LBE in a steel boat can be heated under vacuum and various purified gases with proper temperature controls (Figure.1). This experimental set-up can be operated under vacuum (about 10^{-4} - 10^{-6} mbar) and different gas systems. Special care was taken concerning gas purification to avoid the formation of oxide layers caused by the presence of residual oxygen or moisture. For this purpose, the incoming gas is deoxygenated in a Ta-getter furnace operating at 1000°C. To reduce the formation of oxides that can be formed at high temperatures from air that is penetrating into the evaporation tube through small leaks under vacuum conditions, the evaporation tube and the oven can be transferred to a glove box system containing an inert gas atmosphere.

For a first test of the experimental design, the evaporation behavior of polonium dissolved in liquid LBE was studied at various temperatures between 800-1200 K under a continuous flow of dry Ar/H_2 (60ml/min). Specific activities of ^{210}Po in the samples before and after the experiments were analyzed by the liquid scintillation counting (LSC) method. The results of the experiments described above are compared to earlier experimental results [1].

RESULTS AND CONCLUSION

The designed experimental set-up is tested by studying the evaporation behavior of the radionuclide ^{210}Po from LBE in a continuous flow of Ar/H_2 and comparing the results with those of earlier evaporation experiments. Figure 2 shows the comparison of polonium evaporation under Ar/H_2 using the current apparatus (^{210}Po) and earlier studies (^{206}Po). For the two series of experiments, the evaporation behavior is similar with fractional Po-release of a few % around 700 K and close to complete release at 1200 K. This validates the functionality of the present experimental setup and also confirms that the earlier series of experiments was not much influenced by the presence of oxide layers. As a next step, the setup will be used for studying vacuum release of polonium from LBE. The new setup will also be beneficial for studying the evaporation behavior of electropositive nuclides of rubidium and cesium from LBE.

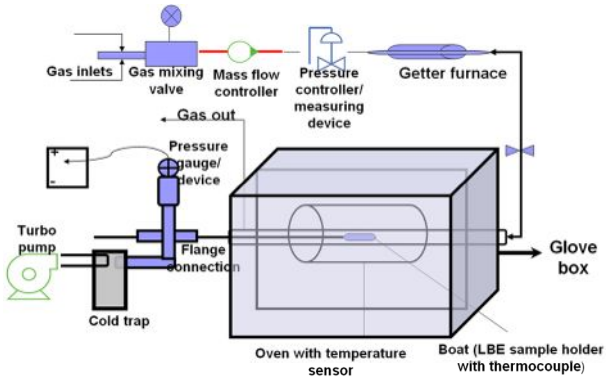

Fig. 1: Schematic view of the evaporation experiment apparatus.

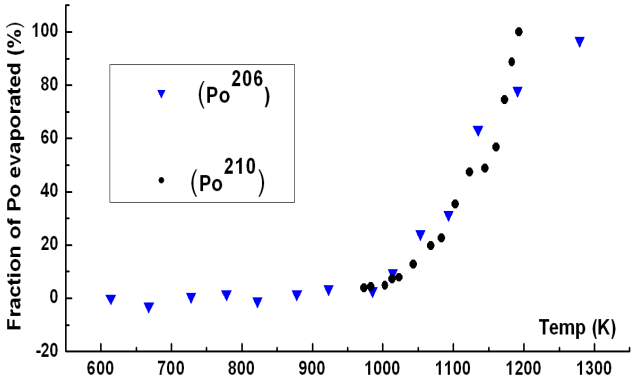

Fig. 2: Comparison of Po release studies of ^{206}Po [1] and ^{210}Po (current experimental set-up).

REFERENCE

[1] J. Neuhausen, U. Köster, B. Eichler, Radiochim. Acta **92**, 917 (2004).

SOLID STATE CHARACTERISATION OF LBE SAMPLES

J. Neuhausen, D. Schumann (PSI), F. v. Rohr (ETH Zürich), R. Brütsch (PSI/AHL), H.K. Grimmer (PSI/LDM)

A fast diffusion of polonium in solidified eutectic lead bismuth alloy leading to an inhomogeneous polonium distribution has been observed. To elucidate the nature of the diffusion process, basic studies of the chemical, crystallographic and micro-structural properties of aged solid samples of the eutectic were performed.

INTRODUCTION

A fast diffusion of polonium has been observed in solidified eutectic lead bismuth alloy (LBE) containing ^{210}Po [1], leading to an inhomogeneous polonium distribution of this hazardous radionuclide [2]. In this work, we report some basic results of bulk and surface solid state analysis that should help to understand driving force and mechanism of the diffusion process.

EXPERIMENTAL

Polonium-containing samples of LBE were prepared in the way described in [2]. The LBE was reduced at 600°C under a stream of H_2 immediately before irradiation. Thus, the samples show a bright metallic luster directly after preparation. However, already after some hours the appearance of the surface changes to a dull grey look. After months or years of storage, a surface layer is clearly visible (Fig. 1). For a phase analysis, such a sample was mounted on a Seifert 3000P powder diffractometer equipped with Cu-anode and multilayer optics. A diffractogram was recorded in the θ-2θ mode using Cu-Kα radiation. For chemical and microstructural analysis, a similar sample was studied using a Scanning Electron Microscope (SEM) equipped with an energy dispersive X-ray spectrometer (EDX). For this purpose, a part of the surface layer was mechanically removed, and EDX analysis was performed on both cleaned and not cleaned areas of the samples. An EDS-mapping of Pb and Bi was performed on the cleaned part of the surface to obtain information about the microstructure of the bulk material.

Fig. 1: Aged sample of neutron irradiated LBE.

RESULTS AND DISCUSSION

In Fig. 2 an x-ray diffractogram of an aged neutron irradiated LBE sample is depicted. Additionally to the lines of a lead rich Pb_7Bi_3-phase and a Bi-phase, lines of PbO are clearly visible. In agreement with this fact, an EDS analysis of the unmodified surface indicates the presence of a significant amount of oxygen, while on a scratched surface only the constituents of the eutectic are detected. An EDS-mapping of a surface cleaned in this way (Fig. 3) shows both grains of a lead-rich and a Bi-rich phase in agreement with the results of x-ray diffraction and the phase diagram known from literature [3]. Already in an early report on Po-distribution in solidified metals [4] an enrichment of Po in grain boundaries of metals was observed after crystallization.

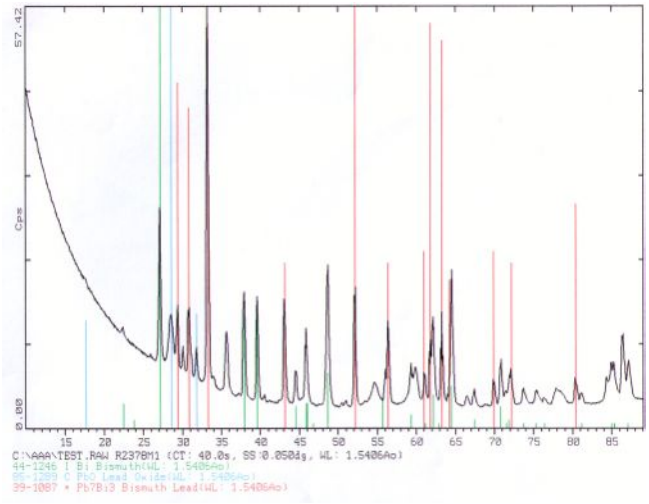

Fig. 2: X-ray diffractogram of a neutron irradiated LBE sample.

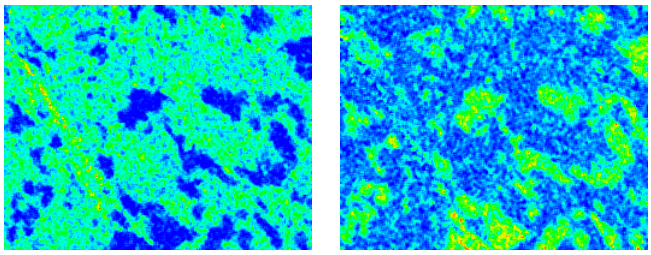

Lead distribution (Lα) **Bismuth distribution (Lα)**

Fig. 3: EDS-Map of a scratched surface of a neutron irradiated LBE sample. Image size ca. 80 × 100 µm.

These results indicate that a grain boundary diffusion process may explain the fast diffusion of Po in LBE, and the binding of Po in a surface oxide layer that is formed on LBE samples is a possible driving force for diffusion. However, a more careful analysis of the process is mandatory to elucidate the diffusion behavior of Po in LBE.

REFERENCES

[1] F. v. Rohr et al., Ann. Rep. Lab. of Radio- & Environ. Chemistry, Uni Bern & PSI (2008).
[2] F. v. Rohr et al., Ann. Rep. Lab. of Radio- & Environ. Chemistry, Uni Bern & PSI (2006).
[3] R. Hultgren et al., Selected Values of the Thermodynamic Properties of Binary Alloys, ASM, Metals Park, Ohio, 1973.
[4] G. Tammann et al., Z. Anorg. Allg. Chem. **205**, 145-162 (1932).

POLONIUM SEGREGATION IN LEAD-BISMUTH EUTECTIC

S. Heinitz, D. Schumann, J. Neuhausen (PSI), S. Müller (Univ. Bern)

The phenomenon of polonium diffusion and surface enrichment in solidified lead-bismuth eutectic samples was studied at different temperatures. Experiments on the diffusion process and its kinetics are still ongoing.

INTRODUCTION

Liquid lead-bismuth eutectic (LBE, T_m = 125°C) is considered as target material in spallation neutron sources, accelerator driven systems and as cooling medium for future Gen-IV nuclear reactors. Since in these systems it is exposed to high proton and neutron fluxes, considerable amounts of highly toxic polonium are formed in the liquid metal. It is of inherent importance to know the behavior of polonium in case of accidents or after disposal of the solidified LBE metal.

It is known from earlier publications, that polonium tends to migrate within solidified lead-bismuth [1] and lead [2, 3]. It is enriched on surfaces and grain boundaries resulting in higher alpha radioactivity than one would expect for its mean bulk concentration. We have studied the increase of surface radioactivity of Po-containing LBE samples with time at different temperatures and gas blankets using alpha spectroscopy.

EXPERIMENTAL

An 8 g LBE ingot was irradiated at SINQ using the NAA rabbit system for 1h to generate ^{210}Po, which is formed by the decay of the activation product ^{210}Bi. To ensure the complete ^{210}Bi decay, the ingot was stored for 1 month before usage. Then, it was diluted and homogenized at 600°C under a hydrogen stream for 30 minutes and an even distribution of polonium within LBE was verified via liquid scintillation counting. The specific activity was 2,5 kBq/g.

To study the enrichment of polonium, nine samples of 200 mg were cut and homogenized in a special specimen holder in order to obtain spherical shaped LBE samples. These were cooled rapidly under a liquid nitrogen flow and immediately placed into the alpha spectroscopy chamber. The alpha counts were registered during 15 minutes at a pressure of p = 10^{-1} mbar. After the measurement, the samples were placed in sealed glass tubes that were evacuated and then filled with different gases (H_2, air) or were left in vacuum. Three glass tubes for each cover-gas were then put in an oven at 100°C, 60°C and at room temperature. The measurement of the surface radioactivity of each sample was performed every day during 4 weeks.

RESULTS

The change of the recorded surface radioactivity with time at different temperatures is illustrated in Figure 1. It can be seen that the activity is increasing rapidly within the first days and almost doubling within four weeks for each measured temperature. This is less than expected from earlier observations [2, 4] where an increase of at least one order of magnitude was observed. However, saturation was reached only for samples stored at 100°C, whereas at room temperature and 60°C the activity was still rising after 25 days.

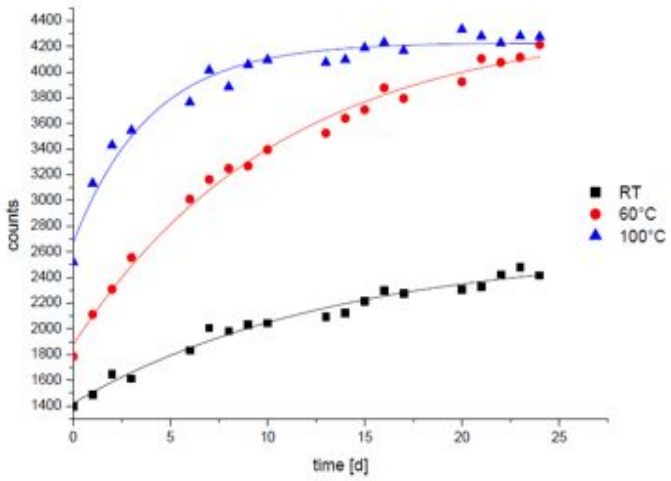

Fig. 1: The increase of surface activity of LBE samples stored in air at different temperatures as a function of time.

This effect is explained by an enhanced segregation rate at higher storage temperature [2]. No clear statement could be made whether the maximum surface activity is equal for every sample.

Note the different initial activities of all three samples in Figure 1 – in theory, they should be equal after homogenization with an activity of 1900 counts / 15min due to calculations based on the measurement geometry and the specific activity. These discrepancies originated from the crystallization process. SEM pictures of inactive LBE spheres show varying surface patterns even if the samples were cooled in the same manner. Therefore, the initial Po concentration at the surface of the samples could also vary due to small changes within the solidification. Experimental procedures to produce samples with reproducible surface activities have to be developed.

REFERENCES

[1] M. T. Stewart et al., Physical Review, **83**, 657 (1951).
[2] A. Zastawny et al., Appl. Radiat. Isot., **36**, 19 (1989).
[3] L. Patrizii et al., Journal of Instrumentation, **3**, P07002, (2008).
[4] F. V. Rohr et al., Ann. Rep. Lab. of Radio- & Environ. Chemistry, Uni Bern & PSI (2008).

MEGAPIE POST IRRADIATION EXAMINATION I: SAMPLING OF LEAD BISMUTH ALLOY FOR RADIOCHEMICAL INVESTIGATIONS

J. Neuhausen, D. Schumann (PSI), Y. Dai (PSI/ASQ), Ch. Zumbach (PSI/AMI), V. Boutellier (PSI/AHL)

The investigation of the radioactive inventory of the MEGAPIE target is mandatory for its safe disposal. Furthermore, studies of irradiated samples from MEGAPIE provide a unique opportunity for gaining insight on the production of radionuclides and their behavior within a liquid metal target. In this report, we discuss the cutting of the MEGAPIE target, the expected behavior of radionuclides within the target system and the resulting sampling strategy.

INTRODUCTION

The MEGAPIE target was the first liquid metal target ever operated in the Megawatt regime, at a power level of 0.8 MW. The liquid lead bismuth eutectic (LBE) target has successfully been irradiated in a period from August until December 2006. During this time the spallation target received a beam charge of 2.8 Ah of 590 MeV protons. After the successful operation of the target it has been stored in the target storage facility of PSI, waiting for its post irradiation examination, PIE. The dismantling of the MEGAPIE target took place in summer 2009. Within this process, the target was cut in cylindrical pieces that will serve for retrieving samples for materials testing and chemical analysis. These comprise the window calotte, several discs from various positions and the expansion tank, indicated by red circles in Fig.1. The remainder of the target will be disposed.

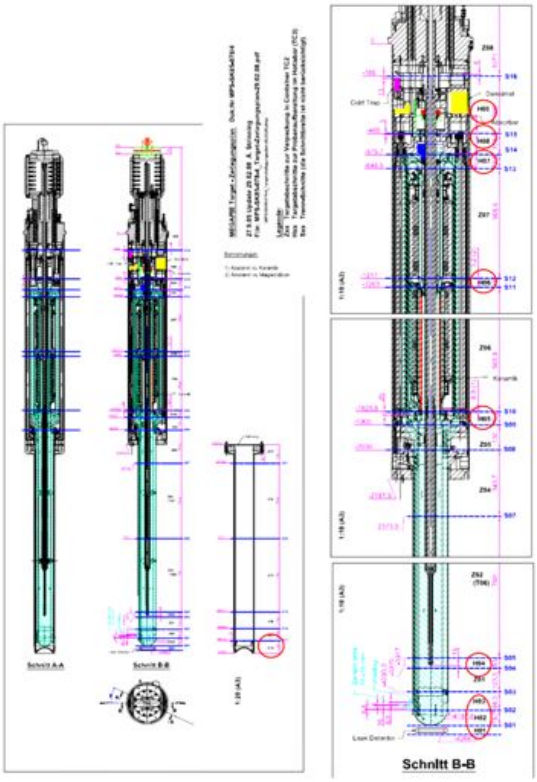

Fig.1: Schematic MEGAPIE cutting plan.

Inhomogeneities of the distribution of radionuclides in LBE are expected resulting from the crystallization process as well as diffusion processes occurring in the solidified metal (see e.g. the preceding reports in this volume). Furthermore, a deposition of nuclear reaction products in form of insoluble compounds is expected on surfaces.

SAMPLE TAKING

Because of the expected inhomogeneous radionuclide distribution in LBE, samples will be drilled from the surfaces of all LBE-containing cuts. To study the longitudinal distribution, various samples will be taken in each cut, at positions corresponding to different flow conditions of the LBE during target operation. For two disks radial profiles will also be determined (see Fig. 2.)

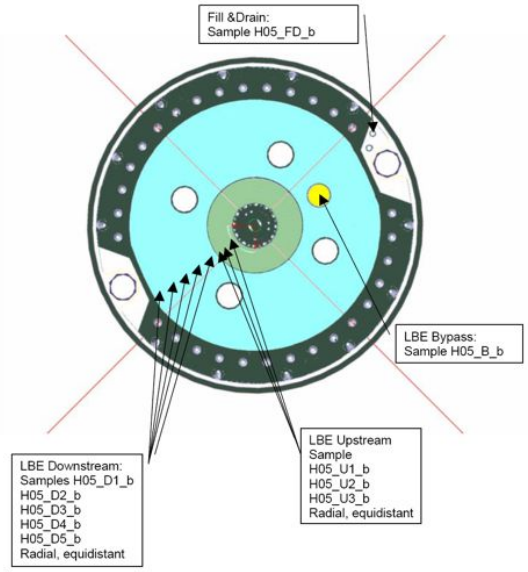

Fig. 2: Example of LBE sampling positions in one disk.

For drilling of the samples, the very heavy disks have to be turned around in the hot-cell and a special positionable drilling-tool (Fig. 3) is developed.

Fig. 3: Turning and drilling tool.

Furthermore, attention will be paid to obtain and analyze samples of solid materials that are deposited on the walls of structural materials and on the free surface of LBE. For more details see [1].

REFERENCE

[1] Y. Dai, J. Neuhausen, D. Schumann, C. Zumbach, MPR-11-DY34-001-2, PSI (2009).

MEGAPIE POST IRRADIATION EXAMINATION II: DISASSEMBLY OF THE EXPANSION TANK SYSTEM FOR RADIOCHEMICAL INVESTIGATIONS

J. Neuhausen, D. Schumann (PSI), Ch. Zumbach (PSI/AMI), M. Dubs (PSI/ATK)

A thorough understanding of the behavior of volatile radioactive material in spallation target systems is crucial for their safe operation. This report discusses the dismantling of the MEGAPIE expansion tank system, which is a prerequisite for gaining new insights on volatiles behavior based on radiochemical studies of their distribution.

THE MEGAPIE COVER-GAS SYSTEM

The MEGAPIE expansion tank system comprises the top part of the target, where the interface of the liquid metal and the cover gas was located while the target was in operation. It will be delivered to the HotLab in three pieces H07, H08, and H09, from which samples will be taken for radiochemical analyses. In the lower part of this section (H07 and H08), the free liquid metal surface moved up and down as a result of thermal variations caused e.g. by changes in the proton current during operation. On the free liquid metal surface, insoluble solids formed from corrosion and nuclear reaction products will accumulate. Because of the changes of the level of the liquid metal during operation and after shutdown, we expect a deposition of these materials not only on the LBE surface but also on the walls of the construction materials. Sampling and analysis of these materials will give insight into the distribution of specific elements between liquid metal and solid phases.

The top part of the expansion tank system, H09 (Fig. 1), contains a free volume of about 2 liters, which during target irradiation contained Ar. The purpose of this gas volume was mainly pressure control, handling and sampling of radioactive gases formed during irradiation. These gases comprise isotopes of hydrogen, noble gases and to a lesser extend volatiles such as polonium, mercury, and iodine. While hydrogen and helium are the main cause of a pressure increase in the target system during operation, the remaining elements do not contribute much to the produced gas volume but may carry a substantial amount of hazardous radioactivity. The release of these hazardous volatiles is a major concern for licensing and safe operation of high power liquid metal targets. Therefore, an understanding of their behavior in such a target system is of special importance.

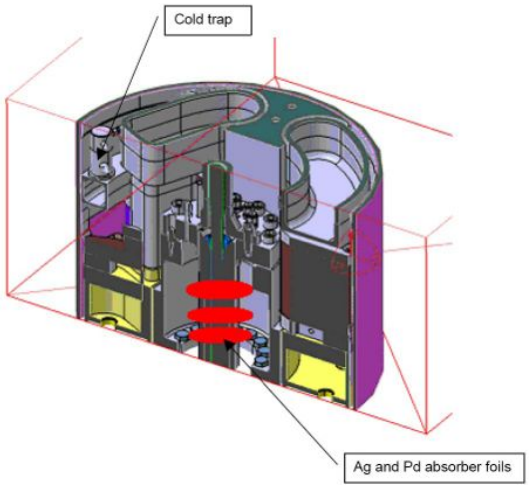

Fig. 1: Sketch of the MEGAPIE expansion tank, H09.

The cover gas system of the MEGAPIE target was equipped with metal foils (Ag and Pd) for the adsorption of gaseous elements such as I, Hg, Po etc., and a cold trap was built into the exhaust line to catch the highly volatile Hg.

DISMANTLING OF H09

The Post Irradiation Examination (PIE) program for the MEGAPIE target provides a unique opportunity to study volatilization and deposition processes in a real high power target system. For this purpose, the top part H09 of the target has to be dismantled in a hot cell to retrieve parts of the cover gas system such as adsorber foils, cold trap and inner surfaces of the gas volume to study the deposition of radioactivity on those parts. The dismantling requires the handling of a very heavy (≅ 250 kg) object in a hot cell, performing operations such as lifting, tilting, unscrewing, cutting, drilling and the like. According to a study of CAD models, the disassembly and retrieval of the most important parts of the expansion tank seems feasible in principle. A possible route for the stepwise disassembly leading to a retrieval of the central rod carrying the absorber foils and cutting of the cold trap is illustrated in Fig.2. More details can be found in [1]. Finally, the procedure has to be validated and optimized by experts of the Hot Laboratory.

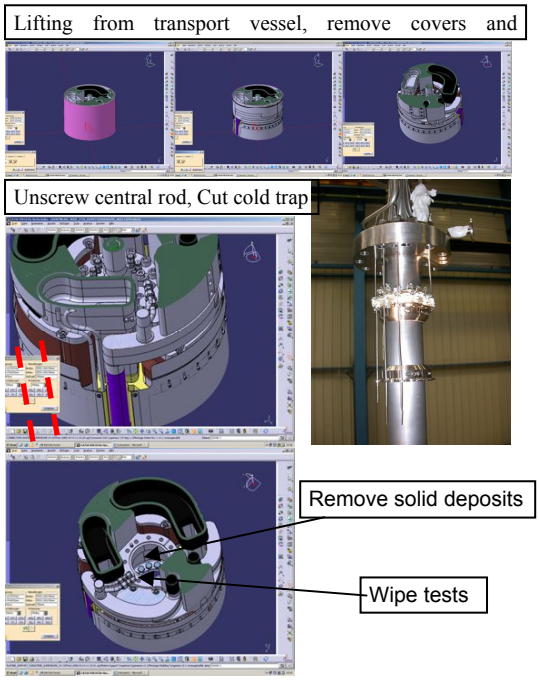

Fig. 2: Stepwise dismantling procedure for H09.

REFERENCE

[1] J. Neuhausen, D. Schumann, Ch. Zumbach, M. Dubs, TM 24-09-01, PSI (2009).

IMPROVED MEASUREMENTS OF GASEOUS ^{14}C SAMPLES AT MICADAS

S. Fahrni (Univ. Bern & PSI), S. Szidat (Univ. Bern), L. Wacker, H.-A. Synal (ETHZ)

Samples of 1 to 40 µg carbon are measured as CO_2 in the gas ion source of the small AMS (Accelerator Mass Spectrometer) facility MICADAS at ETHZ. This measurement technique offers a simple and fast way of ^{14}C measurements without the need of sample graphitization. To improve the performance of gaseous measurements at MICADAS, we tested a number of different cathode geometries and different system settings on a new ion source. The achieved performance allows to close the sample size gap between gaseous and solid samples, increases efficiency and even makes the gas ion source attractive for dating purposes in the 5 permil range.

INTRODUCTION

The gas ion source installed at MICADAS [1] by Ruff et al. [2] is in use for three years now. About one thousand small ^{14}C samples (1-35 µg C) have been measured since then. Gaseous measurements cover many scientific fields like environmental and biomedical applications and the field of applications is still growing. As sample preparation is easier and faster than graphitization and small samples remain difficult to graphitize, gaseous measurements offer a good solution. Up to now, however, there is a major drawback in using the gas ion source. While graphitized samples yield $^{12}C^-$ currents of 40-60 µA [3] on the low energy side of the tandem accelerator, gaseous samples produce only about 2.5 µA at present. This limits the possible applications and precision of any gas sample. Improvements of the negative ion currents and the ionization efficiency can therefore offer the key to new applications, higher precision and shorter measurements.

EXPERIMENTAL

In order to reach higher negative ion currents, we tested a number of cathode geometries, and systematically changed settings as for example the cesium reservoir temperature of the Cs sputter source, the ionizer temperature, cathode cooling, CO_2 concentration and gas inlet pressure. Tests were conducted on a redesigned ion source which is being installed at MICADAS for future operation [3].

RESULTS

With a number of changes to the usual settings we could significantly increase negative ion currents. The most effective changes were:

1. Defocusing the cesium beam by increasing the distance between the Cs ionizer and the cathode by 0.5 mm. This setting allows sputtering a larger area of the cathode.
2. Increasing Cs reservoir temperature (from 154 to 170 °C) to obtain a more intense Cs beam.
3. Increasing sample gas pressure for feeding of the ion source (from 1200 to 1500 mbar) which enhances the carbon mass flow rate from 0.7 to 1.1 µg C/min. A higher gas pressure is favorable, as it allows a faster increase of currents at the beginning of a measurement and higher maximum currents. Too high gas pressures, however, can lead to loss of efficiency as is shown in Figure 1.

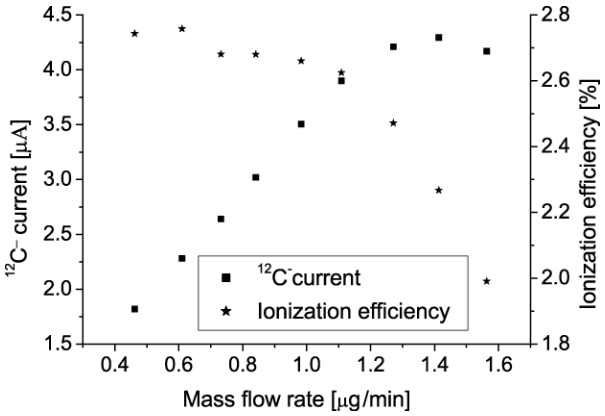

Fig. 1: An example for the carbon mass flow rate (gas pressure) dependency of the negative ion currents in the ion source of MICADAS at 4.5% CO_2 in helium.

With the changes made we have reached about 9 µA negative ion currents and ionization efficiencies have increased from 1.7% to 4% on average. Maximum values obtained are about 7% ionization efficiency and 16 µA negative ion currents. Measurements remain stable and $^{13}C/^{12}C$ ratios are constant over the range of tested settings.
Changes in the cathode geometry mostly led to reduced negative ion production, so that we decided to maintain the old design.
There is still room for improvements, as negative ion currents can vary even between similar samples and currents are dependent on the sample size. These phenomena call for further investigations.

CONCLUSIONS

The gas ion source is now accessible for larger samples up to 80 µg C as higher gas pressures and increased CO_2 content of the carrier enable measurements of such sample sizes. Achieved improvements will also allow radiocarbon dating in the 5‰ range in the near future. As the preparation of gaseous samples is shorter and easier than graphitization, gaseous measurements become a more interesting option for many intermediate size ^{14}C samples.

REFERENCES

[1] H.-A. Synal et al., Nucl. Instr. and Meth. B, **223-224**, 339 (2004).
[2] M. Ruff et al., Radiocarbon, **49**, 307-314 (2007).
[3] T. Schulze-König et al., Nucl. Instr. and Meth. B, in press, doi:10.1016/j.nimb.2009.10.057 (2009).

AGE-1: GRAPHITIZATION PROCEDURE

M. Němec (Univ. Bern), L. Wacker (ETHZ), H.W. Gäggeler (Univ. Bern & PSI)

The Automated Graphitization Equipment (AGE-1) was developed at ETH Zurich and it is now in routine operation producing solid targets for ^{14}C measurement with accelerator mass spectrometry (AMS). The graphitization procedure at AGE-1 uses H_2 for CO_2 reduction to graphite on the iron catalyst. Now, the optimized system is producing quality target graphite in stable and reproducible conditions.

INTRODUCTION

Graphitization of samples is a routine procedure for high-precision AMS ^{14}C measurements. In AGE-1, samples are combusted in a standard elemental analyzer (EA, Elementar, Vario Micro Cube) and the resulting CO_2 is absorbed in a zeolite trap [1,2]. The CO_2 is released by heating the trap and expands to the individual reactors, where it is reduced by H_2 to graphite on the surface of iron catalyst. The iron catalyst plays a very important role in the graphitization system and it is important to understand how it influences the reaction mechanism at given conditions.

For better understanding of the reaction system [3], a more detailed view on equilibrium reactions visualized in a Baur-Glaessner diagram is a helpful option (Fig.1). However, pressure decrease during the graphitization reaction in closed reactors has to be considered.

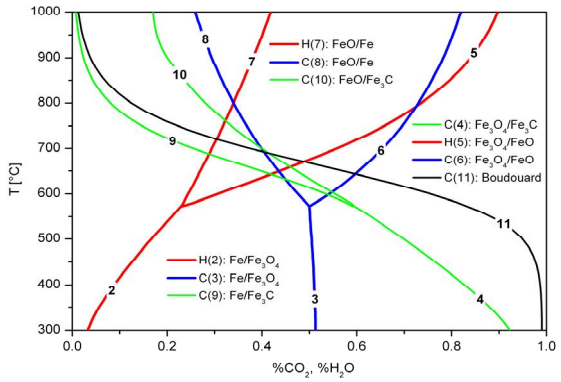

Fig. 1: Extended Baur-Glaessner diagram for Fe/CO_2, Fe/Fe_3C and Fe/H_2O systems.

EXPERIMENTAL

To find optimal reaction parameters [2], blank (brown coal) samples were combusted and the resulting CO_2 was graphitized at various H_2/CO_2 pressure ratios (1.8-2.5) and temperatures (540-620°C). For the graphitization, catalyst (3.20 ± 0.06 mg) preheated to 500°C with air for 240 s followed with 3-step reduction with H_2 was used. At the end of the reaction the reactors were evacuated and flushed with argon to remove all the residual gases.

RESULTS AND DISCUSSION

Resulting graphite samples were measured by AMS with the MICADAS system [4]. The smallest isotopic changes ($\delta^{13}C$) at the minimum of molecular fragment formation (^{13}CH current) and reaction time were taken into account to choose final graphitization conditions; 580°C and 2.3 H_2/CO_2 together with the 240 s catalyst preheating were used.

With the parameters chosen, the set of samples was graphitized to determine the carbon yield and the reaction changes at various catalyst amounts. The amount of total carbon in the reactor was calculated from the CO_2 pressure, carbon mass was determined by iron weight difference before and after the reaction. The results in Fig. 2 show that the ^{12}C current correlates to the C/Fe ratio in the target and that the carbon amount on the iron is practically constant. This implies that the carbon yield of the reaction does not depend on the iron quantity in the tested range and the ^{12}C depends on the carbon density on the catalyst.

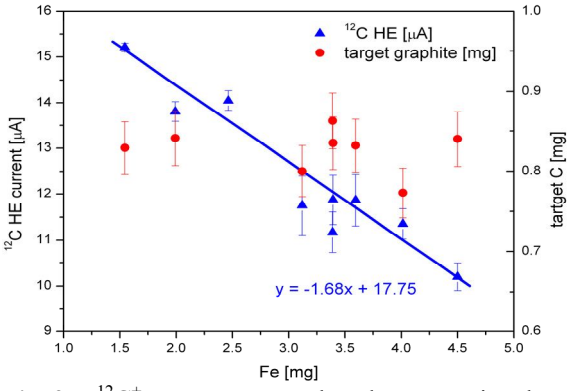

Fig. 2: $^{12}C^+$ HE current and carbon quantity dependence on Fe catalyst amount.

The average final carbon mass of 0.85 mg over all tested samples corresponds to approximately 95% reaction yield. Together with the transport efficiency of about 92%, the total efficiency of the graphitization procedure in carbon production is about 88%.

ACKNOWLEDGEMENT

We are very grateful to the Paul Scherrer Institut and University of Bern for financial support.

REFERENCES

[1] Wacker et al., Nucl. Instr. Meth. Phys. Res. B, in press (2009).
[2] Němec and Wacker, Ann. Rep. Lab. of Radio- & Environ. Chemistry, Uni Bern & PSI (2008), p. 50.
[3] Němec et al., Radiocarbon, submitted (2009).
[4] Synal et al., Nucl. Instr. Meth. Phys. Res. B, **259**, 7-13 (2007).

ALTERNATIVE CELLULOSE SEPARATION METHODS

M. Němec (Univ. Bern), L. Wacker, I. Hajdas (ETHZ), H.W. Gäggeler (Univ. Bern & PSI)

The main methods applied to clean plant material for radiocarbon dating are not compound specific and generally remove only the easily exchangeable components by an acid – base – acid sequence and additional steps like soxhlet extraction or oxidative bleaching with $NaClO_2$. In this work, two more compound specific but still simple methods – viscose extraction and cellulose dissolution in ionic liquid were tested to separate the cellulose from wood.

INTRODUCTION

Radiocarbon dating of various types of wooden artifacts and tree ring sequences is applied very often and plays an important role since the ^{14}C method was established. The chemically stable components of wood are ideal to preserve the original carbon isotopes ratios and thus the age information. The main methods applied to clean plant material for radiocarbon dating are not compound specific and generally remove only the easily exchangeable components. These are normally clean enough for standard radiocarbon measurement, but in some cases it is desirable to have pure cellulose, which is supposed to stay unchanged and immobile over long time ranges, representing the original plant material.

EXPERIMENTAL

In this work, two more compound specific but still simple methods were tested to separate the cellulose from wood [1]. The first one, the viscose method, is based on the xanthification process, where the cellulose converted to alkalicellulose forms with CS_2 a soluble cellulose xanthate, which is then extracted, decomposed and cellulose is recovered. The second procedure is based on the wood/cellulose dissolution in ionic liquid 1-butyl-3-methylimidazolium chloride [BMIM]Cl, where the dissolved cellulose could be precipitated again by simply adding a water-acetone mixture. This process was recently reported in the literature [2], but is still not used in sample preparation procedures for radiocarbon dating.

The standard acid-base-acid (ABA) and its variation called BABAB (base-acid-base-acid-bleaching) methods were used to compare potential contamination of wood samples. Eichstaet wood sequences (1111 – 1269 and 1271 – 1305 calendar age), IAEA C3 cellulose standard and recent Hönggerberg wood were used as standard materials.

RESULTS AND DISCUSSION

The main purpose of these experiments was to develop and test alternative cellulose preparation procedures suitable for AMS measurements, which would show an additional and applicable way to separate cellulose from wood.

None of the wooden samples were fully dissolved, but a reasonable amount of cellulose was prepared in all cases. The α-cellulose yield from the IAEA-C3 cellulose standard was almost 50% for the viscose method and the holocellulose yield for the ionic liquid method was even 75%. For wood samples the absolute yields were approx. 30% for BABAB, 10% - 20% for viscose and 14% for IL.

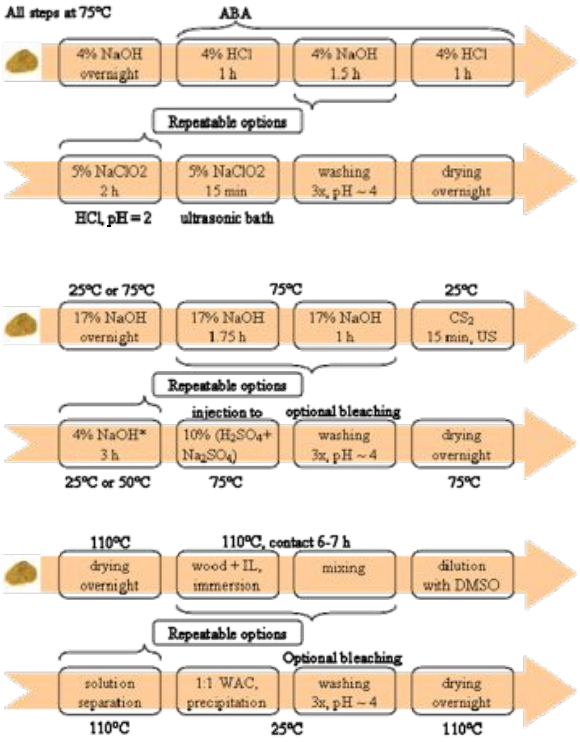

Fig. 1: Sample preparation procedures, from the top: BABAB, viscose, ionic liquid [1].

The goal was to prepare clean products with no "dead" carbon contamination from the chemicals used. These methods showed all satisfactory results, and the radiocarbon results in general fit very well to values obtained in reference BABAB method. Nevertheless, the measured ^{14}C age was for BABAB, viscose and IL methods slightly older then the IntCal04 calibration curve all over the investigated time interval, while the ABA ^{14}C ages fit on the curve or were even slightly younger.

ACKNOWLEDGEMENT

We are very grateful to the Paul Scherrer Institut and University of Bern for financial support.

REFERENCES

[1] Němec et al., Radiocarbon, submitted (2009).
[2] Fort et al., Green Chemistry, **9**, 63-69 (2007).

TOWARDS ONLINE ^{14}C ANALYSES OF CARBONACEOUS AEROSOL FRACTIONS

N. Perron, A.S.H. Prévôt, U. Baltensperger (PSI LAC), S. Szidat (Univ. Bern),
S. Fahrni, M. Ruff (Univ. Bern & PSI), L. Wacker (ETHZ)

A commercial OC/EC analyser was coupled with the gas ion source of the MICADAS and its feeding system. The final goal is to achieve semi on-line ^{14}C analysis of atmospheric filters for source apportionment of carbonaceous aerosol. We present here the set-up and the first measurements of reference materials and blanks.

INTRODUCTION

Atmospheric carbonaceous aerosol is conventionally divided into organic and elemental carbon (respectively OC and EC). Their carbon amounts can be analysed with an OC/EC analyser whereas their fossil and non-fossil origins are determined by ^{14}C analysis [1, 2]. To merge these two operations, we started developing an on-line system connecting a commercial OC/EC analyser with the gas ion source [3] of the Accelerator Mass Spectrometer (AMS) MICADAS [4] using its CO_2 feeding system [5].

METHODS

The RT 3080 thermo-optical OC/EC analyser (Sunset Laboratories Inc.) and the gas ion source of the small AMS system MICADAS [4] were connected via a gas interface [5] which consisted of (Fig. 1):

- a zeolite sieve to trap the CO_2 emitted by the analyser,
- a gas-tight syringe to mix the CO_2 with helium and inject it into the gas ion source,
- a 6-port valve switching between those two elements.

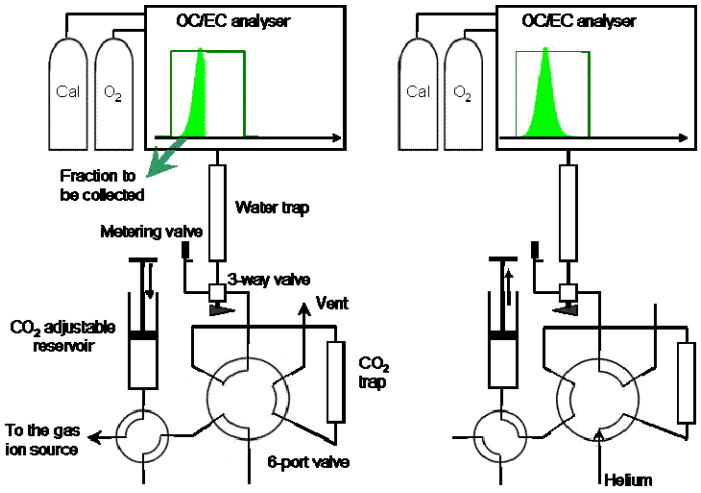

Fig. 1: Coupling system between the OC/EC thermo-optical analyser and the gas interface, during CO_2 trapping (left) and during injection to the gas ion source (right).

In addition, we installed upstream of the interface:

- a $Mg(ClO_4)_2$ water trap,
- a 3-way valve to direct the instrument exhaust either to the interface or to the outside.

OC/EC analyses were run under pure O_2, to anticipate the use of a currently investigated EC/OC separation method.

RESULTS

Prebaked quartz filters punches were spiked with solutions of IAEA standards (10-20 µgC) and frozen until analysis of their ^{14}C content with a one-step temperature program.

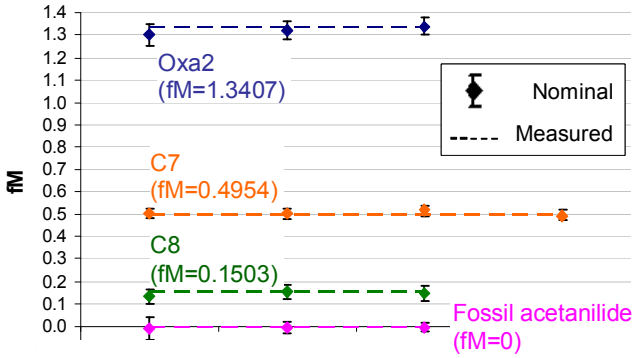

Fig. 2: fM values for filter measurements of standards. A filter blank correction of 2.0±0.4 µgC and fM=0.54 was applied.

The necessary use of quartz filters for this kind of analysis led to the adsorption of volatile organic compounds on the filter fibres during the sample preparation. After correcting for this artefact amounting to 2.0 µgC at fM=0.54, all but two of the ^{14}C signatures agreed within the 1-σ range with the expected nominal values.

CONCLUSIONS AND OUTLOOK

The AMS system MICADAS was successfully coupled with the OC/EC analyser. The first on-line ^{14}C measurements of reference materials were encouraging. Future investigation will focus on adapting the thermal program of the OC/EC analyser to real atmospheric filters in order to achieve on-line ^{14}C measurements of OC and EC.

REFERENCES

[1] S. Szidat et al., Geophys. Res. Lett., **34**, L05820, doi:10.1029/2006GL028325 (2007).
[2] S. Szidat et al., Nucl. Instrum. Methods Phys. Res. B, **223-224**, 829-836 (2004).
[3] M. Ruff et al., Radiocarbon, **49**, 307-314 (2007).
[4] H.-A. Synal et al., Nucl. Instrum. Methods Phys. Res. B, **259**, 7-13 (2007).
[5] M. Ruff et al., Radiocarbon, submitted (2008).

IS ^{210}Pb SUITED FOR THE DETERMINATION OF GLACIER FLOW RATES?

H.W. Gäggeler (Univ. Bern & PSI), S. Szidat, E. Vogel (Univ. Bern), L. Tobler (PSI), H. Boss (Interlaken)

^{210}Pb activity concentrations in surface ice along an 8 km long trajectory was used to evaluate the flow rate of the Aletsch Glacier using samples collected in August 2008.

It is quite unclear which species remain essentially conserved in a temperate glacier and which are depleted by percolating water. This study was initiated by a measurement of tritium and ^{210}Pb of surface ice along the temperate Tasman Glacier, which showed that despite frequent precipitation events in summer in form of rain, the activity concentrations of these two radiotracers seemed to remain essentially unchanged [1]. Between 20 and 22 August 2008 eleven surface samples were retrieved along the Aletsch Glacier to check, whether this observation also holds for this glacier. The coordinates of the sampling sites are summarized in [2] and marked in Fig. 1. The following anion and radionuclides were measured: sulphate as an indicator of melt-water-induced depletion, ^{210}Pb as a possible radiotracer for the determination of the flow rate of the glacier surface, and ^{238}U as source of "supported" ^{210}Pb. The ^{238}U data have been presented previously [2]. It turned out that the supported ^{210}Pb activity concentrations were negligible.

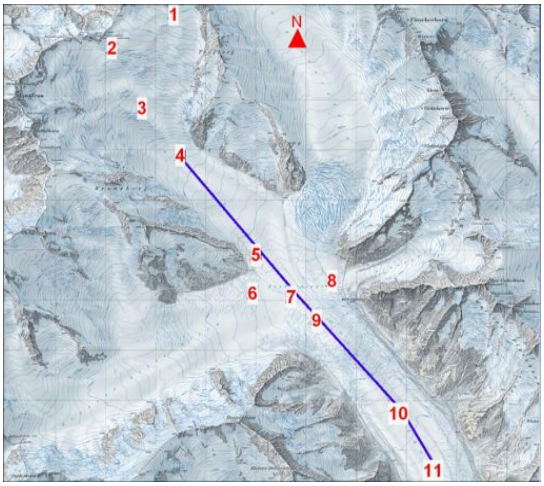

Fig. 1: Sampling sites at the Aletsch Glacier, see also [2].

Fig. 2 depicts the results for sulphate and ^{210}Pb. Sulphate measurements show the expected behaviour of a water-soluble tracer: in fresh snow (samples 1 and 2) the concentrations are high and agree well with expectations. In all other samples concentrations are much lower, obviously depleted by melt water. ^{210}Pb activity concentrations show a distinctly different picture. The ^{210}Pb profile depicts expected activity concentrations for the fresh snow (samples 1 and 2) averaging to 28 mBq/L. On sampling position 3, a strong dirt layer on the surface was assigned to a Saharan dust episode that occurred a few weeks prior to collection [2]. This might explain the exceptional high ^{210}Pb activity concentration. The value at position 4, the end of the snow covered glacier surface from where on ice was sampled instead of firn amounted to 656 mBq/L. The values then steadily decrease to 135 mBq/L for the sample 11, except for samples 7 and 8 with somewhat elevated ^{210}Pb activity concentrations on the Konkordia place.

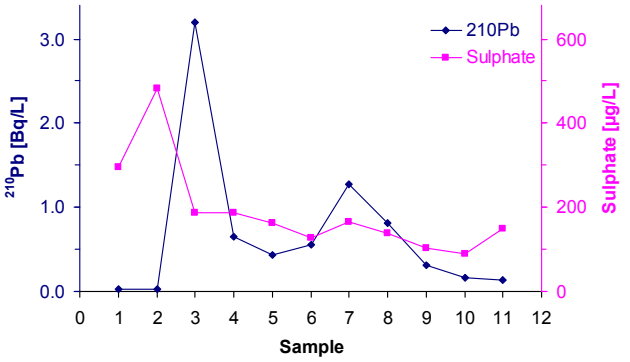

Fig. 2: ^{210}Pb and sulphate concentrations at the 11 sampling sites.

If we take all sampling sites along an approximate trajectory in the middle of the glacier (positions 4, 5, 7, 9, 10, 11, see blue line in Fig. 1), we observe a steady decrease of the activity concentration, except for sample 7 in the middle of the Konkordia place, which is significantly higher for unknown reasons. Excluding this sample we can estimate an average flow rate of the surface of the Aletsch Glacier between position 4 and 11 encompassing 7.92 km distance as 166 m/a (Tab. 1). The estimated statistical uncertainties for the flow rates amount to about 15 % (1σ). The systematic uncertainties (only one single sampling at a given coordinate) might be considerably larger.

Tab. 1: Surface flow rates of the Aletsch Glacier.

Section	Length [km]	Activity ratio	Flow rate [m/a]
4 – 5	2.48	1.52	184
5 – 9	1.62	1.37	159
9 – 10	2.41	1.87	120
10 – 11	1.41	1.24	200
Mean			166

The average flow rate seems to be somewhat high, though a glaciological velocity measurement showed that below the Konkordia place the glacier moves as fast as 200 m/a [3]. Below and above this position the value should be, however, significantly lower [3].

REFERENCES

[1] U. Morgenstern, priv. comm. (2009).

[2] H.W. Gäggeler et al., Ann. Rep. Lab. of Radio- & Environ. Chemistry 2008, Uni Bern & PSI (2009), p. 35.

[3] M. Funk, priv. comm. (2010).

LIST OF PUBLICATIONS

HEAVY ELEMENTS

R. C. Barber, H. W. Gäggeler, P. J. Karol, H. Nakahara, E. Vardaci, E. Vogt
Discovery of the element with atomic number112
Pure Appl. Chem., **81** (7) 1331 (2009).

L. Canella, P. Kudejova, R. Schulze, A. Türler, J. Jolie
PGAA, PGAI and NT with cold neutrons: Test measurement on a meteorite sample
Appl. Rad. Isotopes **67** (12): 2070-2074 (2009).

R. Dressler, R. Eichler, D. Schumann, S. Shishkin
Long-term alpha - and spontaneous fission measurement of a Rf/Db sample chemically prepared in a Ca-48 on Am-243 experiment
Phys. Rev. C 79(5), 054605 (2009).

J. Dvorak, W. Brüchle, C. E. Düllmann, Z. Dvorakova, K. Eberhardt, R. Eichler, E. Jäger, Y. Nagame, Z. Qin, M. Schädel, B. Schausten, E. Schimpf, R. Schuber, A. Semchenkov, P. Thörle, A. Türler, M. Wegrzecki, A. Yakushev
Cross section limits for the Cm-248(Mg-25,4n-5n) Hs-(268,269) reactions
Phys. Rev. C 79(3), 037602 (2009).

C. M. Folden Iii, I. Dragojević, C. E. Düllmann, R. Eichler, M. A. Garcia, J. M. Gates, S. L. Nelson, R. Sudowe, K. E. Gregorich, D. C. Hoffman, H. Nitsche
Measurement of the Pb-208 (Cr-52,n) Sg-259 excitation function
Phys. Rev. C 79(2), 027602 (2009).

X. Lin, H. Gerstenberg, Ch. Lierse von Gostomski, R. Henkelmann, A. Türler, M. Rossbach
Determination of k_0-values for the reactions ^{94}Zr (n,γ) ^{95}Zr and ^{96}Zr (n, γ) ^{97}Zr - ^{97m}Nb by irradiation in highly thermalized neutron flux
Appl. Rad. Isotopes **67** (12): 2092-2096 (2009).

SURFACE CHEMISTRY

B. D'Anna, A. Jammoul, C. George, K. Stemmler, S. Fahrni, M. Ammann, A. Wisthaler
Light-induced ozone depletion by humic acid films and submicron aerosol particles
J. Geophys. Res. **114** (2009).

A. Rouviere, P. F. DeCarlo, A. Schlierf, O. Favez, B. D'Anna, C. George, A. Prevot, M. Ammann
Photosensitized aging of succinic acid aerosol
Geochim. Cosmochim. Acta **73**(13), A1125 (2009).

Y. Sosedova, A. Rouvière, H.W. Gäggeler, M. Ammann
Uptake of NO_2 to deliquesced dihydroxybenzoate aerosol particles
J. Phys. Chem. A **113**(41), 10979-10987 (2009).

M.G.C. Vernooij, M. Mohr, G. Tzvetkov, V. Zelenay, T. Huthwelker, R. Kaegi, R. Gehrig, B. Grobéty
On source identification and alteration of single diesel and wood smoke soot particles in the atmosphere; an X-Ray microspectroscopy study
Environ. Sci. Technol. **43**(14), 5339-5344 (2009).

O. Vesna, M. Sax, M. Kalberer, A. Gaschen, M. Ammann
Product study of oleic acid ozonolysis as function of humidity
Atmos. Environ. **43**(24), 3662-3669 (2009).

A. Vlasenko, T. Huthwelker, H. W. Gäggeler, M. Ammann
Kinetics of the heterogeneous reaction of nitric acid with mineral dust particles: An aerosol flowtube study
Phys. Chem. Chem. Phys. **11**(36), 7921-7930 (2009).

ANALYTICAL CHEMISTRY

A. Eichler, S. Brütsch, S. Olivier, T. Papina, M. Schwikowski
A 750 year ice core record of past biogenic emissions from Siberian boreal forests
Geophys. Res. Lett. **36** (2009).

A. Eichler, S. Olivier, K. Henderson, A. Laube, J. Beer, T. Papina, H. W. Gäggeler, M. Schwikowski
Temperature response in the Altai region lags solar forcing
Geophys. Res. Lett. **36** (2009).

A. Eichler, S. Olivier, K. Hendersen, A. Laube, J. Beer, T. Papina, H.W. Gäggeler, M. Schwikowski
Temperature changes in the Altai are driven by solar and anthropogenic forcing
Chimia **63**, 1 (2009).

U. Heikkila, J. Beer, J. Feichter, V. Alfimov, H. A. Synal, U. Schotterer, A. Eichler, M. Schwikowski, L. Thompson
Cl-36 bomb peak: Comparison of modeled and measured data
Atmos. Chem. Phys. **9**(12), 4145-4156 (2009).

T. M. Jenk, S. Szidat, D. Bolius, M. Sigl, H. W. Gäggeler, L. Wacker, M. Ruff, C. Barbante, C. F. Boutron. M. Schwikowski
A novel radiocarbon dating technique applied to an ice core from the Alps indicating late Pleistocene ages
J. Geophys. Res. **114** (2009).

S. Panebianco, K. Berg, J.C. David, M. Eid, U. Filges, F. Gröschel, A. Guertin, A.Y. Konobeyev, C. Latge, S. Lemaire, S. Leray, A. Letourneau, M. Luthy, F. Michel-Sendis, S. Scazzi, G. Stankunas, N. Thiolliere, L. Tobler, L. Zanini
Neutronic characterization of the MEGAPIE target
Ann. Nucl. Energy **36**, 350 (2009).

M. Schwikowski, A. Eichler, I. Kalugin, D. Ovtchinnikov, T. Papina
Past climate variability in the Altai
PAGES News Vol. **17** N°1, 44-45 (2009).

M. Sigl, T. M. Jenk, T. Kellerhals, S. Szidat, H. W. Gäggeler, L. Wacker, H.-A. Synal, C. Boutron, C. Barbante, J. Gabrieli, M. Schwikowski
Towards radiocarbon dating of ice cores
J. Glaciol. **55** (194), 986-996 (2009).

F. Thevenon, F. S. Anselmetti, S. M. Bernasconi, M. Schwikowski
Mineral dust and elemental black carbon records from an alpine ice core (Colle Gnifetti glacier) over the last millennium
J. Geophys. Res. **114** (2009).

F. Vimeux, P. Ginot, M. Schwikowski, M. Vuille, G. Hoffmann, L. G. Thompson, U. Schotterer
Climate variability during the last 1000 years inferred from Andean ice cores: A review of methodology and recent results
Palaeogeogr., Palaeoclim., Palaeoeco. **281**(3-4), 229-241 (2009).

RADWASTE ANALYTICS

M. Ayranov, U. Krähenbühl, S. Röllin, M. Burger
Sensitivity of DF-ICP-MS, PERALS and alpha spectrometry for the determination of actinides: A comparison
J. Radioanal. Nucl. Chem. **279**(2), 475 - 480 (2009).

M. Ayranov, J. Cobos, K. Popa, V.V. Rondinella
Determination of REE, U, Th, Ba, and Zr in simulated hydrogeological leachates by ICP-AES after matrix solvent extraction
Journal of Rare Earths **27**(1), 123 (2009).

C. Domingo-Pardo, I. Dillmann, T. Faestermann, U. Giesen, J. Gorres, M. Heil, S. Horn, F. Kappeler, S. Köchli, G. Korschinek, J. Lachner, M. Maiti, J. Marganiec, J. Neuhausen, R. Nolte, M. Poutivtsev, R. Reifarth, R. Rugel, D. Schumann, E. Uberseder, F. Voss, S. Walter, M. Wiescher
S-process nucleosynthesis in massive stars: New results on Fe-60, Ni-62 and Ni-64
Capture Gama-Ray Spectroscopy and Related Topics **1090** 230-237 (2009).

G. Rugel, T. Faestermann, K. Knie, G. Korschinek, M. Poutivtsev, D. Schumann, N. Kivel, I. Günther-Leopold, R. Weinreich, M. Wohlmuther
New measurement of the Fe-60 half-life
Phys. Rev. Lett. **103**(7), 072502-4 (2009).

D. Schumann, J. Neuhausen, J. Eikenberg, M. Rüthi, M. Wohlmuther, P. W. Kubik, H.-A. Synal, V. Alfimov, G. Korschinek, G. Rugel, T. Faestermann
Radiochemical analysis of a copper beam dump irradiated with high-energetic protons
Radiochim. Acta **97**(3), 123-131 (2009).

E. Uberseder, R. Reifarth, D. Schumann, I. Dillmann, C. D. Pardo, J. Gorres, M. Heil, F. Kappeler, J. Marganiec, J. Neuhausen, M. Pignatari, F. Voss, S. Walter, M. Wiescher
Measurement of the Fe-60(n,gamma)Fe-61 cross section at stellar temperatures
Phys. Rev. Lett. **102**(15), (2009).

ENVIRONMENTAL RADIONUCLIDES UNIVERSITÄT BERN

R. Fisseha, M. Saurer, M. Jaggi, R.T.W. Siegwolf, J. Dommen, S. Szidat, V. Samburova, U. Baltensperger
Determination of primary and secondary sources of organic acids and carbonaceous aerosols using stable carbon isotopes
Atmos. Environ. **43**(2), 431-437 (2009).

K. Hippe, F. Kober, H. Baur, M. Ruff, L. Wacker, R. Wieler
The current performance of the in situ ^{14}C extraction line at ETH
Quaternary Geochronology **4**, 493-500, doi:10.1016/j.quageo.2009.06.001 (2009).

K. Li, E. Vogel, U. Krähenbühl
Measurement of I-129 in environmental samples by ICP-CRI-QMS: possibilities and limitations
Radiochim. Acta **97**, 453-458, doi:10.1524/ract.2009.1639 (2009).

S. Szidat
Atmosphere sources of Asian haze
Science **323**(5913), 470-471 (2009).

S. Szidat, M. Ruff, N. Perron, L. Wacker, H.A. Synal, M. Hallquist, A.S. Shannigrahi, K.E. Yttri, C. Dye, D. Simpson
Fossil and non-fossil sources of organic carbon (OC) and elemental carbon (EC) in Goteborg, Sweden
Atmos. Chem. Phys. **9**(5), 1521-1535 (2009).

S. Szidat
Radiocarbon analysis of carbonaceous aerosols: Recent developments
Chimia **63**(3), 157-161 (2009).

TECHNICAL REPORT

J. Neuhausen, D. Schumann, Ch. Zumbach, M. Dubs
Arbeitsschritte zur Zerlegung der Megapie-Schnitte H07, H08 und H09 (Expansionstank) und zur Probennahme für radiochemische Untersuchungen
TM 24-09-01, 2009.

REPORTS

Y. Dai, J. Neuhausen, D. Schumann, C. Zumbach
Specimen extraction plan for MEGAPIE PIE
MEGAPIE-Report MPR-11-DY34-001-2, 2009.

J. Neuhausen, D. Schumann, R. Dressler, S. Horn, S. Lüthi, St. Heinitz, S. Chiriki, T. Stora, M. Eller
Innovative waste management in the mercury loop of the EURISOL Multi-MW converter target
EURISOL-DS project, Task2 Deliverable D2, 2009.
http://www.eurisol.org/site02/doc_details.php?operation=download&docu=951&type=25

PATENT

J.M. Moreno, A. Türler, R. Henkelmann, E. Kabai, E. Huenges
Method for purification of ^{225}Ac from irradiated ^{226}Ra targets
US Patent No: US 2009/0191122 A1, 30.7.2009.

CONTRIBUTIONS TO CONFERENCES, WORKSHOPS AND SEMINARS

HEAVY ELEMENTS

L. Canella, P. Kudejova, R. Schulze, A. Türler, J. Jolie
The PGAA facility at FRM II
FRM-II Seminar, Garching, Germany, 18 May 2009.

R. Dressler
Estimation of statistical uncertainties in the case of rare events
Seminar of the Laboratory of Radiochemistry and Environmental Chemistry, Paul Scherrer Institut and University of Bern, 6 March 2009.

R. Dressler, P. Rasmussen, R.Eichler, N.Schlumpf
pureCOLD for beta-alpha pile-up suppression: a status report
7-th Workshop on the Chemistry of the Heaviest Elements, Mainz, Germany, 11-13 October 2009.

R. Dressler for a PSI-University Bern-FLNR-LLNL-ITE-FZD collaboration
The challenge of using a physical preseparator in chemical experiments with super heavy elements: the stopping force problem
The fourth Asia-Pacific Symposium on Radiochemistry APSORC09, Napa, USA, 29 November - 4 December 2009.

R. Eichler
Chemical investigation of transactinide elements
Seminar on New Horizons in Actinide Chemistry Research , BARC, Mumbai, India, 6 January 2009.

R. Eichler
Gas phase chemistry with transactinide elements
NUCAR 2009 symposium, Mumbai, India, 7-10 January 2009.

R. Eichler for a PSI-University of Bern-FLNR-LLNL-ITE collaboration
Chemical investigation of element 114
237th ACS National Meeting, Salt Lake City, UT, USA, 22-26 March 2009.

R. Eichler for a PSI-University of Bern-FLNR-LLNL-ITE collaboration
Chemical investigation of superheavy elements 112 and 114
ACTINIDES´09, San Francisco, CA, USA, 12-17 July 2009.

R. Eichler
Gas phase chemistry with transactinides (The last 10 years and what's next)
GDCH Wissenschaftsforum Chemie, Frankfurt am Main, Germany, 30 August - 2 September 2009.

R. Eichler for a PSI-University of Bern-FLNR-LLNL-ITE collaboration
Chemical investigation of element 114
7-th Workshop on the Chemistry of the Heaviest Elements, Mainz, Germany, 11-13 October 2009.

H.W. Gäggeler
Actinides Research at the Laboratory of Radiochemistry and Environmental Chemistry
Radiochemistry Seminar on New Horizons in Actinide Chemistry Research, BARC, Mumbai, India, 6 January 2009.

H.W. Gäggeler
Radiochemical research in Switzerland
NUCAR 2009 symposium, Mumbai, India, 7-10 January 2009.

H.W. Gäggeler
From Mendeleev's principle to Einstein's relativity: news from the chemistry of superheavy elements
Int. Symp. Periodic Table of D.I. Mendeleev. The new superheavy elements, Dubna, Russia, 20-21 January 2009.

H.W. Gäggeler
Misserfolge und erfolglose Suchexperimente,
25 Jahre Labor für Radio- und Umweltchemie, Paul Scherrer Institut, Switzerland, 28 August 2009.

H.W. Gäggeler
Chemical studies of the currently heaviest members of the Periodic Table
Symposium of the occasion of 175 anniversary of D.I. Mendeleev, Tobolsk, Russia, 16-19 September 2009.

H.W. Gäggeler
Chemistry experiments with elements 112 and 114
EXON Conf., Sochi, Russia, 28 September - 2 October2009.

H.W. Gäggeler
From Mendeleev's principle to Einsteins relativity: news from the chemistry of superheavy elements
Institute of Advanced Study, Massey University, Albany (Auckland), New Zealand, 6 November 2009.

S. M. Lehenberger, K. P. Zhernosekov, A. Türler, S. Cohrs, K. Zimmermann, J. Grünberg, R. Schibli
Production and application of the low energy electron emitter ^{161}Tb for endoradiotherapy as a better alternative to ^{177}Lu
EANM 09, Annual Congress of the European Association of Nuclear Medicine, Barcelona Spain, 10-14 October 2009.

A. Serov
Model experiments with homologues of superheavy elements (SHE)
Seminar of the Laboratory of Radiochemistry and Environmental Chemistry, Paul Scherrer Institut and University of Bern, 2 October 2009.

A. Serov, R. Eichler, H.W. Gäggeler
Adsorption interaction of In-113m and Tl-200-202 isotopes with quartz.
7-th Workshop on the Chemistry of the Heaviest Elements, Mainz, Germany, 11-13 October 2009.

D. Wittwer
Gas phase chemical studies of superheavy elements using the Dubna gas-filled recoil separator - stopping range determination
DCB Unibe 1st year graduate students symposium, Switzerland, 7 July 2009.

D. Wittwer
Stopping force estimations for element 114 in Mylar and argon gas
7-th Workshop on the Chemistry of the Heaviest Elements, Mainz, Germany, 11-13 October 2009

D. Wittwer
Gas phase chemical studies of superheavy elements using the Dubna gas-filled recoil separator - stopping range determination
TOURS 2009 - Tours Symposium on Nuclear Physics and Astrophysics VII, Kobe, Japan, 16-20 November 2009.

A. Türler
Nuclear structure and reaction studies near and at Z = 108 and N =162
Symposium of the occasion of 175 anniversary of D.I. Mendeleev, Tobolsk, Russia, 16-19 September 2009.

A. Türler
Grundlagen der Nuklearchemie in 60 Minuten
GDCh Kolloquium Institut für Chemie, Martin-Luther-Universität Halle-Wittenberg, Halle, Germany, 13 May 2009.

A. Türler
Ausgewählte Themen nuklearchemischer Grundlagenforschung - ein Streifzug durch die Nuklidkarte
GDCh Kolloquium Institut für Chemie, Martin-Luther-Universität Halle-Wittenberg, Halle, Germany, 13 May 2009.

SURFACE CHEMISTRY

M. Ammann, T. Huthwelker, M. Kerbrat, T. Bartels-Rausch, A. Křepelová
Flow tube, diffusion tube and molecular level spectroscopic studies of nitrous, nitric and pernitric acid uptake on ice
SCOUT-O3 Laboratory Activity 5 Annual Meeting, Mainz, Germany, 16-18 February 2009.

M. Ammann, V. Zelenay, A. Křepelová, J. Raabe, B. Watts, T. Huthwelker
The climate effect of atmospheric particles caught in act
JUM@P'09: Joint Users' meeting at PSI, Villigen, 12-13 October 2009.

M. Ammann, A. Rouvière, Y. Sosedova, C. George, B. D'Anna, V. Zelenay, A. Křepelová, T. Huthwelker
Microchemistry and microstructure of organic particles
EUCAARI Annual Meeting, Stockholm, Sweden, 16-20 November 2009.

M. Ammann, A. Rouvière
Effect of fatty acid coatings on ozone uptake to deliquesced KI/NaCl aerosol particles
AGU Fall Meeting, San Francisco, California, USA, 14-18 December 2009.

T. Bartels-Rausch, M. Kerbrat, A. Křepelová, M. Ammann
Snow as reactor
10th Swiss Global Change Day, Bern, Switzerland, 31 March 2009.

T. Bartels-Rausch, J. Kleffmann, Y. Elshorbany, M. Brigante, C. George, B. D'Anna, A. Bernhard, M. Schläppi, M. Schwikowski, M. Ammann
HONO and Hg: Photo-enhanced reductions in ice by organics
European Geosciences Union General Assembly Vienna, Austria, 20-24 April 2009.

T. Bartels-Rausch, M. Kerbrat, T. Huthwelker, A. Křepelová, T. Ulrich, M. Ammann
Beyond adsorption: Recent approaches in the laboratory to study uptake of trace gases to ice
Fifth SCOUT-O3 Annual Meeting, Schliersee, Germany, 15-17 June 2009.

T. Bartels-Rausch
Recent approaches in the laboratory to study uptake and reactivity of trace gases on ice
Laboratoire de Physique et de Chimie de l'Environnement et de l'Espace, CNRS and University of Orleans, France, 3-5 September 2009.

T. Huthwelker, A. Křepelová, V. Zelenay, T. Bartels-Rausch, M. Janousch, M. Ammann
X-ray spectroscopy of frozen salt solutions: Are inclusions solid or liquid below eutectic temperature?
European Geosciences Union General Assembly Vienna, Austria, 20-24 April 2009.

T. Huthwelker, A. Křepelová, M. Janousch, T. Bartels-Rausch, M. Ammann
X-ray spectroscopy of frozen salt solutions: The liquid nature of ions in frozen solutions
XAFS XIV, Camerino, Italy, 26-31 July 2009.

T. Huthwelker, A. Křepelová, T. Bartels-Rausch, V. Zelenay, M. Janousch and M. Ammann
The aqueous nature of ions in frozen salt solutions at temperatures below the eutectic temperature
JUM@P'09: Joint Users' meeting at PSI, Villigen, 12-13 October 2009.

M. Kerbrat, T. Huthwelker, A. Křepelová, T. Ulrich, T. Bartels-Rausch, M. Ammann
Flow tube and molecular level spectroscopy studies of nitrous, nitric and pernitric acid uptake on ice
Fifth SCOUT-O3 Annual Meeting, Schliersee, Germany, 15-17 June 2009.

A. Křepelová, T. Huthwelker, M. Janousch, M. Ammann
X-ray studies of halogen salt impurities in ice
Seminar of the Laboratory of Radiochemistry and Environmental Chemistry, University of Berne and Paul Scherrer Institut 3 April 2009.

A. Křepelová, M. Ammann, J.T. Newberg, H. Bluhm, T. Huthwelker
The effect of strong acids on the ice - air interface studied by X-ray photoelectron spectroscopy
European Geosciences Union General Assembly Vienna, Austria, 20-24 April 2009.

A. Křepelová, M. Ammann, T. Huthwelker, J.T. Newberg, H. Bluhm
X-ray photoelectron spectroscopy of halogen salt impurities in ice
JUM@P'09: Joint Users' meeting at PSI, Villigen, Switzerland, 12-13 October 2009.

A. Křepelová, M. Ammann, J.T. Newberg, H. Bluhm, T. Huthwelker
Impact of strong acids on ice surface melting studied by XPS and NEXAFS
Advanced Light Source Users' Meeting Lawrence Berkeley National Laboratory, Berkeley, USA, 15-17 October 2009.

A. Rouvière, Y. Sosedova, M. Ammann, H. W. Gäggeler
Determination of bulk accommodation coefficient of NO_2 and O_3 to inorganic/organic aerosols
European Aerosol Conference, Karlsruhe, Germany, 6-11 September 2009.

A. Rouvière, P. F. DeCarlo, A. Schlierf, O. Favez, B. D'Anna, C. George, A. Prévôt, M. Ammann
Photosensitized transformation of dicarboxylic acid in aerosols
European Aerosol Conference, Karlsruhe, Germany, 6-11 September 2009.

A. Rouvière, P. F. DeCarlo, B. D'Anna, C. George, A. Prévôt, M. Ammann
Influence of a photosensitizer on the aging of succinic acid aerosol
INTROP Conference on "Tropospheric Chemistry", Portoroz, Slovenia, 14-17 April 2009.

A. Rouvière, M. Ammann
Effect of organic coating on ozone uptake to deliquesced potassium iodide particles
Seminar of the Laboratory of Radiochemistry and Environmental Chemistry, Paul Scherrer Institut and University of Bern, 8 Mai 2009.

A. Rouvière, M. Ammann
Reactive uptake of O_3 on deliquesced KI particles coated with fatty acids and SDS
13th IACIS International Conference on Surface and Colloid Science New-York, U.S.A, 14-19 June 2009

A. Rouvière, P. F. DeCarlo, A. Schlierf, O. Favez, B. D'Anna, C. George, A. Prévôt, M. Ammann
Photosensitized aging of succinic acid aerosol
Goldschmidt 2009 - "Challenges to Our Volatile Planet", Davos, Switzerland, 21-26 June 2009.

A. Rouvière, P. DeCarlo, T. Bartels-Rausch, M. Ammann
Effect of photosensitized chemistry on organic aerosol evolution
AGU Fall Meeting, San Francisco, California, USA, 14-18 December 2009.

Y. Sosedova, A. Rouvière, M. Birrer, M. Ammann
Bulk reaction limited uptake of NO_2 by aerosols containing hydroquinone and gentisic acid
INTROP Conference on "Tropospheric Chemistry", Portoroz, Slovenia, 14-17 April 2009.

Y. Sosedova
NO_2 uptake on aqueous phenolic aerosols:Dark and illuminated conditions
Seminar of the Laboratory of Radiochemistry and Environmental Chemistry, Paul Scherrer Institut and University of Bern, 2 October 2009.

V. Zelenay, T. Huthwelker, A. Křepelová, M. Birrer, M. Ammann
Observation of water uptake in aerosol particles using microspectroscopy
Seminar of the Laboratory of Radiochemistry and Environmental Chemistry, Bern, Switzerland, 3 April 2009.

V. Zelenay, T. Huthwelker, A. Křepelová, M. Birrer, M. Ammann
Observations of water uptake in ammonium sulfate particles using x-ray microspectroscopy
INTROP Conference on "Tropospheric Chemistry", Portoroz, Slovenia, 14-17 April 2009.

V. Zelenay, A. Křepelová, M. Birrer, T. Tritscher, R. Chirico, T. Huthwelker, M. Ammann
Soot- water uptake
NEADS Workshop, PSI, Villigen, Switzerland, 7 July 2009.

V. Zelenay, A. Křepelová, M. Birrer, T. Huthwelker, M. Ammann
Fulvic acids: Tracking morphological changes upon water uptake
JUM@P'09: Joint Users' meeting at, PSI, Villigen, 12-13 October 2009.

V. Zelenay, A. Křepelová, M. Birrer, T. Tritscher, R. Chirico, T. Huthwelker, M. Ammann
Water uptake in single soot particles- an X-ray microspectroscopy study
ETH Seminar, ETHZ, Zürich, Switzerland, 2 December 2009.

ANALYTICAL CHEMISTRY

A. Eichler
Gletscher als Klima- und Umweltarchive
Metrohm Schweiz IC User Meeting, Zofingen, Switzerland, 22 October 2009.

J. Gabrieli, G. Cozzi, P. Vallelonga, M. Schwikowski, M. Sigl, C. Boutron, C. Barbante
A fast semi-quantitative method for plutonium determination in an alpine firn/ice core
European Geosciences Union General Assembly Vienna, Austria, 20-24 April 2009.

J. Gabrieli, P. Vallelonga, W. Cairn, G. Cozzi, F. Decet, M. Schwikowski, M. Sigl, C. Boutron, C. Barbante
A novel firn/ice-core melter system for semi-continuous extraction of PAHs and continuous ICP-QMS trace element analysis
EGU General Assembly, Vienna, Austria, 19–24 April 2009.

H.W. Gäggeler
On the way to quantify human impact on climate: pollution records and climatic information from alpine ice cores
University of Waikato, Hamilton, New Zealand, 13 November 2009.

H.W. Gäggeler
On the way to quantify human impact on climate: pollution records and climatic information from alpine ice cores
Massey University, Albany (Auckland), New Zealand, 18 December 2009.

S. Kaspari, M. Schwikowski, M. Gysel, P.A. Mayewski, S. Kang, S. Hou
Recent increase in black carbon concentrations from a Mt. Everest ice core spanning 1860-2000 AD
AGU Fall Meeting, San Francisco, California, USA, 14–18 December 2009.

M. Schläppi, T. Jenk, A. Rivera, G. Casassa, M. Schwikowski
Analytical tools for the investigation of climate parameters stored in an ice core from the Southern Patagonia Ice Field
Analytical Chemistry Symposium, ETH Zürich, Switzerland, 13 May 2009.

M. Schläppi
Carbonaceous particles in Pio XI glacier
Seminar of the Laboratory of Radiochemistry and Environmental Chemistry, Paul Scherrer Institut and University of Bern, 6 November 2009.

M. Schwikowski
Schnee von gestern - Gletschereis als Klimaarchiv
Veranstaltung für die Aktionäre, Obligationäre, Geschäftspartner und Freunde der Edisun Power Gruppe, Zürich, Switzerland, 20 January 2009.

M. Schwikowski
High-alpine glaciers as archives of atmospheric pollution and climate
Workshop on Muon Tomography and Emulsions, University of Bern, Switzerland, 29 January 2009.

M. Schwikowski
Klimageschichte aus alpinen Eisbohrkernen
SAC Lindenberg, Wohlen, Switzerland, 13 March 2009.

M. Schwikowski
High-mountain glaciers as climate archives
Conference High Mountain Glaciers and Climate Change, Tromsø, Norway, 7-10 June 2009.

M. Schwikowski
Gletscher - lesen in den Klimaarchiven der Erde
Lions Club Brugg, Untersiggenthal, Switzerland, 11 August 2009.

M. Schwikowski
Von kalten Füssen und warmen Gletschern
25 Jahre Labor für Radio- und Umweltchemie, Paul Scherrer Institut, Switzerland, 28 August 2009.

M. Sigl, H.W. Gäggeler, A. Kress, M. Schwikowski
The variability of $\delta^{18}O$ in an Alpine ice core reflects long-term trends of past summer (May-July) temperatures
Millennium European Climate 3rd Milestone Meeting, Cala Millor Mallorca, Spain, 2-6 March 2009.

M. Sigl, H.W. Gäggeler, M. Schwikowski
The variability of $\delta^{18}O$ in an Alpine ice core reflects long-term trends of past summer (May-July) temperatures
10th Swiss Global Change Day, Bern, Switzerland, 31 March 2009.

M. Sigl
1.000 year history of Saharan dust recorded in an Alpine ice core
Seminar – WSL Dendro Sciences, Birmensdorf, Switzerland, 16 September 2009.

RADWASTE ANALYTICS

M. Ayranov
*Currents status of the remotely controlled system for the radiochemical separation of exotic isotopes from accelerator waste*s
Seminar of the Laboratory of Radiochemistry and Environmental Chemistry, Paul Scherrer Institut and University of Bern, 6 March 2009.

M. Ayranov, D. Schumann
Production of ^{7}Be, ^{44}Ti and ^{60}Fe from proton irradiated copper beam dump and SINQ cooling water
Nuclear Physics in Astrophysics IV, Frascati, Italy, 8-12 June 2009.

M. Ayranov, Z. Tosheva, A. Kies
Determination of ^{210}Pb and ^{210}Po in water samples
International Topical Conference on Po and Radioactive Pb Isotopes, Seville, Spain, 26-28 October 2009.

M. Ayranov, D. Schumann
^{60}Fe samples for nuclear astrophysics experiments
TOURS 2009, Kobe, Japan, 16-20 November 2009.

S. Heinitz
Environmental compliance report concerning the chemical reactivity of Lead Bismuth – Estimations for ESS
ESS-PP Meeting Lund, Sweden, 1 October 2009.

S. Heinitz
Extraction and migration of polonium out of Lead-Bismuth Eutectic
ITC-9, Tokai, Japan, 3 December 2009.

J. Neuhausen, L. Zanini, St. Heinitz, D. Schumann, V. Boutellier, M. Ruethi, J. Eikenberg
Nuclear reaction product distribution in a p-irradiated liquid LBE target and Po-extraction from LBE
EUROTRANS DM4 Technical Review Meeting, Karlsruhe Institute of Technology, Karlsruhe, Germany, 3 March 2009.

J. Neuhausen
Recent results on the chemistry of liquid lead-bismuth and mercury targets
Information Exchange Meeting on activated LBE-Handling techniques, SCK-CEN, Mol, Belgium, 25 May 2009.

J. Neuhausen, D. Schumann, Ch. Zumbach, M. Dubs
Radiochemische Untersuchungen am Megapie-Target
MEGAPIE PIE-Meeting, Paul Scherrer Institute, Villigen, Switzerland, 20 August 2009.

J. Neuhausen, St. Heinitz, F. v. Rohr, D. Schumann, S. Lüthi, S. Horn, R. Dressler, B. Eichler, M. M. Marin Marmol, St. Keller, S. Müller, L. Zanini, V. Boutellier, M. Ruethi, J. Eikenberg
Mechanisms of spallation product release and deposition: Summary of achieved results
EUROTRANS DM4 Technical Meeting, Bologna, Italy, 16 September 2009.

J. Neuhausen
HLM-Handbook chapter 5
8-th Meeting of the OECD-NEA Expert Group for Heavy Liquid Metal Technology, Bologna, Italy, 17 September 2009.

J. Neuhausen, D. Schumann, Ch. Zumbach, M. Dubs
Radiochemical investigations of the Megapie-target
MEGAPIE Project Coordination Group and Steering Committee Meeting, Paul Scherrer Institute, Villigen, Switzerland, 5 November 2009.

J. Neuhausen, D. Schumann, R. Dressler, S. Horn, S. Lüthi, St. Heinitz, S. Chiriki
Radiochemistry of the EURISOL mercury target
Seminar of the Laboratory of Radiochemistry and Environmental Chemistry, Paul Scherrer Institut and University of Bern, 11 December 2009

D. Schumann
Radiochemical analysis of proton-irradiated lead targets
NUDATRA-meeting, Madrid, Spain, 3-5 March 2009.

D. Schumann
Exotic radionuclides from accelerator waste for science and technology
Seminar at University of Vienna, Austria, 19. March 2009.

D. Schumann
Bestimmung des Radionuklidinventars von Proben aus der Spallationsneutronenquelle (SINQ) des Paul Scherrer Instituts
Jahrestagung Kerntechnik, Dresden, Germany, 8-14 May 2009.

D. Schumann
Preparation of ^{60}Fe samples for nuclear physics experiments
NPA4 Gran Sasso, Italy, 8-12 June 2009.

D. Schumann
Working plan task 8.2.
ESS-PP meeting Jülich, Germany, 18 June 2009.

D. Schumann
Intermediate report
ESS-PP meeting Lund, Sweden, 30 September - 1 October 2009.

D. Schumann
Determination of the radionuclide inventory of samples from a spallation neutron source
ICEM Liverpool, Great Britain, 12-15 October 2009.

D. Schumann
Accurate nuclear data for nuclear energy sustainability
MEGAPIE PCG meeting, Villigen, Switzerland, 5 November 2009.

D. Schumann
Separation of ^{60}Fe samples from an irradiated beam dump for nuclear astrophysics experiments
APSORC09, Napa, USA, 29 November - 4 December 2009.

Environmental Radionuclides Universität Bern

D. Ceburnis D, C.D. O'Dowd, A. Garbaras, V. Remeikis, M. Rinaldi, S. Szidat, S. Fahrni, A.S.H. Prévôt, N. Perron, L. Wacker, S. Leinert
Proof of biogenic origin of marine aerosol by ^{13}C and ^{14}C analysis
19th Goldschmidt Conference, Davos, Switzerland, 21-26 June 2009.

S. Fahrni
Compound-specific radiocarbon analysis
Seminar Ion Beam Physics, ETH Zürich, Switzerland, 29 April 2009.

S. Fahrni
Compound-specific radiocarbon analysis – part II
Seminar of the Laboratory of Radiochemistry and Environmental Chemistry, Paul Scherrer Institut and University of Bern, 8 May 2009.

S. Fahrni, H.W. Gäggeler, M. Ruff, L. Wacker, S. Szidat
A preparative 2D-chromatography method for compound-specific radiocarbon analysis of aerosol components
20th International Radiocarbon Conference, Kona/Hawaii, USA, 31 May - 5 June 2009.

H.W. Gäggeler
Micro-radiocarbon determination with the table-top AMS system MICADAS
Methods and Applications of Radioanalytical Chemistry – MARC VIII, Kailua-Kona, Hawaii, USA, 5–10 April 2009.

H.W. Gäggeler, S. Szidat,
Microanalytical ^{14}C measurements on carbonaceous aerosol particles
APSORC'09 Conference, Napa, CA, USA, 29 November - 4 December 2009.

M. Němec
Optimisation of graphitisation procedure at AGE-1
Seminar of the Laboratory of Radiochemistry and Environmental Chemistry, Paul Scherrer Institut and University of Bern, 3 April 2009.

M. Němec, L. Wacker
AGE: Optimization of the graphitization procedure
DPG Frühjahrstagung, Hamburg, Germany, 2-6 March 2009.

M. Němec, L. Wacker
Optimization of the automated graphitization system AGE-1
20th International Radiocarbon Conference, Kona/Hawaii, USA, 31 May - 5 June 2009.

M. Němec, L. Wacker, I. Hajdas
Alternative methods for cellulose preparation for AMS measurement
20th International Radiocarbon Conference, Kona/Hawaii, USA, 31 May - 5 June 2009.

N. Perron, S. Szidat, A. S. H. Prévôt, U. Baltensperger
EC: not easy
Seminar Laboratory of Atmospheric Chemistry, Paul Scherrer Institut, Switzerland, 6 April 2009.

N. Perron, S. Szidat, S. Fahrni, L. Wacker, A.S.H. Prévôt, U. Baltensperger
Radiocarbon on-line analysis of atmospheric samples
20th International Radiocarbon Conference, Kona/Hawaii, USA, 31 May - 5 June 2009.

N. Perron, S. Szidat, A. S. H. Prévôt, U. Baltensperger
Particulate matter characterisation in the Swiss Rhone Valley
Seminar of the Laboratory of Radiochemistry and Environmental Chemistry, Paul Scherrer Institut and University of Bern, 6 November 2009.

N. Perron, S. Szidat, A. S. H. Prévôt, U. Baltensperger
Carbonaceous aerosol characterisation in the Swiss Rhone Valley
Seminar Laboratory of Atmospheric Chemistry, Paul Scherrer Institut, Switzerland, 16 November 2009

A.S.H. Prévôt, S. Szidat, N. Perron, V. Lanz, M.R. Alfarra, P. DeCarlo, C. Mohr, U. Baltensperger
Fossil and non-fossil primary and decondary organica aerosol
19th Goldschmidt Conference, Davos, Switzerland, 21-26 June 2009.
A.S.H. Prévôt, S. Szidat, N. Perron, V. Lanz, M.R. Alfarra, P. DeCarlo, C. Mohr, U. Baltensperger
Assessment of fossil and non-fossil primary and secondary organic aerosol
European Aerosol Conference, Karlsruhe, Germany, 6-11 September 2009.

S. Szidat, S. Schmoker, B. Gasser, H.W. Gäggeler, I. Hajdas, L. Wacker, H. Veit
Isolation of different soil components for radiocarbon dating of an alluvial fan
20th International Radiocarbon Conference, Kona/Hawaii, USA, 31 May - 5 June 2009.

S. Szidat, S. Fahrni, N. Perron, A.S.H. Prévôt, M. Ruff, L. Wacker, U. Baltensperger
Fossil and non-fossil sources of carbonaceous aerosols from ^{14}C
19th Goldschmidt Conference, Davos, Switzerland, 21-26 June 2009.

S. Szidat
Bestimmung von Aerosolquellen mit ^{14}C: Erster Schritt zur Verbesserung der Luftqualität
GDCh-Wissenschaftsforum Chemie 2009, Frankfurt/Main, Germany, 30 August - 2 September 2009.

S. Szidat, N. Perron, S. Fahrni, M. Ruff, L. Wacker, A.S.H. Prévôt, U. Baltensperger
Optimized separation of OC and EC for radiocarbon source apportionment
European Aerosol Conference, Karlsruhe, Germany, 6-11 September 2009.

M. Viana, T.A.J. Kuhlbusch, X. Querol, A. Alastuey, R.M. Harrison, P.K. Hopke, W. Winiwarter, M. Vallius, S. Szidat, A.S.H. Prévôt, C. Hueglin, H. Bloemen, P. Wåhlin, R. Vecchi, A.I. Miranda, A. Kasper-Giebl, W. Maenhaut, R. Hitzenberger
Source apportionment analysis of transport-related PM sources in Europe
17th Transport and Air Pollution Symposium, 3rd Environment and Transport Symposium, Toulouse, France, 2-4 June 2009.

L. Wacker, M. Ruff, S. Fahrni, M. Němec, S. Szidat, H.-A. Synal
How to measure small samples with a gas ion source
20th International Radiocarbon Conference, Kona/Hawaii, USA, 31 May - 5 June 2009.

L. Wacker, G. Bonani, I. Hajdas, B. Kromer, M. Němec, M. Ruff, H.-A. Synal
MICADAS: Routine and high-precision radiocarbon dating
20th International Radiocarbon Conference, Kona/Hawaii, USA, 31 May - 5 June 2009.

PUBLIC RELATIONS

Analytical Chemistry

- Media release
  EAWAG
  Neue Ergebnisse der Klimaforschung mit Eisbohrkernen
  8 January 2009.

- SF Schweizer Fernsehen, Schweizaktuell
  Fliegende Eisklötze
  19 January 2009.

- Spiegel Online
  Wie sich Klimawandel-Skeptiker die Erderwärmung kaltrechnen
  23 January 2009.

- Ecologist
  New studies disprove cosmic ray and solar influence theories of global warming
  6 February 2009.

- Die Zeit
  Der Heilige Krieg um die Erderwärmung
  26 February 2009.

- SF Schweizer Fernsehen, Schweizaktuell
  Fliegende Eisklötze
  3 March 2009.

- NewScientist
  Swiss paradise
  7 November 2009.

- New Delhi Television NDTV, http://www.ndtv.com/news/world/climate_change_frozen_in_time.php
  Climate change: Frozen in time
  23 November 2009.

Environmental Radionuclides Universität Bern

- Schweizer Fernsehen
  Tagessschau: Feinstaub-Studie
  http://www.sf.tv/sf1/tagesschau/index.php?docid=20090122
  22 January 2009.

- Schweizer Fernsehen
  10 vor 10: Es ist wieder Feinstaub-Saison
  http://www.sf.tv/sf1/10vor10/index.php?docid=20090122
  22 January 2009.

- NZZ Online
  Woher kommt der Feinstaub wirklich
  http://www.nzz.ch/nachrichten/panorama/woher_kommt_der_feinstaub_wirklich_1.1757227.html
  22 January 2009.

- soitu.es
  La nube de hollín que cubre media Asia
  http://www.soitu.es/soitu/2009/01/22/medioambiente/1232637846_130339.html
  22 January 2009.

- Tribune de Genève
  Le "Nuage brun d'Asie" disséqué au carbone 14
  23 January 2009.

- Radio SWR 2
  Campus: Braune Wolken über Asien
  24 January 2009.

- n-tv.de
  Rußpartikel aus Privathaushalten – Braune Wolke über Asien
  http://www.n-tv.de/1092874.html
  27 January 2009.

- BioChemie am Samstag, Uni Bern
  Vortrag S. Szidat: Ursachen und Risiken von Feinstaub
  24 October 2009.

LECTURES AND COURSES

Prof. Dr. H.W. Gäggeler
Universität Bern, FS2009:
Bachelor
- Instrumentalanalytik II (with others) (3 ECTS)
- Allgemeine Chemie (Einführung Radioaktivität) (with others) (4 ECTS)

Master
- Kolloquium Radio- und Umweltchemie in collaboration with the Paul Scherrer Institut (organized by D. Schumann)

Prof. Dr. Andreas Türler
TU München, WS2008/2009, SS2009
Master
- Radioaktivität und Radiochemie (4 ECTS)
- Spezielle Aspekte der Radiochemie (4 ECTS)
- Praktikum in Radiochemie und Radioanalytik (3 ECTS)
- Seminar Radioaktivität und Radiochemie (1 ECTS)
- Seminar Spezielle Aspekte der Radiochemie (1 ECTS)
- Seminar über wissenschaftliche Arbeitsmethoden der Radiochemie

Universität Bern, HS2009:
Bachelor
- Physikalische Chemie IV (with Prof. T. Wandlowski) (3,75 ECTS)
- Praktikum Phys. Chemie II (with others) (4 ECTS)

- *Master*
- Nuclear and Radiochemistry (3 ECTS)
- Lab course Nuclear and Radiochemistry (with others) (4 ECTS)
- Lab course Paul Scherrer Institut (with others) (4 ECTS)
- Kolloquium Radio- und Umweltchemie in collaboration with Paul Scherrer Institut (organized by D. Schumann)

Prof. Dr. M. Schwikowski
Universität Bern, FS2009:
Bachelor
- Instrumentalanalytik II (with others) (3 ECTS)

Universität Bern, HS2009:
Master
- Atmospheric and Aerosol Chemistry (3 ECTS)

Dr. M. Ammann
ETH Zürich, FS 2009:
- Course 'Atmospheric Interface Chemistry (3 ECTS)

Dr. T. Bartels-Rausch
HS 2009
- Lab course Paul Scherrer Institut (with Prof. A. Türler and S. Szidat) (4 ECTS)

Dr. R. Eichler
Universität Bern, HS2009:
- Praktikum Phys. Chemie II (with Prof. A. Türler) (4 ECTS)
- Lab course Nuclear and Radiochemistry (with Prof. A. Türler and S. Szidat) (4 ECTS)

Dr. D. Schumann
- Kolloquium Radio- und Umweltchemie in collaboration with Paul Scherrer Institut

PD Dr. S. Szidat

Universität Bern, FS2009:

- Ergänzungen zur analytischen Chemie für Pharmazeuten (Vorlesung und praktische Übungen) (1.5 ECTS)

Universität Bern, HS2009:

- Chemie für Studierende der Veterinärmedizin (with C. Leumann) (4.5 ECTS)
- Environmental Radionuclides and Nuclear Dating (1.5 ECTS)
- Praktikum Physikalische Chemie II (with others) (4 ECTS)
- Lab Course Nuclear and Radiochemistry (with Prof. A. Türler and R. Eichler) (4 ECTS)

MEMBERS OF SCIENTIFIC COMMITTEES EXTERNAL ACTIVITIES

Dr. Markus Ammann:
- Air-Ice Chemical Interactions (AICI), Member of Steering Committee
- Atmospheric Chemistry and Physics: member of editorial board
- Member of the IUPAC Subcommittee on gas kinetic data evaluation
- PSI internal research commission (FoKo), member

Dr. Robert Eichler:
- PSI internal research commission (FoKo), member

Prof. Dr. Heinz W. Gäggeler:
- Nuklearforum Schweiz, Member of the Executive Board and Member of the Science Board
- Schweizerische Kommission für die hochalpine Forschungsstation Jungfraujoch der SANW, member
- Astronomische Kommission der Stiftung Jungfraujoch und Gornergrat, member
- Joint IUPAC/IUPAP Working Party (JWP) on the discovery of new elements, member
- International Union of Pure and Applied Chemistry (IUPAC), fellow
- Steering Committee of EURISOL, member
- Division of Nuclear and Radiochemistry, European Association for Chemical and Molecular Sciences (EuCheMS), Chairman
- Oeschger Centre for Climate Change Research, Member of the Scientific Board

Dr. Dorothea Schumann:
- Nuklearforum Schweiz, member
- Schweizerische Gesellschaft der Kernfachleute, member
- PSI internal Neutron Source Development Group, member

Prof. Dr. Margit Schwikowski:
- Expert of the Matura Examination of Kantonsschule Baden
- Coordinating Committee of the Pages/IGBP initiative LOTRED SA (Longterm climate reconstruction and Diagnosis of (southern) South America), member
- Schweizerische Gesellschaft für Schnee, Eis und Permafrost (SEP), board member
- Oeschger Centre for Climate Change Research, member

PD Sönke Szidat:
- Oeschger Centre for Climate Change Research (OCCR), member

Prof. Dr. Andreas Türler:
- Research Center Dresden-Rossendorf (FZD), member of the advisory board
- GSI Helmholtzzentrum für Schwerionenforschung GmbH, member of the General Program Advisory Committee
- (G-PAC) and GSI Users Group, member of the Executive Committee (UEC)
- Forschungs-Neutronenquelle Heinz Maier-Leibnitz (FRM-II), member of the committee on instrumentation
- Gesellschaft Deutscher Chemiker (GDCh), Fachgruppe Nuklearchemie, Vorsitzender
- Radiochimica Acta, member of the advisory board

BACHELOR THESIS

Benjamin Gasser

Isolierung von Huminsäuren und Cellulose aus Bodenproben für die AMS ^{14}C-Bestimmung

Dr. S. Szidat / Uni Bern
Prof. Dr. H.W. Gäggeler / PSI & Uni Bern
May 2009

Nicolas Millius

Molsiebfalle zum Einfangen von Kohlenstoffdioxid für anschliessende ^{14}C-Messung zur Feinstaubanalyse

Dr. S. Szidat / Uni Bern
Prof. Dr. H.W. Gäggeler / PSI & Uni Bern
May 2009

DOCTORAL THESIS

Nadzeya Homazava

Development of a novel microflow-capillary technique online hyphenated to the inductively coupled plasma mass spectrometry for the spatial- and time-resolved investigation of local corrosion

Prof. Dr. U. Krähenbühl / Uni Bern
May 2009

Anita Ciric

ENSO related climate variability recorded in an ice core from Cerro Mercedario, Central Andes

Prof. Dr. Margit Schwikowski / PSI & Uni Bern
Prof. Dr. H.W. Gäggeler / PSI & Uni Bern
October 2009

Michael Sigl

Ice core based reconstruction of past climate conditions from Colle Gnifetti, Swiss Alps

Prof. Dr. Margit Schwikowski / PSI & Uni Bern
Prof. Dr. H.W. Gäggeler / PSI & Uni Bern
October 2009

HABILITATION

Sönke Szidat

Source apportionment of carbonaceous particles in the atmosphere

Universität Bern, October 2009

TITULAR PROFESSOR

Margit Schwikowski

was awarded *titular professor* of the University of Bern
for her outstanding contributions to palaeo-climate science, October 2009

AWARDS

Sönke Szidat received the *Fritz-Strassmann-Preis*
by the Nuclear Chemistry Section of the German Chemical Society (GDCh)
for his achievements on the determination of the radionuclide ^{14}C in environmental samples with miniaturized accelerator mass spectrometry, September 2009

M. Sigl, H.W. Gäggeler, M. Schwikowski
Poster Award from the World Climate Research Program
The variability of $\delta^{18}O$ in an Alpine ice core reflects long-term trends of past summer (May-July) temperatures
10th Swiss Global Change Day, Bern, Switzerland, 31 March 2009

SUMMER STUDENTS

Marko Markovic
Separation of titanium from an irradiated stainless steel sample
Universität Bern
July - August 2009

Nicolas Millius
Advancement of the online melting analysis with ICP-SFMS (Inductively Coupled Plasma Sector Field Mass Spectrometry) for firn cores
Universität Bern
July - August 2009

Silvana Müller
Behaviour of ^{210}Po in LBE
Universität Bern
July - August 2009

Patrick Steinegger
Alloys of a noble metal containing a rare earth element
Universität Bern
July - August 2009

Michael Wagner
Uptake of ozone on deliquesced KI/NaCl aerosol particles coated with surfactants
Universität Bern
July - August 2009

Benjamin Christian Wyler
Analysis of the upper five meters of an ice core from Spitsbergen with ion chromatography
Universität Bern
July - August 2009

Pascal Albrecht
1-wöchiges Berufspraktikum (BOGY) zur Analyse von Gletschereis
Klettgau-Gymnasium Waldshut-Tiengen
19-23 October 2009

Michelle Ernst
Maturarbeit Luftverschmutzung archiviert in Gletschereis
Kantonsschule Olten
August-December 2009

VISITING GUESTS AT PSI 2009

13-14 January
Peter Schwertfeger, Massey University Auckland, New Zealand
Relativistic effects in the chemistry of gold

24-31 January
Francisco Cereceda, Universidad Tecnica Federico Santa Maria, Chile
Swiss-Chilean collaboration on air pollution

28 January – 10 February
Binita Dutta, Sahel Institute of Nuclear Physics, India
Collaboration in the frame of EURISOL

01-13 February
Irene Wientjes, University Utrecht, Netherlands
Analyses of ice cores

11-21 February
Susanta Lahiri, Sahel Institute of Nuclear Physics, India
Collaboration in the frame of EURISOL

06 March
Frank Rösch, University Mainz, Germany
Potential medical application of Ti-44:
^{44}Ti/^{44}Sc radionuclide generators for ^{44}Sc-PET radiopharmaceuticals

14 April
Arbeitsgruppe Atmosphärische Strömungssysteme von Prof. H. Wernli, Universität Mainz, Germany
Klimaarchiv Gletschereis, Laborbesuch

04 May - 31 July
Manabu Shiraiwa, Max Planck Institut, Mainz, Germany
Experiment PROTRAC protein aerosol nitration

7 May 2009
Lehrerfortbildung Geographie Kantonsschule Wettingen, Switzerland
Klimaarchive, Vortrag und Laborbesuch

08 May
Hubertus Fischer, University of Bern, Switzerland
Polar ice core reconstructions of annual to glacial/interglacial changes in atmospheric circulation: Reality or wishful thinking

29 June
Schülergruppe Gymnasium und Handelsmittelschule Thun-Schadau, Ergänzungsfach Chemie, Switzerland
Klimaarchiv Gletschereis, Laborbesuch

28 August
Tatyana Papina, Institute for Water and Environmental Problems (IWEP), SBRAS, Barnaul, Russia
Discussion of Mongolian ice core project

31 August
Walter Kutschera, University Wien, Austria
Meeting on future work with ^{60}Fe

27-30 August
A. Popeko, Flerov Laboratory for Nuclear Reactions, Dubna, Russia
Discussion of experiment, element 114 at Dubna

20-22 September
Pamela Santibanez Avila, Centro de Estudios Cientificos, Valdivia, Chile
Ice sample preparation, discussion of a joint publication

24-25 September
Paul Mayewski, Daniel Dixon, Climate Research Institute, Maine
Discussion of future collaboration in ice core science

02 October
Marcus Christl, ETHZ, Zurich, Switzerland
Actinide measurements with a small accelerator - recent developments and applications in environmental sciences

02 October
Christian Bogdal, ETHZ, Zurich, Switzerland
The haunting legacy: Persistent organic pollutants in remote Alpine sites

07-08 October
Fabienne Riche, SLF Davos, Switzerland
Experiment PROTRAC snow diffusion chamber

12 October
Doug Hardy, University of Massachusetts, USA
Discussion of radiocarbon dating of Kilimanjaro ice samples

15-16 October
Barbara May, Institute for Environmental Physics, University of Heidelberg, Germany
Investigating ^{14}C in DOC and POC extracted from Alpine ice

20-25 October
Dimitry Divine, NPI, Tromsö, Norwegen
Discussion of ice core results within EU FP6 project MILLENNIUM

5 November
Dr. Hans-Arno Synal, ETH Zürich
New and future possibilities of low-energy AMS (accelerator mass spectrometry)

06 November
Georg Kaser, Institut für Geographie, Innsbruck, Austira
Learning about climate from glacier changes: a multi-method and multi-scale approach on Kilimanjaro

06 November
Walter Kutschera, University of Wien, Austria
The prospect of a $^{26}Al/^{10}Be$ chronometer to date old ice

19-27 November
Vladimir N. Loginov, Flerov Laboratory for Nuclear Reactions, Dubna, Russia
Setup ECR-ION source at LCH

08-22 November
Manabu Shiraiwa, Max Planck Institut, Mainz, Germany
Experiment PROTRAC protein aerosol nitration

11 December
Rainer Moormann, FZ Jülich, Germany
Safety aspects of high power spallation sources

PAUL SCHERRER INSTITUT

LABOR FÜR RADIO- UND UMWELTCHEMIE
DES PAUL SCHERRER INSTITUTS UND DER UNIVERSITÄT BERN
31.12.2009

UNIVERSITÄT BERN

PSI **Prof. Dr. Andreas Türler** **Uni Bern**

Angela Blattmann (Secretary / 80 %)

Catrina Veraguth (Secretary / 40 %)

Prof. Dr. Margit Schwikowski (Deputy)

SURFACE CHEMISTRY
Dr. Markus Ammann
Dr. Thorsten Bartels-Rausch
Dr. Aurélie Rouviere
Dr. Adèla Krepelovà
Mario Birrer
Yulia Sosedova [1]
Veronika Zelenay [1]
Thomas Ulrich [1]
Sepp Schreiber [1]

ANALYTICAL CHEMISTRY
Prof. Dr. Margit Schwikowski
Leonhard Tobler
Dr. Anja Eichler (50%)
Thomas Aemmer
Sabina Brütsch
Silvia Köchli
Michael Sigl [1]
Anita Ciric [1]
Manuel Schläppi [1]
Pierre-Alain Herren [1]
Isabella Mariani [1]

ENVIRONMENTAL RADIONUCLIDES
PD Dr. Sönke Szidat
Edith Vogel
Simon Fahrni [1]

HEAVY ELEMENTS
Dr. Robert Eichler
Dr. Rugard Dressler
Dave Piguet
Alexander Vögele
Alexey Serov [1]
David Wittwer [1]

RADWASTE ANALYTICS
Dr. Dorothea Schumann
Dr. Jörg Neuhausen
Dr. Marin Ayranov
Sabrina Lüthi
Tanja Stowasser (50%)
Suresh Chiriki
Stephan Heinitz [1]

[1] Graduate student

AUTHOR INDEX

AFFILIATION INDEX

ABE	High Intensity Proton Accelerators, Paul Scherrer Institut, CH-5232 Villigen PSI, Switzerland
AHL	Hot Laboratory Division, Paul Scherrer Institut, CH-5232 Villigen PSI, Switzerland
AMI	Abteilung Maschinen-Ingenieurwissenschaften, Paul Scherrer Institut, CH-5232 Villigen PSI, Switzerland
ASQ	Spallation Neutron Source Division, Paul Scherrer Institut, CH-5232 Villigen PSI, Switzerland
BMR	Biomolecular Research, Paul Scherrer Institut, CH-5232 Villigen PSI, Switzerland
CECS	Centro de Estudios Cientificos, Valdivia, Chile
CWU	Central Washington University, Department of Geological Sciences, 400 E. University Way, Ellensburg, WA 98926, USA
EAWAG Dübendorf	Eidgen. Anstalt für Wasserversorgung, Abwasserreinigung und Gewässerschutz, Überlandstrasse 133, CH-8600 Dübendorf, Switzerland
ETHZ	Eidgen. Technische Hochschule Zürich, CH-8092 Zürich, Switzerland
FLNR Dubna	Flerov Laboratory of Nuclear Reactions, Joliot Curie 6, 141980 Dubna, Russia
EMPA	Eidgenössische Materialprüfungs- und Forschungs-Anstalt, Überlandstrasse 129, CH-8600 Dübendorf, Switzerland
FS INVENTOR	FS Inventor AG, Muristr. 18, CH-3132 Riggisberg, Switzerland
IMAU	Institute for Marine and Atmospheric Research Utrecht, Utrecht University, Princetonplein 5, 3584 CC Utrecht, The Netherlands
IRCELYON	Institut de recherches sur la catalyse et l'environnement de Lyon, Université Lyonand Centre national de la recherche scientifique, 69622 Villeurbanne cedex, France
Isotope Prod. GmbH	13125 Berlin, Germany
ITE	Instytut Technologii Elektronowej, al. Lotnikow 32,46, 02-668 Warszawa, Poland
ITP, China	Institute of Tibetan Plateau Research, Chinese Academy of Sciences, Beijing 100085, China
IWEP	Institute for Water and Environmental Problems, Siberian Branch of the Russian Academy of Sciences, 105 Papanintsev Str., RU-Barnaul 656099, Russia
LAC	Laboratory of Atmospheric Chemistry, Paul Scherrer Institut, CH-5232 Villigen PSI, Switzerland
LBNL	Lawrence Berkeley National Laboratory, Berkeley, CA 94720, USA
LDM	Laboratory for Development and Methods, Paul Scherrer Institut, CH-5232 Villigen PSI, Switzerland
LGGE	Laboratoire de Glaciologie et Geophysique de l'Environnement, 38402 Saint Marin d'Hère, Cedex, France
MPI-CH	Max Planck Institute for Chemistry, Biogeochemistry Department, 55128, Mainz, Germany
NCCR Climate	NCCR National Climate Management Centre for Competence in Research, University of Bern, Erlachstrasse 9a, CH-012 Bern, Switzerland
CIC Niels Bohr Inst.	Centre for Ice and Climate, Juliane Maries Vej 30, DK-2100 København Ø, Denmark
NPI	Norwegian Polar Institute, N-9296 Tromsø, Norway
Oeschger Center	University of Bern, Zähringerstrasse 25, CH-3012 Bern, Switzerland

PSI	Radio- and Environmental Chemistry Paul Scherrer Institut, CH-232 Villigen PSI, Switzerland
SLS	Swiss Light Source, Paul Scherrer Institut, CH-5232 Villigen PSI, Switzerland
Univ. L'Aquila	Universita 67100, L'Aquila, Italy
Univ. Bern	Departement für Chemie und Biochemie, Universität Bern, Freiestr. 3, CH-3012 Bern, Switzerland
Univ. Bern, Plant Sci.	University of Bern, Institute of Plant Sciences, Altenbergrain 21, CH-3013 Bern, Switzerland
Univ. Luxembourg	University of Luxembourg, Department for Physics, 162 a avenue de la Faiencerie, L-1511 Luxembourg
Univ. Maine	Climate Change Institute and Department of Earth Sciences, University of Maine, Orono ME 04469, USA
Univ. Milano Bicocca and INFN	University of Milano, 20126, Milano, Italy
Universidad Austral de Chile	Instituto de Botanica, Facultad de Ciencias, Universidad Austral de Chile, Valdivia, Chile
Univ. Orleans	Laboratoire de Physique et Chimie de l'Environnement), UMR 6115 CNRS, Université d'Orléans, F-45071 Orleans, France
Univ. Tallinn	Institute of Geology, Tallinn University of Technology, 10143 Tallinn, Estonia
Univ. Venice	University of Venice Ca' Foscari, Environmental Science Department, Calle Larga Santa Marta 2137, IT-30123 Venezia, Italy
Uni Zürich	University of Zurich, Winterthurerstr. 190, CH-8057 Zürich, Switzerland
UU	Department of Earth Sciences, Uppsala University, Villavägen 16, S-752 36 Uppsala, Sweden
Weizmann	Department of Environmental Sciences, Weizmann Institute, Rehovot 76100, Israel

Paul Scherrer Institut, 5232 Villigen PSI, Switzerland
Tel. +41 (0)56 310 21 11, Fax +41 (0)56 310 21 99
www.psi.ch